Vacuum Contributions

to the Nucleon Energy Sum Rule

Devon Neil Crowther

Departement Fisika · Department of Physics

Universiteit · Stellenbosch · University

December 2023

DECLARATION

By submitting this thesis electronically, I declare that the entirety of the work contained therein is my own, original work, that I am the sole author thereof (save to the extent explicitly otherwise stated), that reproduction and publication thereof by Stellenbosch University will not infringe any third party rights and that I have not previously in its entirety or in part submitted it for obtaining any qualification.

Date: 12 January 2024

ABSTRACT

Vacuum Contributions to the Nucleon Energy Sum Rule

Devon Crowther

Department of Physics
Stellenbosch University

Thesis: MSc (Theoretical Physics)

December 2023

Within the Nambu Jona-Lasinio(NJL) chiral soliton model nucleon structure functions were previously explored. One of the structure functions, namely the iso-singlet unpolarized nucleon structure function (IUSF), displayed results that did not agree with experimental data. The simulations described in this paper aim to investigate this behaviour of the IUSF. The central means of this investigation is the energy sum rule that relates an integral of the IUSF to the mass of the nucleon. Through this investigation, it was discovered that the cut-off constant Λ had not been properly computed in that earlier study. This constant is not a numerical parameter but is fully determined by physical constants, such as the pion mass and pion decay constant. Even though the correction was only minor, the adjusted calculation of the IUSF resulted in a significant problem with the sum rule — a numerical inaccuracy that became more apparent at higher grand spins. These inaccuracies in the sum rule become apparent regardless of the Λ value but were signifcantly more so for the corrected Λ. With the validity of our sum rule in numerical jeopardy, an investigation is launched into why this is so and obtaining the appropriate numerical parameters to fix it. Following this, we investigated the deviation from empirical data exhibited by the IUSF. This was done in two ways, first the numerical parameters that encode the discretisation of the quantum fields were changed, secondly the contribution from the non-solitonic background, which defines the reference energy, was changed to better reflect its spatial invariance. In essence a strong dependence of the IUSF on the treatment of the vacuum subtraction was found.

UITTREKSEL

Vakuum Bydraes na die Nukleon Energie Som Reël

Devon Neil Crowther

Departement Fisika
Universiteit Stellenbosch

Tesis: MSc (Teoretiese Fisika)

Desember 2023

Voorheen was die Nambu Jona-Lasinio(NJL) chirale solitonmodel is nukleonstruktuurfunksies ondersoek. Een van die struktuurfunksies, die iso-singlet ongepolariseerde nukleonstruktuurfunksie (IUSF), het resultate geleuer wat nie met eksperimentele data ooreenstem nie. In die skripsie, word hierdie gedrag van die IUSF word deur simulasies ondersoek. Die hoof doel lê in die energiesomreël wat 'n integraal van die IUSF koppel met die massa van die nukleon. Hierdie konstante is nie 'n numeriese parameter nie, maar word ten volle bepaal deur fisiese konstantes, soos die pion massa en verval konstantes. Alhoewel die regstelling slegs minimaal was, het die aangepaste berekening van die IUSF tot 'n beduidende probleem met die somreël gelei - 'n numeriese onakkuraatheid wat meer beklemtoon word by hoër grand spins. Hierdie onakkuraathede in die somreël is opvallend ongeag die Λ-waarde, maar was aansienlik meer so vir die gekorrigeerde Λ. Met die geldigheid van ons somreël in numeriese gevaar, is 'n ondersoek geloods om die oorsprong te vind en die nodige toepaslike numeriese parameters te bepaal. Hierna volg 'n ondersoek van afwyking in empiriese data wat vertoon word deur die IUSF. Dit word op twee maniere gedoen, eerstens die verandering van numeriese parameters wat die diskretisering van die kwantumvelde kodeer, tweedens die bydrae van die nie-solitoniese agtergrond, wat die verwysingsenergie definieer, is verander om die ruimtelike invariansie beter te weerspieël. In wese is 'n sterk afhanklikheid van die IUSF op die hantering van die vakuumaftrekking gevind.

ACKNOWLEDGMENTS

First and foremost, I extend my deepest appreciation to my supervisor, Professor Weigel, for his invaluable insights and dedicated mentorship throughout this research endeavor. His expertise and encouragement have been instrumental in shaping the direction of this master's degree. I would like to express my profound thanks to Stellenbosch University and its Postgraduate Scholarship Programme for financing my studies. I also give thanks to Dr I. Takyi for his valuable correspondence, helping me understand some details of his work.

I extend my gratitude to the Stellenbosch University Physics Department for providing the necessary resources and facilities that I have utilized throughout my research. The academic environment and resources have played a crucial role in the development and completion of my master's degree.

Special thanks are due to my parents, Russell and Tracy Crowther, and my brother, Callum Crowther, for their unwavering support during this academic journey. I would also like to express special thanks to my friend, Erin Matthews, for staying up with me all night to get work done.

Last but not least, I want to express my gratitude to Chris Boshoff, Chad Rath, and Damian Robson for being great friends who kept me company throughout my master's degree.

CONTENTS

List of Figures

CHAPTER 1

INTRODUCTION

1.1 QUANTUM CHROMODYNAMICS

Humanity's goal of finding the fundamental structure of matter first led to the discovery of the atom by John Thomson in 1897 who proposed the so-called plum pudding model according to which the atom was made of small electrically charged particles called electrons embedded in a positively charged soup[3]. In 1911 Ernest Rutherford scattered α-particles off gold foils. He successfully explained the result through a model in which a positively charged nucleons surrounded by a cloud of electrions[4]. In 1932 James Chadwick further improved on the model by introducing particles within the nucleus called protons (positively charged particles) and neutrons (neutrally charged particles). By the end of these studies it was revealed that the atom was made of a nucleus composed of positively charged protons (p) and neutral neutrons (n) and orbiting around this nucleus were negatively charged electrons[5]. It was at this point that these particles were thought of as the fundamental particles of matter. Yet, the question still remained, what held the nucleus together, since as far as they knew the positively charged particles should repel each other and the nucleus should blow apart. This lead to the discovery of the nuclear force that acted between nucleons. This force is strongly attractive at short distances, overcoming the repulsive electric force between the protons. One of the early attempts to understand the nature of this force was made by Hideki Yukawa[6].

Further studies conducted throughout the 1950's and 1960's using particle colliders of increasingly high energy revealed that additional particles also existed such as muons (μ), tau (τ) and neutrinos (ν). These particles with the addition of the electron were called leptons. Towards the end of the 1960's deep inelastic scattering (DIS) was used to probe the structure of nucleons. Through these experiments it was discovered that protons and neutrons were made of small particles called quarks. These leptons and quarks which are considered $\frac{1}{2}$-fermions, form the fundamental structure of matter. While leptons are only subject to the electromagnetic and weak nuclear force [7], quarks also interact via the strong force.

With the discovery of these particles it is also important to be able to calculate the interaction between them. Gauge field theories have been proven successful in describing the interactions of these particles. These theories describe forces as (virtual) gauge bosons propagating between the fundamental spin-$\frac{1}{2}$ fermions. These gauge theories usually are unitary ($U(N)$) or special unitary ($SU(N)$) Lie groups, where the dimension N, of the Lie group is the number of elementary fermions. With this there are N^2 and $N^2 - 1$ gauge bosons for unitary and special unitary gauge theories, respectively. For the electromagnetic field, the interactions are mediated by a gauge boson called photon and the gauge theory, called Quantum Electrodynamics (QED), is a $U(1)$ gauge symmetry. Strong interactions are mediated by the gluon gauge field with the gauge theory called Quantum Chromodynamics (QCD), gauge symmetry of $SU(N_C)$, with $N_C = 3$ colour charges. Colour is a new quantum number of the quarks which is introduced to make the nucleon wave function totally antisymmetric under the exchange of its spin-$\frac{1}{2}$ constituents. With the nucleon being composed of three quarks we must have equally many colour charges. In QED the photon has no charge, however in QCD the gluons do have colour charge and interact directly with each other. As a result QCD is much more complicated than QED. An introduction to Quantum Field Theory and Quantum Chromodynamics is given in Refs. [8, 9].

To introduce QCD as a gauge theory we first define the non-abelian field strength tensor for the gluon fields[9]

$$F^a_{\mu\nu} = \partial_\mu A^a_\nu - \partial_\nu A^a_\mu + g_{\text{QCD}} f^{abc} A^b_\nu A^c_\mu, \tag{1.1}$$

where $a = 1, \cdots, N_C^2 - 1$ is a colour label while $\mu, \nu = 0, 1, 2, 3$ are Lorentz indices. The interaction strength is measured by the coupling constant g_{QCD} The structure constants f^{abc} emerge from the $SU(N_C)$ algebra

$$\left[\frac{\lambda^a}{2}, \frac{\lambda^b}{2}\right] = i f^{abc} \frac{\lambda^c}{2} \tag{1.2}$$

of the $N_C^2 - 1$ hermitian traceless $N_C \times N_C$ matrices. For $N_C = 3$ these are the eight Gell-Mann matrices. With this definition The QCD Lagrangian is

$$\mathcal{L}_{\text{QCD}} = \bar{q}\left(i\partial\!\!\!/ - m_0\right) q - \frac{1}{4} F^{a\mu\nu} F^a_{\mu\nu} + g_{QCD} \bar{q} \gamma^\mu A^a_\mu \frac{\lambda^a}{2} q. \tag{1.3}$$

This describes the interaction of the quarks mediated by the gluons. As these are the components of particles that are subject to the strong interaction (called hadrons, to be specified in Section 1.2) this Lagrangian will eventually describe their structure and dynamics. The quarks spinors (q) have three labels (not explicitly shown for notational convenience): $\alpha = 1, 2, 3, 4$ for Dirac space, $a = 1, 2, 3, \ldots, N_C$ for colour and $i = 1, 2, \ldots, 6$ for flavour. Typically, the various flavours are called by name: up, down, ..., top. This quantum number dictates the observable quantum numbers of the hadrons. Colour interaction is not affected by the flavour of the particle. Due to this the different flavours are only distinct by the mass matrix in Eq. (1.3)

$$m_0 = \text{diag}\left(m_0^u, m_0^d, m_0^s, m_0^c, m_0^b, m_0^t\right), \tag{1.4}$$

that acts on the flavour index of the quark spinors.

The second term in the Lagrangian is the Yang-Mills Lagrangian. Due to the non-Abelian structure of QCD the gluons couple to the quarks and with themselves. The last term is the coupling of gluons to the colour currents of the quarks

$$j^a_\nu = \bar{q} \frac{\lambda^a}{2} \gamma_\mu q. \tag{1.5}$$

Here the Gell-Mann matrices act on the colour index of the quark spinors.

QCD is an asymptotically free theory [10]: as the interaction energy increases, the interaction itself becomes weaker: quarks and gluons behave like (almost) free particles. As a result, techniques from perturbative quantum field theory can be applied, for example to deep inelastic scattering (DIS) for which structure functions are an important ingredient. On the other hand, at low interaction energies the interaction strength increases which makes it more and more difficult to separate individual quarks and gluons. Ultimately this leads to the confinement hypothesis.

Colour Confinement. *One cannot observe a single quark on its own.*

This leads us to one of the peculiarities of the strong interaction. The total amount of observed colour for isolated particles is either zero or the N_C colours occurring in equal proportions. This means all hadron states and physical observables are invariant under the colour SU(N_C) transformation, with the only colourless combinations being $q\bar{q}$ mesons, and if $N_C = 3$, qqq (baryons) and $\bar{q}\bar{q}\bar{q}$ (anti-baryons).

Pulling quarks apart requires energy supply. Since the colour force becomes larger as the quarks are pulled further apart, the amount of energy needed eventually becomes large enough to create a new quark anti-quark pair. This effectively creates another hadron.

Flavour	Electric Charge	Mass(MeV)
up (u)	$\frac{2}{3}$	2.3
down (d)	$-\frac{1}{3}$	4.8
strange (s)	$-\frac{1}{3}$	95
charm (c)	$\frac{2}{3}$	1275
bottom (b)	$-\frac{1}{3}$	4180
top (t)	$\frac{2}{3}$	173500

Table 1.1: The flavours and their respective electric charge and mass [11]

1.2 Hadrons

There are two main types of hadrons, baryons and mesons. The low-lying baryons have quantum numbers of bound states from N_C quarks, while mesons are associated with quark-antiquark pairs. There are six flavours of quarks, these are given in the table 1.1. The hadrons of interest in this project are protons and neutrons. Since protons and neutrons are similar with respect to the strong interaction they are grouped within the so-called "nucleon" iso-doublet. The name arises as it is the building block of atomic nuclei. These are fermions and are the lightest of the baryons, as their quantum numbers are made of up (u) and down (d) quarks. The proton has the quantum numbers (flavours) of two up (u) quarks and one down (d) quarks, uud, with integer electric charge one and mass m = 938MeV, whilst the neutron has one up (u) quark and two down (d) quarks, udd, with zero charge and mass, m = 939.6MeV[11]

1.3 Chiral Symmetry and the QCD Langrangian

In the absence of current masses Quantum Chromodynamics becomes a chiraly symmetric theory. This means that left and right-handed fermions decouple according to the projection:

$$q_R = P_R q, \quad q_L = P_L q, \text{ with } \quad q = q_R + q_L, \tag{1.6}$$

with the projectors

$$P_{R,L} = \frac{1}{2}(1 \pm \gamma_5). \tag{1.7}$$

That is, for $m_0 = 0$ the quark part of the Lagrangian, Eq. (1.3) is a sum of two forms; one only contains q_L, the other only q_R.

Hence, we find that for $m_0 = 0$ the Lagrangian is invariant under global unitary flavour transformations, on the left and right-hand side fields, corresponding to a $U_L(N_f) \times U_R(N_f)$, where N_f is the number of flavours.

As mentioned above chiral symmetry is broken by the current masses, however when dealing with light quarks, i.e. the up and down flavours it is a good approximation with their masses only being of the order of a few MeV, much less than the typical QCD scale, Λ_{QCD}. In the above symmetry we should therefore take N_f to be the number of quarks with $m_q \lesssim \Lambda_{\text{QCD}}$.

Empirically the chiral symmetry suggests the existence of parity doublets. However, this is not observed; rather the light pseudoscalar meson (pions, kaons) stand out while the scalar mesons emerge as heavy and wide resonances. Hence, the symmetry must be broken spontaneously (or dynamically). The non-vanishing scalar vacuum expectation value is the quark condensate $\langle \bar{q}q \rangle \neq 0$. The pseudoscalar mesons are the Goldstone bosons associated with this symmetry breaking. Or rather they are "would-be" Goldstone bosons because they have a small non-zero mass from the explicit breaking $m_0 \neq 0$.

1.4 Effective Models of Strong Interactions in QCD

Since at low energies the QCD interaction strength is large, standard perturbation techniques cannot be applied when exploring this quantum field theory. Rather certain effective models of strong interactions should be used to mimic the low-energy behaviour of QCD as closely as possible. For this purpose we use the approximate chiral symmetry of the QCD Lagrangian as a guide to construct such effective models[10]. The requirement of the known explicit, spontaneous and anomalous chiral symmetry breaking puts significant constraints on possible models for the strong interaction of quarks. We can also generalise QCD to a gauge theory with an arbitrary number of colours N_C. Then for a large N_C QCD will reduce to an effective theory of an infinite number of weakly interacting meson and glueballs[12]. Here weakly means that the interaction strength between those particles decreases as N_C increases. This will be further discussed in chapter 2.

While this meson theory cannot be constructed explicitly, the light mesons should be most relevant. Consequently, the effective theory's Lagrangian subjects these mesons to the dynamics of chiral symmetry (breaking). Furthermore, Witten gave arguments that within this effective theory, baryons emerge as solitons[13]. Witten's conjecture has been applied quite successfully recently. The most popular effective meson theories are the Skyrme and gauged σ-models.

Formally these effective theories should be derived from QCD by integrating out the quark and gluon fields. Unfortunately this seems infeasible for the latter. We therefore start from the Nambu-Jona Lasinio (NJL) model in which quarks self-interact according to the rules of chiral symmetry. The force associated

with the gluon exchange is approximated by a point interaction. So-called bosonisation techniques can be applied to the NJL model, i.e. local quark bilinears can be replaced integer spin fields, yielding an effetive meson theory. Further advantages of this model are that it is simple enough that such complicated field configurations like solitons can be determined self-consistently. It contains the correct chiral symmetry breaking pattern and reproduces a lot of meson properties such as masses, decay constants, scattering lengths etc. using only few input parameters. Lastly it allows for two pictures of baryons, as either ordinary three-valence-quark bound state or as a chiral soliton.

Unfortunately the model comes with some drawbacks. The model is non-renormalisable and only uniquely defined when the necessary regularisation prescription is specified. Due to the non-renormalisability a ultra-violet cutoff is introduced which then indicates the range of applicability of the model. Leading onto this quantitative results for some observables differ in various regularisation schemes.

1.5 Deep Inelastic Scattering (DIS)

This section will go over the inelastic scattering of electrons off a nucleon at high energy and large momentum transfer. The scattering process is given by:

$$e(k) + N(p) \to e(k') + X(p_n) \tag{1.8}$$

where e is the electron, N is the nucleon and X is the system of hadrons produced due to the scattering. The arguments are their respective momenta. The electron has momentum k and k', pre-collision and post-collision, respectively. The nucleon has a momentum of p and the system of hadrons has momentum p_n with n denoting the number of hadrons. In this experiment the known values are the initial values k and p and the final momentum value for the electron k'. DIS relies on the fact that from the final state particles we only measure the electrons and allow X to be any collection of hadrons.

The Lorentz invariant kinematical variables for the scattering process are defined by

$$s = (p+k)^2, \quad q^2 = (k-k')^2 \quad \text{and} \quad \nu = \frac{p\cdot q}{M} \tag{1.9}$$

where s is the total energy squared, q^2 the squared momentum transferred by the virtual photon to the hadrons. In the nucleon rest frame we have the $p = (M,0,0,0)$ where M is the mass of the proton, $k_\mu = (E,\vec{k})$, $k'_\mu = (E',\vec{k}')$ and $\nu = E - E'$: the electron energy loss. Neglecting the electron mass we have that

$$s = (2E+M)M \geq M^2 \tag{1.10}$$

$$q^2 = -4EE'\sin^2(\frac{\theta}{2}) \leq 0 \tag{1.11}$$

$$W = (p+q)^2 = q^2 + M^2 + 2M(E-E') \geq M^2 \tag{1.12}$$

where θ is the scattering angle of the electron and W is the effective mass of X. (Note that the case where $X \equiv N$ and $W = M^2$ is elastic scattering). It is also customary to introduce $Q^2 = -q^2 > 0$. Furthermore, one defines the Bjorken variable

$$x = \frac{-q^2}{2M\nu} = \frac{Q^2}{2M\nu} \tag{1.13}$$

which is bounded by $0 \leq x \leq 1$. The upper bound represents elastic scattering.

The scattering amplitude is then given as

$$\langle e'X|\,T\,|eN\rangle = e^2\bar{u}_{\lambda'}(k')\gamma^\mu u_\lambda(k)\frac{1}{q^2}\langle X|\,J_\mu(0)\,|p,s\rangle \tag{1.14}$$

where λ', λ and s are the spins of the final and initial electromagnetic current operator and the nucleon, respectively. The final state of the hadron system is $|X\rangle$ and $|p,s\rangle$ is the state of the initial nucleon with spin projection s. J_μ is the hadronic part of the electromagnetic current operator.

By summing over all possible final hadron states $\sum_{n,p_n} |\langle\ldots\rangle|$ we can get the inclusive cross-section for

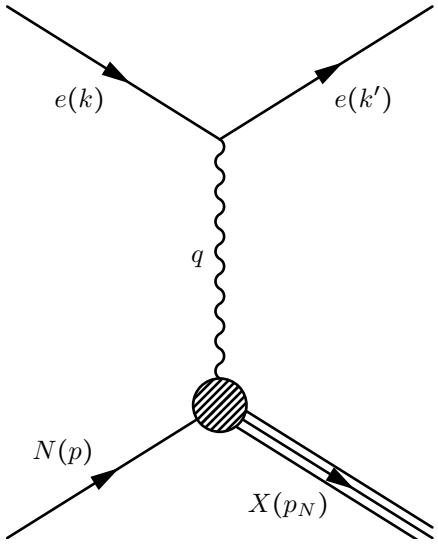

Figure 1.1: Deep inelastic scattering for electron-nucleon scattering.

unpolarised electron scattering[1] [9, 10]

$$\frac{d^2\sigma}{d\Omega dE'} = \frac{\alpha^2}{q^4}\left(\frac{E'}{E}\right)L^{\mu\nu}W_{\mu\nu}, \tag{1.15}$$

where $\alpha = \frac{e^2}{4\pi}$ is the fine structure constant, $L^{\mu\nu}$ and $W_{\mu\nu}$ are the leptonic and hadronic tensors. The leptonic tensor is computed by standard techniques of Dirac spinors:

$$L^{\mu\nu} = \frac{1}{4}\mathrm{tr}(\not{k}\gamma^\mu \not{k}'\gamma^\nu) = 2(k'^\mu k^\nu + k'^\nu k^\mu + \frac{q^2}{2}g^{\mu\nu}), \tag{1.16}$$

where electron mass is approximated to zero. Since the hadronic state is not observed we sum over all possible configurations

$$\begin{aligned} W_{\mu\nu}(p,q) &= \sum_X \langle p,s|\, J_\mu(0)\,|X\rangle\,\langle X|\, J_\nu(0)\,|p,s\rangle\,(2\pi)^4\delta^4(p_n - p - q) \\ &= \int d^4\xi e^{iq\cdot\xi}\,\langle p,s|\, J_\mu(\xi)J_\nu(0)\,|p,s\rangle\,, \end{aligned} \tag{1.17}$$

by translational invariance. The opposite order $\langle p,s|\, J_\nu(0)J_\mu(\xi)\,|p,s\rangle$ involves $\delta^4(p_n - p + q)$. In the lab frame this requires $p_n^0 = M - \nu \leq M$, which is impossible since the proton is the lightest baryon and baryon number is conserved. Thus, we can introduce the current commutators

$$W_{\mu\nu}(p,q) = \int d^4\xi e^{iq\cdot\xi}\,\langle p,s|\,[J_\mu(\xi), J_\nu(0)]\,|p,s\rangle\,. \tag{1.18}$$

A similar calculation for the time ordered product yields ($\epsilon \to 0^+$):

$$\begin{aligned} T_{\mu\nu}(p,q) &= i\int d^4\xi e^{iq\cdot\xi}\,\langle p,s|\, T(J_\mu(\xi)J_\nu(0))\,|p,s\rangle \\ &= (2\pi)^3\sum_{n,\vec{p}_n}\left\{\frac{\delta^3(\vec{p}_n - \vec{p} - \vec{q})}{p_n^0 - p^0 - q^0 - i\epsilon}\,\langle p,s|\, J_\mu(0)\,|n\rangle\,\langle n|\, J_\nu(0)\,|p,s\rangle\right. \\ &\left. + \frac{\delta^3(\vec{p}_n - \vec{p} + \vec{q})}{p_n^0 - p^0 + q^0 - i\epsilon}\,\langle p,s|\, J_\nu(0)\,|n\rangle\,\langle n|\, J_\mu(0)\,|p,s\rangle\right\}. \end{aligned} \tag{1.19}$$

Using the Dirac formula $\frac{1}{x-i\epsilon} = \mathcal{P}\left(\frac{1}{x}\right) + i\pi\delta(x)$ we find that the imaginary part of the first term in Eq. (1.19) yields Eq. (1.17). The second term of Eq. (1.19) has no imaginary part, which can be shown by a similar

[1] Summation over final and average over initial electron spins.

kinematical argument used to introduce the commutator in Eq. (1.18). With this in mind we can write

$$W_{\mu\nu}(p,q) = \frac{1}{2\pi}\mathrm{Im}T_{\mu\nu}(p,q). \tag{1.20}$$

This equation is useful since a matrix element of the time ordered product is easier to calculate in any path integral formulation of a quantum field theory. Physically $T_{\mu\nu}$ can be seen as the Compton scattering amplitude and $\mathrm{Im}T_{\mu\nu}$ is its absorptive part.

Using current conservation, Lorentz covariance and parity invariance the general decomposition of the hadronic tensor can be

$$\begin{aligned} W_{\mu\nu}(p,q) = {} & MW_1(\nu,Q^2)\left(-g_{\mu\nu}+\frac{q_\mu q_\nu}{q^2}\right)+\frac{W_2(\nu,Q^2)}{M}\left(p_\mu-\frac{p\cdot q}{q^2}q_\mu\right)\left(p_\nu-\frac{p\cdot q}{q^2}q_\nu\right) \\ & + i\epsilon_{\mu\nu\lambda\sigma}q^\lambda\left\{MG_1(\nu,Q^2)s^\sigma+\frac{G_2(\nu,Q^2)}{M}((p\cdot q)s^\sigma-(q\cdot s)p^\sigma)\right\}, \end{aligned} \tag{1.21}$$

where W_1 and W_2 are the unpolarised form factors of the nucleon, G_1 and G_2 are the polarised form factors of the nucleon and s^σ is the nucleon spin. These functions only depend on Q^2 and ν, which are the only dynamical Lorentz scalars. Scalars like $p^2 = M^2$ are not dynamical.

1.6 Bjorken Scaling

In this section we will consider the symmetric part of the hadronic tensor

$$\begin{aligned} W^S_{\mu\nu} = {} & MW_1(\nu,Q^2)\left(-g_{\mu\nu}+\frac{q_m u q_\nu}{q^2}\right) \\ & + \frac{W_2(\nu,Q^2)}{M}\left(p_\mu-\frac{p\cdot q}{q^2}q_\mu\right)\left(p_\nu-\frac{p\cdot q}{q^2}q_\nu\right). \end{aligned} \tag{1.22}$$

Substituting this into Eq. (1.15) and using Eq. (1.16) yields

$$\frac{d^2\sigma}{d\Omega dE'} = \frac{\alpha^2}{4E^2}\frac{\cos^2\frac{\theta}{2}}{4\sin^4\frac{\theta}{2}}\left[2W_1\tan^2\left(\frac{\theta}{2}\right)+W_2\right]. \tag{1.23}$$

From this we see that the form factors W_1 and W_2 carry all the information on unpolarised inclusive cross-section $eN \to eX$.

Let the target nucleon (N) be a proton (p) and assume it to be made of point-like, spin-$\frac{1}{2}$ particles referred to as partons. Then at small wave-lengths (large Q^2) this point-charge proton behaves like a free Dirac particle. By contrasting this behaviour with that for the elastic electron-proton scattering $ep \to ep$, figure 1.2, one would expect the differential cross-section for the point-like proton to be that of the electron-muon ($e\mu \to e\mu$) cross-section, which in the muon rest (laboratory) frame is

$$\left(\frac{d\sigma}{d\Omega}\right)_{e\mu\to e\mu} = \frac{\alpha^2\cos^2\frac{\theta}{2}}{4E^2\sin^4\frac{\theta}{2}}\left[\frac{Q^2}{2M_\mu^2}\tan^2\frac{\theta}{2}+1\right]\frac{E'}{E}, \tag{1.24}$$

where

$$\frac{E'}{E} = \frac{1}{1+\frac{2E}{M_\mu}\sin^2\frac{\theta}{2}}. \tag{1.25}$$

It turns out that the differential cross-section is instead given by the Rosenbluth formula

$$\frac{d\sigma^{\text{elastic}}}{d\Omega} = \frac{\alpha^2}{4E^2}\frac{\cos^2\frac{\theta}{2}}{\sin^4\frac{\theta}{2}}\left[G_M^2\frac{Q^2}{2M^2}\tan^2\frac{\theta}{2}+\frac{G_E^2+G_M^2\frac{Q^2}{4M^2}}{1+\frac{Q^2}{4M^2}}\right]\frac{E'}{E}, \tag{1.26}$$

where

$$G_E = F_1 - \frac{Q^2}{4M^2}F_2 \quad \text{and} \quad G_M = F_1 + \kappa_p F_2, \tag{1.27}$$

are the electric and magnetic form factors, respectively that only depend on Q^2. The Lorentz invariant form factors are introduced as modifications of the proton matrix elements of the electromagnetic current to model

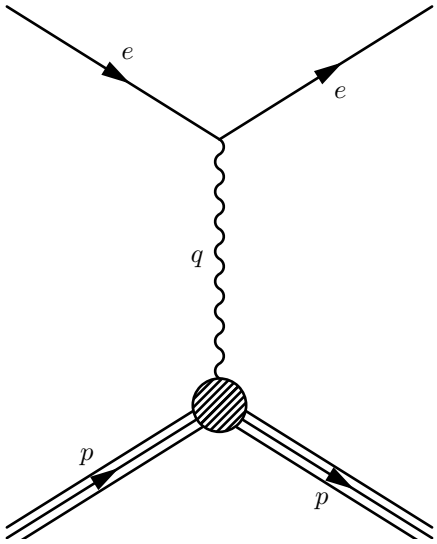

Figure 1.2: Feynman diagram of electron proton scattering

the structure of the proton

$$\langle p'|\, J_\mu(0)\,|p\rangle = \bar{u}(p')\left[\gamma_\mu F_1(q^2) + i\sigma_{\mu\nu}q^\nu \frac{\kappa_p}{2M_N}F_2(q^2)\right]u(p). \tag{1.28}$$

Here u is the free Dirac spinor for the proton and $\sigma_{\mu\nu} = \frac{i}{2}[\gamma_\mu, \gamma_\nu]$. Empirically these form factors are well approximated by the (double) dipole formula:

$$\frac{G_M}{\kappa_p} = G_E = \left(1 + \frac{Q^2}{0.7(\text{GeV})^2}\right)^{-2}. \tag{1.29}$$

Finally $\kappa_p = 2.79$ is the proton magnetic moment.

Let us, for the time being, approximate the hadronic tensor by restricting the sum in Eq. (1.17) to n =proton and compare the resulting differential cross-sections. Integrating over the final momenta reduces $\delta^4(p_n - p - q)$ in Eq. (1.17) to

$$\begin{aligned}\delta(E'_N - M - E + E') &= \delta(E'_N - M - \nu)\\ &= 2M\delta(2M' - 2ME'_N + 2M\nu)\\ &= 2M\delta(q^2 + 2M\nu)\end{aligned} \tag{1.30}$$

Then we identify

$$W_1^{\text{el}} = -\delta(2M\nu - Q^2)\frac{Q^2}{2M}G_M^2(Q^2) \tag{1.31}$$

$$W_2^{\text{el}} = \delta(2M\nu - Q^2)\frac{2M}{1 + \frac{Q^2}{4M^2}}\left[G_E^2(Q^2) + \frac{Q^2}{4M^2}G_M^2(Q^2)\right]. \tag{1.32}$$

For the case of a point-like nucleon we thus have

$$2W_1^{\text{point}} = \frac{Q^2}{2M}\delta\left(\nu - \frac{Q}{2M}\right) = \frac{Q^2}{2M\nu}\delta\left(1 - \frac{Q^2}{2M\nu}\right), \tag{1.33}$$

$$W_2^{\text{point}} = 2M\delta\left(\nu - \frac{Q^2}{2M}\right) = \frac{2M}{\nu}\delta\left(1 - \frac{Q^2}{2M\nu}\right). \tag{1.34}$$

1.6.1 Parton Model

At large Q^2, we can view the inelastic electron-proton scattering as an elastic system where the 'free' quarks within the proton are bombarded with electrons. Gluons are not affected since they do not have an electric

charge. The equations (1.33) and (1.34) reveal that the form factors depend only on the variable

$$x = \frac{Q^2}{2M\nu} \text{ with } 0 \leq x \leq 1. \tag{1.35}$$

In this case the form factors are called structure functions. This shows a well-known approximate scaling (Bjorken scaling) which states that, the structure function are constant at large Q^2 and ν with x held fixed.

This observation motivates the parton model. In this model the nucleon is viewed as a composite of point-like spin-$\frac{1}{2}$ fermions carrying momenta $P_x = xp$. Each of the partons (i) has a probability density $f_i(x)$ so that $\sum_i \int dx f_i(x) = 1$.

When Q and ν are large we may neglect the parton masses (if they are non-zero). Let $f_i(x)$ be the probability density to find parton i with momentum fraction x: $\int_0^1 dx f_i(x) = 1$. We then take that parton to have electric charge e_i; momentum xp and scatter elastically off the electron. This yields form factors as in (1.33) and (1.34) with appropriate substitutions. We then sum overall partons and integrate out the momenta weighted by the respective probability. This removes the δ-function factors in (1.33) and (1.34):

$$MW_1 = \sum_{i=1} e_i^2 f_i(x) = F_1(x), \tag{1.36}$$

$$\nu W_2 = 2\sum_{i=1} e_i^2 x f_i(x) = F_2(x). \tag{1.37}$$

Though the notation is confusing, the structure functions on the right-hand sides do not equal the nucleon form factors in Eq. (1.28). Not only does this parton model show that W_1 and νW_2 are only functions of the Bjorken scaling variable x, it also gives a relation between these two form factors:

$$F_2(x) = 2xF_1(x), \tag{1.38}$$

the so-called Callan-Gross relation. Its experimental verification proves that the electrically charged partons are indeed spin-$\frac{1}{2}$ Dirac particles. Assuming the contrary, that they are spinless, yields $F_1(x) = 0$.

Similar analysis for antisymmetric part of the hadronic tensor. Let $\delta f_i(x)$ be the difference of distributions with opposite spin orientation. The first unpolarised structure function is then given as

$$M^2\nu G_1(x) = \sum e_i^2 \delta f_i(x) =: g_1(x). \tag{1.39}$$

The second polarised structure function

$$M\nu G_2(x) =: g_2(x) \tag{1.40}$$

does not have a simple parton interpretation[14].

In the Bjorken limit (for x fixed and Q^2 large) the structure functions measure the momentum and spin distributions of the partons in the target nucleon and the hadronic tensor of Eq. (1.21) becomes

$$\begin{aligned} W_{\mu\nu}(p,q) = {} & F_1(x)\left(-g_{\mu\nu} + \frac{q_\mu q_\nu}{q^2}\right) + \frac{F_2(x)}{p\cdot q}\left(p_\mu - \frac{p\cdot q}{q^2}q_\nu\right)\left(p_\nu - \frac{p\cdot q}{q^2}q_\nu\right) \\ & + i\epsilon_{\mu\nu\lambda\sigma}\frac{q^\lambda M}{p\cdot q}\left\{g_1(x)s^\sigma + g_2(x)\left(s^\sigma - \frac{q\cdot s}{q\cdot p}p^\sigma\right)\right\}. \end{aligned} \tag{1.41}$$

1.7 Thesis Outline

The ultimate aim of this paper is to investigate the abnormal behavior of the sea contribution to the iso-singlet unpolarized nucleon structure function within the Nambu-Jona Lasinio (NJL) model with Pauli-Villars regularisation, as previously explored by I. Takyi[1, 2]. The abnormalities manifest in the structure function's behavior not aligning with experimental results; see Figure 1.3 for the simulated behavior and Ref.[15] for the expected sea contribution to the structure function.

To investigate this behavior in Chapter 2, we first introduce the NJL model Lagrangian. We then proceed to bosonize it to create an effective action and employ the Pauli-Villars regularisation scheme. The relevant constants in the model are confirmed to be related to physical values used in our simulations.

Following this, in Chapter 3, we introduce the hedgehog configuration, acting as the static chiral field for the NJL model soliton that describes the nucleon. We formulate the energy functional of the soliton and

provide a brief introduction to the diagonalization of the model's Hamiltonian to obtain quark wavefunctions and energy eigenvalues. We show how the equation of motion for our soliton emerges from extremizing the energy functional with respect to the chiral angle (a function determining the shape of the soliton). We use this equation of motion to simulate the structure of the soliton for a single baryon, gather information on the quark wavefunctions and energy eigenvalues using the Hartree-Fock method, and conclude the chapter by discussing the cranking corrections, necessary for creating quark wavefunctions with good spin and isospin quantum numbers. This correction is required since the solutions attained previously had zero grand spin [2] and, as a result, did not conserve spin and isospin.

Chapter 4 will focus on the derivation of the structure functions in the NJL model, particularly the iso-singlet unpolarized nucleon structure function. We begin by considering the derivation of the structure function for the pion, revealing a trick that we can then apply to derive the structure functions for the nucleon in the subsequent section. Lastly, an explanation of how the iso-singlet unpolarized nucleon structure function (IUSF) is simulated, will be provided.

Chapter 5 concerns the derivation and investigation of the energy sum rule and an investigation of the IUSF. During the simulations, it is found that, after a correction to a certain numerically calculated physical value Λ[3], the sum rule, which should hold independent of Λ, becomes incredibly inaccurate. After thorough investigation, a solution is found through an adjustment to the numerical parameters of the simulations. Lastly, an attempt is made to correct the abnormality of the structure function through the alteration of a subtraction introduced within the regularisation programme setting the energy scale.

Chapter 6 briefly summarises the project. Various technical aspects are collected in four appendices.

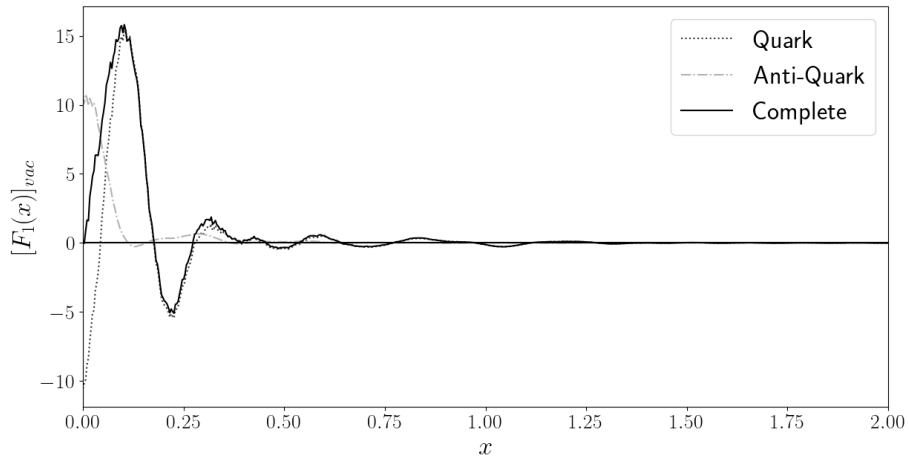

Figure 1.3: Sea contribution to the iso-singlet unpolarised structure function using the numerical values given from Ref.[1, 2].

[2] This is the sum of spin and isospin operators. Each quark energy level has a grand spin value. Grand spin will be explored further in chapter 3

[3] The Λ value is introduced during the regularisation of the model discussed in Chapter 2; it takes on a physical value when we tie the model to physical parameters.

CHAPTER 2

THE NJL MODEL

In this chapter we will first give a brief motivation as to why soliton models can be used in the large N_C limit of QCD. We then go on to describe the Nambu-Jona-Lasinio (NJL) model as an effective, chirally invariant theory with the two light flavour quarks (up and down). The main motivation to consider this model is that it allows us to derive an effective meson theory that has soliton solutions from a quark model via bosonisation. In turn this facilitates the computation of structure functions in a soliton model.

2.1 MOTIVATIONS FOR SOLITON MODELS IN THE LARGE N_C LIMIT

First we will briefly go over the ideas of soliton models as descriptions of baryons. We find that at low energies QCD becomes impossible to be treated perturbatively. As a result other methods have been introduced to get reliable results in this area. These results are based primarily on two considerations, these being that the number of colours N_C is large and that of the chiral symmetry of massless QCD and its spontaneous symmetry breaking.

First note that in QCD quarks have a single colour label, in this case there are N_C possible colour degrees of freedom, their interactions are mediated by gluons which are said to have two colour labels, one that couples to the spinor and another that couples to the conjugated-spinor. A result of this is that gluons have N_C^2 degrees of freedom. As QCD is gauge with a special unitary group turns this into $N_C^2 - 1$. However, for large N_C that subtraction is not relevant. We consider the combinatorics of Feynman diagrams and write gluons as a pair of a quark and anti-quark line of figure 2.1.

In the 1970's t'Hooft[12] and Witten[13] demonstrated that by making N_C large and generalising the QCD gauge group from SU(3) to SU(N_C), one can use $\frac{1}{N_C}$ as an implicit expansion parameter. The conclusions from this expansion are an essential motivation as to why we can consider soliton models for baryons.

For the gluon propagator having a finite limit for $N_C \to \infty$ we need to scale $g_{\text{QCD}} \sim \frac{1}{\sqrt{N_C}}$ by considering confinement with $N_C \to \infty$ and having $g^2 N_C$ fixed. This results in a limit that leaves only planar Feynman diagrams[12]. Non-planar Feynman diagrams and those with gluon handles are suppressed by a factor N_C^{-2}. Diagrams with quark loops are suppressed by a factor N_C^{-1}. To demonstrate this consider figures 2.2 and 2.3, they are planar and non-planar respectively.

For the combinatorial factor of the one gluon loop interaction in figure 2.2 we note that the colour index of the outer quark lines contracts with that of the initial and final states, which are specified once these states are known. The inner quark loop contracts with itself and its indices are not specified. This results in a factor N_C. The interaction contains two three-gluon vertices, each vertex contributes a factor g_{QCD} resulting in an overall factor of g_{QCD}^2. The total Feynman diagram has the total combinatorial factor of $g_{\text{QCD}}^2 N_C$. This, by definition, is of the order unity therefore is smooth when $N_C \to \infty$.

Now we take a look at the non-planar diagram 2.3. The tangled inner quark loop contributes a factor N_C to the diagram. The diagram has two three-gluon interaction vertices and two four-gluon interaction vertices,

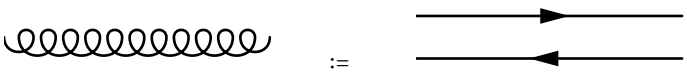

Figure 2.1: Gluon as a double-line fermion in a Feynman diagram

the resulting contributing factor being g_{QCD}^6. Consequently, the Feynman diagram has a total combinatoric factor of $N_C g_{\text{QCD}}^6 = \frac{1}{N_C^2}$ so in the limit $N_C \to \infty$ this diagram is suppressed.

2.1.1 An Effective Theory for QCD in the Large N_C Limit

Hadrons are colour singlet particles whose quantum numbers are determined by the flavour content of its constituent quarks. Hence, in the large N_C application to hadrons we consider colour singlet quark bilinears, examples of these are $\bar{q}\gamma^\mu q$ and $\bar{q}(i\partial_\mu - g_{\text{QCD}} A_\mu)q$ where A_μ is the gluon field. We denote such operators as $J(x)$. This requires considering Feynman diagrams in which these quark bilinears couple to gluon loops, an example of which is given in figure 2.4. This diagram is of the order $N_C^2 g_{\text{QCD}}^2 \sim N_C$ and is the leading order coupling to quark bilinears. In general leading order diagrams have the following properties[13]:

- They are planar diagrams (non-planar diagrams are suppressed in the large N_C limit),
- internal lines are only gluons,
- external lines, i.e. their edges, are only quark lines.

Intermediate states are defined by cutting through these mentioned diagrams using Cutkosky's rules. In the large N_C limit only planar diagrams contribute to the matrix elements of the quark bilinears. In this case, the colour indices along any cut combine into a single trace resulting to a single hadron (assuming the confinement hypothesis). For non-planar diagrams colour indices along any cut form separated saturated sums, resulting in the product of two or more colour singlet hadrons. Hence, for $N_C \to \infty$ all intermediate states are quark bilinear colour singlets i.e. one meson intermediate states.

Since intermediate states are one meson states, for large N_C we can decompose the quark bilinear operator as

$$\langle J(x)J(y)\rangle = \int \frac{d^4k}{(4\pi)^4} e^{ik(x-y)} \sum_j \frac{a_j(k)a_j^\dagger(k)}{k^2 - m_j^2} \tag{2.1}$$

the sum of all meson states that couple to $J(x)$ and $a_j = \langle 0|\, J\, |j\rangle$ is the matrix element of J to create the j^{th} (with mass m_j) meson from the vacuum. Using the properties of the planar diagrams mentioned above a few observations can be made from Eq. (2.1).

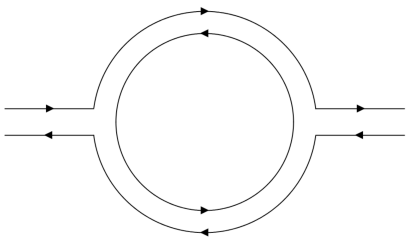

Figure 2.2: A planar Feynman diagram of a gluon interaction

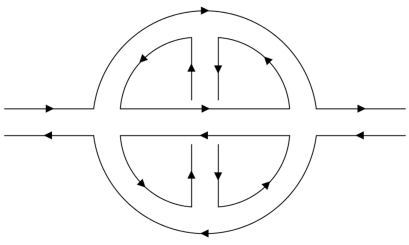

Figure 2.3: A non-planar Feynman diagram of a gluon interaction

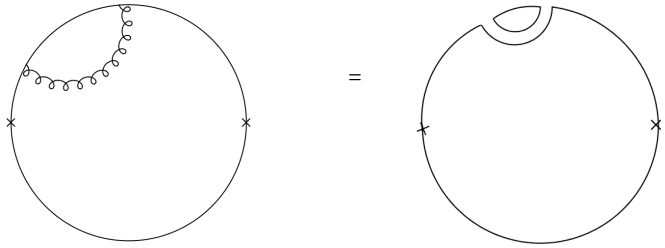

Figure 2.4: Gluon as a double-line fermion in a Feynman diagram

- We note that the left-hand side of the equation has a smooth limit for $N_C \to \infty$ while the right-hand side is the sum of all the planar diagrams. Hence, $m_j \sim \mathcal{O}(N_C^0)$.
- Due to the asymptotic freedom of QCD, (2.1) must by logarithmically divergent for large k^2 so it must contain an infinite number of meson states. Eq. (2.1) formally is a spectral representation. Hence, m_j must be real, so the mesons are stable.
- Since the diagrams under consideration are planar, with one of their properties being that they are of the order N_C, the right-hand side of Eq. (2.1) must be as well. Hence, the meson amplitude is of the order $\sqrt{N_C}$.

Accordingly, any interaction of n mesons is described by a product of n such operators and their vertex functions. This interaction must be of the order N_C i.e.

$$N_C \sim \langle 0|\, J\, |j_1\rangle \cdots \langle 0|\, J\, |j_n\rangle \Rightarrow N_C \sim N_C^{\frac{n}{2}} \Gamma^{(n)}_{j_1,\ldots,j_n} \tag{2.2}$$

where $\Gamma^{(n)}_{j_1,\ldots,j_n}$ is the vertex function for the interaction of n mesons. Therefore, the coupling constant of the interaction is of the order

$$\Gamma^{(n)}_{j_1,\ldots,j_n} = \mathcal{O}(N_C^{1-\frac{n}{2}}) \tag{2.3}$$

In particular the four meson vertex decreases like $\frac{1}{N_C}$. The above results lead to the conjecture that in the large N_C limit, QCD is equivalent to a theory of (infinitely many) interacting mesons(and glueballs) with meson loops and coupling constants being suppressed as N_C becomes large. The latter property means that the mesons interact weakly with $\frac{1}{N_C}$ being the effective coupling.

2.1.2 Baryon Properties in the Large N_C Limit

Baryons are totally antisymmetric colour singlets made of N_C quarks. Upon a quick evaluation the combinatorial factor for Feynman diagrams of baryons with m gluon exchanges between interior quarks is $g_{\text{QCD}}^{2m} \frac{1}{m!}[N_C(N_C-1)]^m$.[1] These diagrams clearly diverge as N_C becomes large, this makes it quite inconvenient to study baryons in the large N_C limit using Feynman diagrams.

For the reason above we will now use classical many body theory to describe the properties of baryons. To do this we assume that the N_C quarks bound to the baryon are heavy and do not experience relativistic effects[13]. We use the Hartree-Fock approximation in treating the non-relativistic many body problem by assuming the quark interaction to be small. This is acceptable since when one quark interacts with another the strength is proportional to $\frac{1}{N_C}$ and the mean field is of the order one. This result in the Hamiltonian is

$$H = N_C M + \sum_{i=1}^{N_C} \frac{-\vec{\partial}^2}{2M} - \frac{g^2}{M} \sum_{i>j}^{N_C} \frac{1}{|\vec{r}_i - \vec{r}_j|}, \tag{2.4}$$

where M is the quark mass and $g = \sqrt{N_C} g_{\text{QCD}}$ is of the order unity. The construction of the ground state wave function requires to place each quark in the ground state of the mean field potential. With this reasoning

[1] The g_{QCD}^2 factor is a result of each gluon creating two vertices. The other factor is obtained from each gluon having $[N_C(N_C-1)]$ possible connections amongst the N_C quarks, the division by $m!$ is necessary since gluons are not distinguishable from one another.

we write the many body wave function $\Psi(r_1,\ldots,r_{N_C})$ as the product of the normalised one-particle quark wave functions $\phi(r_i)$.

$$\Psi(r_1,\ldots,r_{N_C}) = \prod_{i=1}^{N_C}\phi(\vec{r}_i). \tag{2.5}$$

Here the antisymmetrisation from the colour degress of freedom is not made explicit. To determine ϕ, we write the total energy $E = N_C\epsilon$ where ϵ is the energy of an individual quark. Applying the variational principle to

$$\begin{aligned}\langle\Psi|\, H - E\,|\Psi\rangle = &- N_C\epsilon + N_C M + \frac{N_C}{M}\int d^3r\vec{\partial}\phi^*(\vec{r})\cdot\vec{\partial}\phi(\vec{r}) \\ &- \frac{N_C(N_C-1)}{2}\frac{g^2}{N_C}\int d^3r_1\int d^3r_2\frac{|\phi(\vec{r}_i)|^2\,|\phi(\vec{r}_2)|}{|\vec{r}_1-\vec{r}_2|}\end{aligned} \tag{2.6}$$

and taking $N_C\to\infty$, yields the one particle eigenvalue equation

$$-\frac{\vec{\partial}^2}{2M}\phi(\vec{r}_1) - g^2\phi(\vec{r}_1)\int d^3r_2\frac{|\phi(\vec{r}_2)|^2}{|\vec{r}_1-\vec{r}_2|} - \epsilon\phi(\vec{r}_1) = 0. \tag{2.7}$$

The N_C from (2.6) has been factored out in Eq. (2.7) showing that both the wavefunction ϕ and its energy ϵ are of the order unity. There are two results that are deduced from this study, firstly the baryon mass is then of the order $\mathcal{O}(N_C)$, additionally the baryon radius

$$|r^2| = \frac{1}{N_C}\langle\Psi|\sum_i r_i^2\,|\Psi\rangle \tag{2.8}$$

is of the order unity $\mathcal{O}(N_C^0)$. A bit later we will see that soliton models also predict similar dependencies on the effective coupling.

Our next aim is to investigate both baryon-baryon and baryon-meson scattering. In our baryon-baryon scattering picture we find that our Feynman diagrams for a single gluon exchange between the two baryons have a combinatoric factor proportional to $N_C^2 g_{\rm QCD}^2 = {N_C}^2$[2]. Hence the Feynman diagram is not smooth in the large N_C limit. We will again consider it as a many body problem in the non-relativistic framework. To do this we consider the $2N_C$ quarks to be heavy and using the Hartree approximation. Within a baryon-baryon interaction the baryons will either repel or attract one another, as a result we will make use of the time dependent Schrödinger equation for the $2N_C$ quarks. Since there are only N_C colours and $2N_C$ quarks the Pauli exclusion principle forbids us from considering a single space-spin wave function. We instead consider time dependent normalised space spin wave functions $\phi_i(\vec{r},t)$, $i=1,2$ one for each of the quarks in the $2N_C$ quark system. Our many body wave function can then be defined as

$$\Psi(\vec{r}_1,\ldots,\vec{r}_{2N_C}) = \sum_p(-1)^p\prod_{i=1}^{N_C}\phi_1(\vec{r}_i,t)\prod_{j=1}^{N_C}\phi_2(\vec{r}_{N_C+j},t). \tag{2.9}$$

This wavefunction is antisymmetrised between the quarks from the two baryons. We apply the time dependent variational principle, i.e. $\langle\Psi|\, H-E\,|\Psi\rangle$ to determine the normalised wave functions ϕ_i. We consequently obtain the variational equation[13]

$$\begin{aligned}&g^2\phi_1(\vec{r}_1,t)\int d^3r_2\frac{|\phi_1(\vec{r}_2,t)|^2}{|\vec{r}_1-\vec{r}_2|} + g^2\phi_2(\vec{r}_1,t)\int d^3r_2\frac{\phi_2(\vec{r}_2,t)\phi_1(\vec{r}_2,t)}{|\vec{r}_1-\vec{r}_2|} + \frac{\vec{\partial}^2}{2M}\phi_1(\vec{r}_1,t) \\ &+ i\frac{\partial}{\partial t}\phi_1(\vec{r}_1,t) = 0\end{aligned} \tag{2.10}$$

for ϕ_1. A similar equation exists for ϕ_2. This shows that the scattering wave function is smooth in the large N_C limit and so is the scattering amplitude.

For meson-baryon scattering we find the Feynman diagram to be $\mathcal{O}(N_C^0)$, so in the large N_C picture it should be smooth. We shall, however, again work in the many body regime. In order to do so we first note that there are N_C+1 quarks and one anti-quark. Since the baryon can be considered to have infinite mass in the large N_C limit as it contains N_C quarks, the problem can then by interpreted as a meson scattering off a baryon. The baryon will again be written is a product of single quark wave functions $\phi(\vec{r}_i,t)$. The meson will be written as one wave function $u(\vec{r},\vec{y},t)$, where $\vec{r}$ is the position of the quark and $\vec{y}$ is the position of

[2] N_C^2 is from the number of choices for each of the two gluon vertices in a single gluon exchange between the baryons

the anti-quark. Hence we write the many body wave function as

$$\Psi(\vec{r}_1,\ldots,\vec{r}_2,\vec{r},\vec{y},t) = \sum_p (-1)^P \prod_{i=1}^{N_C} [\phi_i(\vec{r}_i,t)] u(\vec{r},\vec{y},t). \tag{2.11}$$

Applying the time dependent variational principle results in a wave equation without factors of N_C

$$\begin{aligned} i\frac{\partial}{\partial t}u(\vec{r},\vec{y},t) &= \frac{1}{2M}(\vec{\partial}_r^2 + \vec{\partial}_y^2)u(\vec{r},\vec{y},t) - g^2\frac{u(\vec{r},\vec{y},t)}{|\vec{r}-\vec{y}|} \\ &\quad - g^2\phi(\vec{r})\int d^3z\phi^*(\vec{z},t)u(\vec{z},\vec{y},t)\Big[\frac{1}{|z-r|}+\frac{1}{|z-y|}\Big]. \end{aligned} \tag{2.12}$$

This equation shows the meson wave equation is $\mathcal{O}(N_C^0)$, and we conclude that the meson-baryon scattering amplitude is smooth as well.

2.1.3 Baryons as Solitons

Solitons (more precisely solitary waves) are solutions in non-linear field theory with localised energy densities. This allows a particle interpretation.

In the previous section we had shown that at large N_C QCD can be regarded as a weakly coupled meson field theory. We will now find a effective coupling constant g_{eff} that defines these interactions. By considering meson-meson scattering we find that

$$g_{\text{eff}} = \Gamma^2 \propto \frac{1}{N_C} \tag{2.13}$$

where Γ^2 is a four point vertex for two interacting mesons. From this identification we found that the mass of the baryon is $M_B = \frac{1}{g_{\text{eff}}}$ and the amplitude of the meson-baryon scattering as well as the baryon radii are $\mathcal{O}(g_{\text{eff}}^0)$. This leads to the conjecture that baryons emerge as soliton solutions in the large N_C limit[13].

We will now verify this with a typical example of a soliton, the kink soliton in the ϕ^4 field theory in one space and one time dimensions. The Lagrange density for this model is

$$\mathcal{L} = \frac{1}{2}[(\partial_t\phi)^2 - (\partial_x\phi)^2] - \frac{\lambda}{4}(\phi^2 - \frac{m^2}{\lambda})^2 \tag{2.14}$$

where m is a real constant. Obviously λ is the (classical) four point vertex coupling constant. The classical equation of motion shows that the Lagrangian has two degenerate stable vacuum solutions $\phi_{\text{vac}} = \pm\frac{m}{\sqrt{\lambda}}$. There are two stationary solutions

$$\phi_\pm(x) = \pm\frac{m}{\sqrt{\lambda}}\tanh(\frac{m}{\sqrt{\lambda}}x) \tag{2.15}$$

that connect these vacua. Here ϕ_+ is the kink soliton while ϕ_- function is the anti-kink.

Then classically, for static configurations we obtain the energy functional as

$$E[\phi] = -\int_{-\infty}^{\infty} dx\mathcal{L} = \int_{-\infty}^{\infty} dx\Big\{\frac{1}{2}(\partial_x\phi_+)^2 + (\phi_+^2 - \frac{m^2}{\lambda})^2\Big\} = \frac{2\sqrt{2}}{3}\frac{m^3}{\lambda} = \mathcal{O}(\frac{1}{g_{\text{eff}}}), \tag{2.16}$$

which satisfies the first property of the soliton solutions, namely that for the mass. The expectation value of $|x^2|$ with respect to the energy density is the radius

$$|x^2| = \frac{1}{E}\int_{-\infty}^{\infty} x^2\mathcal{L} = -\frac{1}{m}(1-\frac{\pi^2}{6}) = \mathcal{O}(g_{\text{eff}}^0). \tag{2.17}$$

This is again consistent with our previous calculation. To confirm the similarities for meson-baryon scattering we introduce fluctuations $\phi(x,t) = \phi_+(x) + \eta(x,t)$. These fluctuations describe the meson field in the background of the kink. For linear terms of these fluctuations, the equation of motions is

$$\begin{aligned} 0 &= \frac{\partial^2\eta}{\partial t^2} - \frac{\partial^2\eta}{\partial x^2} - m^2 + 3\lambda\phi_+^2(x)\eta(x,t) \\ &= \frac{\partial^2\eta}{\partial t^2} - \frac{\partial^2\eta}{\partial x^2} - m^2 + 3m^2\tanh(\frac{m}{\sqrt{2}x})\eta(x,t). \end{aligned} \tag{2.18}$$

This is the kink analog of Eq. (2.12). We can see that the coupling does not appear in this equation. Hence, the scattering data obtained are $\mathcal{O}(g_{\text{eff}}^0)$. From this we can conclude that the ϕ^4 soliton matches the features of baryons in the large N_C limit of QCD.

2.2 The NJL Model Lagrangian

The NJL model was first introduced in Ref.[16] to investigate the dynamical breaking of chiral symmetry. In this investigation we will only consider the simplest $SU(2)$ version limited to just the two up and down quark flavours. The model is defined by the Lagrangian

$$\mathcal{L}_{\text{NJL}} = \bar{q}(i\partial\!\!\!/ - m_0)q + \frac{G}{2}[(\bar{q}q)^2 + (\bar{q}\vec{\tau}i\gamma_5 q)^2], \tag{2.19}$$

which can be written as the sum $\mathcal{L}_{\text{NJL}} = \mathcal{L}_{\text{free}} + \mathcal{L}_{\text{int}}$

$$\mathcal{L}_{\text{free}} = \bar{q}(i\partial\!\!\!/ - m_0)q \tag{2.20}$$

$$\mathcal{L}_{\text{int}} = \frac{G}{2}\left[(\bar{q}q)^2 + (\bar{q}\vec{\tau}i\gamma_5 q)^2\right] \tag{2.21}$$

of the free and interaction pieces. The Lagrangian contains a local four-fermion (quark) interaction via a chiraly symmetric contribution of scalar and pseudoscalar components. The quark field is demarcated through discrete labels $q = q_{\alpha i\nu}(x)$; where $\alpha = 1,2,3,4$ are the Dirac components, $i = u,d$ stands for the two flavours and $\nu = 1,2,\ldots,N_C$ is the colour label. The Dirac matrices γ_μ in $\partial\!\!\!/ = \gamma_\mu\partial^\mu$ act on α, while the Pauli matrices $\vec{\tau} = (\tau_1,\tau_2,\tau_3)$ are in isospace and act on i. The quark interaction can be thought of as originating from integrating out the gluons (at the expense of losing confinement). Then there is no further colour interaction, and we merely obtain factors of N_C when summing over ν. We neglect isospin breaking by setting $m_0 = m_u^0 = m_d^0$. These mass parameters will later be fitted to empirical hadron data, as will the coupling constant G.

The Lagrangian has the following properties:

- The Lagrangian (2.19) is symmetric under the global $U(1)$ transformation

  $$q(x) \to \exp(i\theta)q(x) \tag{2.22}$$

  where θ is a real constant. This symmetry leads to the conserved baryon number.

- Assuming isospin symmetry, the Lagrangian is invariant under the global isospin rotation

  $$q(x) \to \exp(i\frac{1}{2}\vec{\epsilon}\cdot\vec{\tau})q(x) \tag{2.23}$$

  where $\vec{\epsilon}$ is a real constant vector that characterises the transformation. Noether's theorem then implies conservation of the isovector current $\vec{V}_\mu = \bar{q}\gamma_\mu\frac{\vec{\tau}}{2}q$.

- Additionally, if $m_0 = 0$ the Lagrangian is invariant under the global axial-chiral rotation

  $$q(x) \to \exp(i\frac{1}{2}\gamma_5\vec{\epsilon}'\cdot\vec{\tau})q(x). \tag{2.24}$$

  This leads to the concept of the partially conserved axial vector current (PCAC). Partial conservation relates to the fact that $m_0 \neq 0$ in the real world. The current is $\vec{A}_\mu = \bar{q}\gamma_\mu\gamma_5\frac{\vec{\tau}}{2}q$.

- There is also the symmetry

  $$q(x) \to \exp(i\epsilon\frac{\gamma_5}{2})q(x) \tag{2.25}$$

  on the classical level. Once photon fields are added by minimal substitutions this symmetry is broken at the one-loop quantum level. This is the axial anomaly[17, 18]. On the experimental side this anomaly manifests itself through the decay of the electrically neutral pion into two photons.

These continuous symmetries give rise to the following Noether's currents

$$B_\mu = \bar{q}\gamma_u q \quad \text{(baryon current)}, \tag{2.26}$$

$$\vec{V}_\mu = \bar{q}\gamma_\mu \frac{\vec{\tau}}{2} q \quad \text{(vector current)}, \tag{2.27}$$

$$\vec{A}_\mu = \bar{q}\gamma_\mu\gamma_5 \frac{\vec{\tau}}{2} q \quad \text{(axial vector current)} \tag{2.28}$$

with divergences:

$$\partial_\mu B^\mu = 0 \tag{2.29}$$

$$\partial_\mu \vec{V}^\mu = i\bar{q}[m_0, \frac{\vec{\tau}}{2}]q \tag{2.30}$$

$$\partial_\mu \vec{A}^\mu = i\bar{q}\{m_0, \frac{\vec{\tau}}{2}\}q. \tag{2.31}$$

The commutator and anti-commutator above act on the flavour indices of the quark fields.

Looking at the isospin and axial transformations infinitesimally Eq.(2.23) and (2.24) we see that

$$\begin{aligned} q &\to (1 + i\vec{\epsilon}\cdot\vec{\tau} + i\vec{\epsilon'}\cdot\vec{\tau}\gamma_5)q + \cdots \\ &\to (1 + i(\vec{\epsilon}+\vec{\epsilon}')\cdot\vec{\tau}P_R + i(\vec{\epsilon}-\vec{\epsilon}')\cdot\vec{\tau}P_L)q + \cdots. \end{aligned} \tag{2.32}$$

Hence,

$$q_R \to (1 + i(\vec{\epsilon}+\vec{\epsilon}')\cdot\vec{\tau})q_R + \cdots \tag{2.33}$$

and

$$q_L \to (1 + i(\vec{\epsilon}-\vec{\epsilon}')\cdot\vec{\tau})q_L + \cdots. \tag{2.34}$$

From this we can see that the NJL Lagrangian (2.19) has the

$$\mathrm{SU}(2)_R \otimes \mathrm{SU}(2)_L \otimes \mathrm{U}(1) \tag{2.35}$$

chiral symmetry in the limit of $m_0 \to 0$. This is the same as in QCD.

For $m_0 \neq 0$ the mass term

$$\mathcal{L}_{\text{mass}} = -(\bar{q}_R m_0 q_L + \bar{q}_L m_0 q_R) \tag{2.36}$$

couples the left and right-handed fields. This breaks chiral symmetry, however since $m_0 \ll \lambda_{\text{QCD}}$ it is considered a good approximation to take $m_0 \approx 0$, at least within up-down flavour space.

2.3 Bosonisation

We will now use a technique called bosonisation to derive an effective meson theory from the NJL model, Eq (2.19). First we replace the four quark interaction Lagrangian by terms quadratic in quark bilinears[19–22]. We rewrite Eq. (2.21) as:

$$\mathcal{L}_{\text{int}} = 2G(\bar{q}\Lambda_\alpha q)^2, \tag{2.37}$$

where

$$\Lambda_\alpha = \mathbf{1}_c \otimes \left(\frac{\vec{\tau}}{2}\right) \otimes \Gamma_\alpha,\ \Gamma_\alpha \in \{1, i\gamma_5\} \tag{2.38}$$

is a tensor product of colour, flavor and Dirac matrices.

Note that the functional integral [3]

$$\begin{aligned} &\int \mathcal{D}\Phi_\alpha \exp(-\frac{i}{8G}\int d^4x \Phi_\alpha^2) = \int \mathcal{D}\Phi_\alpha \exp\big(-\frac{i}{8G}\int d^4x[\Phi_\alpha + 4G\bar{q}\Lambda_\alpha q]^2\big) \\ &= \int \mathcal{D}\Phi_\alpha \exp(-\frac{i}{8G}\int d^4x(\Phi_\alpha^2 + 8G\bar{q}\Lambda_\alpha q\Phi_\alpha) - i\int d^4x\mathcal{L}_{\text{int}}) \end{aligned} \tag{2.39}$$

is just a number that does not depend on $\bar{q}\Lambda_\alpha q$ since we introduced it by shifting the integration variable.

[3] The explicit form of the integration measure is $\Pi_\alpha \mathcal{D}\phi_\alpha$ while the exponential is $\sum_\alpha \phi_\alpha^2$.

Hence, we can write the vacuum-to-vacuum transition amplitude (VVTA) for the NJL model as

$$\begin{aligned}\mathcal{Z}_{\text{NJL}} &\sim \int \mathcal{D}\Phi_\alpha e^{-\frac{i}{8G}\int d^4x\Phi_\alpha^2} \int \mathcal{D}q\mathcal{D}\bar{q}e^{\int d^4x(\mathcal{L}_{\text{free}}+\mathcal{L}_{\text{int}})} \\ &= \int \mathcal{D}\Phi_\alpha\mathcal{D}q\mathcal{D}\bar{q}e^{i\int d^4x(\mathcal{L}_{\text{free}}-\frac{1}{8G}(\Phi_\alpha^2+8G\bar{q}\Lambda_\alpha q\Phi_\alpha))} \\ &= \int \mathcal{D}\Phi_\alpha e^{-\frac{i}{8G}\int d^4\Phi_\alpha^2} \int \mathcal{D}q\mathcal{D}\bar{q}e^{i\int d^4x\bar{q}(i\partial\!\!\!/-m_0-\Lambda_\alpha\Phi_\alpha)q} \\ &= \int \mathcal{D}\Phi_\alpha e^{-\frac{i}{8G}\int d^4x(\Phi_\alpha-m_0)^2}\det[i\partial\!\!\!/-\Lambda_\alpha\Phi_\alpha],\end{aligned} \tag{2.40}$$

where, in the last step, we shifted the scalar singlet component of Φ_α by the mass matrix. By writing the interaction as the square of a quark bilinear we reduced the VVTA to an integral over quark bilinears whose functional integral is standard. We note that overall factors, pure numbers are irrelevant for $\ln\mathcal{Z}_{\text{NJL}}$. The result is a functional integral over the boson field $\phi=\Lambda_\alpha\Phi_\alpha$ and defines the effective meson action[4]

$$\begin{aligned}\mathcal{A}_{\text{NJL}}[\phi] &= \frac{-1}{8G}\int d^4x\phi^2 - i\ln\text{Det}[i\partial\!\!\!/-\phi] \\ &= \frac{-1}{8G}\int d^4\phi^2 - i\text{Tr}\ln[i\partial\!\!\!/-\phi]\end{aligned} \tag{2.41}$$

The VVTA can then be expressed as

$$\mathcal{Z}_{\text{NJL}} = \int \mathcal{D}\phi e^{i\mathcal{A}_{\text{NJL}}[\phi]}. \tag{2.42}$$

To analyse the particle content we decompose the boson field ϕ into two irreducible Lorentz components:

$$\phi = S + i\gamma_5 P. \tag{2.43}$$

Here S and P are scalar and pseudo-scalar fields, respectively. They are Hermitian matrices in flavour space:

$$S = S_0\boldsymbol{I} + \frac{1}{2}\vec{S}\cdot\vec{\tau}, \quad \text{and} \quad P = P_0\boldsymbol{I} + \frac{1}{2}\vec{P}\cdot\vec{\tau}. \tag{2.44}$$

It is also customary to introduce a single multiplet $M = S + iP$ and $M^\dagger = S - iP$, so that

$$\phi = \frac{1}{2}\left(M+M^\dagger\right) + \frac{1}{2}\gamma_5\left(M-M^\dagger\right) = P_R M + P_L M^\dagger. \tag{2.45}$$

Then the tra can be written as

$$\begin{aligned}Z_{NJL} &= \int \mathcal{D}\phi\exp\left(i\mathcal{A}[M,M^\dagger]\right) \text{ with} \\ \mathcal{A}[M,M^\dagger] &= -\frac{1}{4G}\int d^4x\text{tr}[MM^\dagger - m_0(M+M^\dagger)] - iN_C\text{Tr}_\Lambda\log iD,\end{aligned} \tag{2.46}$$

being the effective mesonic action. The trace "tr" is over flavour space and the functional trace is $\text{Tr}_\Lambda = \int_\Lambda d^4x\text{tr}$. This theory is ultraviolet divergent and thus requires regularisation. This is indicated by the subscript Λ on the integral. Since the model is not renormalisable the cut-off will acquire a physical meaning, i.e. Λ is an additional model parameter.

We now describe the details of this regularisation. There are many scenarios, like a sharp cut-off for three or four momenta, or Schwinger proper time, to name two popular ones. However, we will employ a version of the Pauli-Villars scheme since it does not require analytic continuation to Euclidean space[23]. In fact that will allow us to extract the absorptive parts of correlation functions via Cutkosky's rule. In Eq. (2.46) the Dirac operator is expanded as

$$iD = i\partial\!\!\!/ - (MP_R + M^\dagger P_L) = i\partial\!\!\!/ - (S + i\gamma_5 P). \tag{2.47}$$

We also introduce

$$iD_5 = -i\partial\!\!\!/ - (S - i\gamma_5 P) = -i\partial\!\!\!/ - \left(MP_L + M^\dagger P_R\right). \tag{2.48}$$

This operator is obtained from iD by performing a Wick rotation ($\partial_t \to i\partial_t, \beta\to i\beta, \partial^i\to\partial_i$ and $\gamma^i\to-\gamma^i$) to iD_E. From there we take $iD_E^\dagger$ and rotate it back to Minkowski space. As we will see in the following equations the operator iD_5 is relevant only for the purpose of regularisation. With this in mind we can write

[4] We use uppercase 'Det' and 'Tr' for continuous variables and lowercase 'det' and 'tr' for discrete ones.

the effective action as [24, 25]

$$\mathcal{A}\left[M, M^\dagger\right] = \mathcal{A}_R + \mathcal{A}_I + \mathcal{A}_m \tag{2.49}$$

with

$$\mathcal{A}_{\mathrm{R}} = -i\frac{N_c}{2}\sum_{i=0}^{2} c_i \mathrm{Tr}\log\left[-DD_5 + \Lambda_i^2 - i\epsilon\right], \tag{2.50}$$

$$\mathcal{A}_{\mathrm{I}} = -i\frac{N_c}{2}\mathrm{Tr}\log\left[-D(D_5)^{-1} - i\epsilon\right], \tag{2.51}$$

$$\mathcal{A}_{\mathrm{m}} = \frac{1}{4G}\int d^4x \mathrm{tr}\left[m_0\left[M + M^\dagger\right] - MM^\dagger\right]. \tag{2.52}$$

The subscript "R" and "I" have been attached because in Euclidean space $\mathcal{A}_{\mathrm{R}}$ and $\mathcal{A}_{\mathrm{I}}$ would be real and imaginary, respectively. The real part $\mathcal{A}_R$ turns out to be ultraviolet divergent. To cancel all ultraviolet divergences the Pauli-Villars scheme imposes the conditions[26]

$$c_0 = 1, \qquad \Lambda_0 = 0, \qquad \sum_{i=0}^{2} c_i = 0 \qquad \text{and} \qquad \sum_{i=0}^{2} c_i\Lambda_i^2 = 0. \tag{2.53}$$

To reduce the number of model parameters we always take $\Lambda_1 \to \Lambda_2 = \Lambda$. This enables us to eliminate the coefficients c_i using the identity (see Appendix B) [27]

$$\lim_{\Lambda_1\to\Lambda_2 = \Lambda}\sum_{i=0}^{2} c_i g(\Lambda_i^2) = g(0) - g(\Lambda^2) + \Lambda^2\frac{\partial g(\Lambda^2)}{\partial\Lambda^2}, \tag{2.54}$$

for any function $g(\Lambda^2)$. The imaginary part $\mathcal{A}_{\mathrm{I}}$ is conditionally convergent, by imposing a principal value description for the integration over the time coordinate. This does not imply it should not be regularised. Later we will observe that the baryon number current originates from $\mathcal{A}_{\mathrm{I}}$. In order to maintain integer baryon number we are, however forced to leave $\mathcal{A}_{\mathrm{I}}$ unregularised[19, 28].

2.4 Relating the Cutoff to Physical Values

We have explained the unique role of the pion in the strong interaction as the (would-be) Goldstone boson associated with the breaking of chiral symmetry in QCD. The non-zero vacuum expectation value is the (scalar) quark condensate and thus this Goldstone boson must be pseudo-scalar. We will now see that these features are also incorporated in the NJL model; moreover, we will employ pion properties to determine the model parameters.

First, we need to show that there is a non-zero scalar quark condensate; $\langle\bar{q}q\rangle \neq 0$. After bosonisation this amounts to a non-trivial solution for the scalar $\langle S\rangle \neq 0$. For symmetry reasons, this matrix vacuum expectation value should be proportional to the unit matrix. We therefore write $\langle S\rangle = mI$. Similarly, the vacuum expectation values of the pseudoscalar (matrix) field vanishes $\langle P\rangle = 0$. The field equation for constant S (or m) then reads.

$$\frac{1}{2G}[m_0 - m] = -i4N_C m\sum_{i=0}^{2} c_i\int\frac{d^4k}{(2\pi)^4}\left[-k^2 + m^2 + \Lambda_i^2 - i\epsilon\right]^{-1} \tag{2.55}$$

Adopting the single cut-off prescription, (2.54), we get

$$-i4N_C m\sum_{i=0}^{2} c_i\int\frac{d^4k}{(2\pi)^4}\left[-k^2 + m^2 + \Lambda_i^2 - i\epsilon\right]^{-1} \to \frac{mN_C}{4\pi^2}\left[\Lambda^2 - m^2\log\left(1 + \frac{\Lambda^2}{m^2}\right)\right]. \tag{2.56}$$

We see that by substituting $m \neq 0$ into the Dirac operator (2.47), that m plays the role of a mass parameter. It is therefore called the constituent quark mass; in contrast to the current quark mass m_0. The non-zero value of $\langle S\rangle$ in the vacuum sector signals the dynamical breaking of chiral symmetry with the quark condensate of the corresponding order parameter. This spontaneous symmetry breaking suggests pseudoscalar meson fields to be Goldstone bosons. As a result we will see below that physical mesons (pions) emerge as low-lying quark-antiquark excitations of the translationally invariant vacuum field configuration $\langle S\rangle = mI$.

We now turn to the discussion of pion properties. To introduce the isovector pion field $\vec{\pi}$, we adopt the

non-linear relation

$$M = mU \quad \text{with} \quad U = \exp(i\frac{g}{m}\vec{\pi}\cdot\vec{\tau}). \tag{2.57}$$

Here U is the chiral field. The exponential function contains the constituent quark mass for dimensional reasons. The role of the dimensionless coupling constant g will become clear soon. In contrast to the pseudo scalar field P, it has a well-defined global chiral transformation

$$U \to LUR^{\dagger}, \tag{2.58}$$

where L and R are representations of the unitary transformation associated with the left and right-handed charges discussed earlier.

We then expand the action to quadratic order in the pion field $\vec{\pi}$. Expanding the chiral field we get

$$U = 1 + i\frac{g}{m}\vec{\pi}\cdot\vec{\tau} - \frac{g^2}{2m^2}\vec{\pi}^2 + \cdots. \tag{2.59}$$

The mesonic part of the action expands as

$$\mathcal{A}_m = \frac{1}{2G}\int d^4x\left(m^2 + 2mm_0 - \frac{m_0}{m}g^2\vec{\pi}^2\right) + \mathcal{O}\left(\vec{\pi}^4\right). \tag{2.60}$$

We introduce the Fourier transform

$$\tilde{\phi}(q) = \int d^4x\phi(x)e^{iqx} \tag{2.61}$$

or

$$\phi(x) = \int \frac{d^4q}{(2\pi)^4}\tilde{\phi}(q)e^{-iqx}. \tag{2.62}$$

So the bilinear term of the mesonic action $\mathcal{A}_m$ is given by[20, 29]

$$\mathcal{A}_m^{(2)} = \frac{g^2}{2G}\frac{m_0}{m}\int \frac{d^4q}{(2\pi)^4}\vec{\pi}(q)\cdot\vec{\pi}(-q), \tag{2.63}$$

where the Fourier transformed $\vec{\pi}(q)$ is indicated by its argument.

For the non-local term we first expand $-DD_5 = \partial^2 + m^2 + g\gamma_5\left[\not{\partial}, \vec{\pi}\cdot\vec{\tau}\right] + \frac{g^2}{2m}\left[i\not{\partial}, \vec{\pi}^2\right] + \mathcal{O}(\vec{\pi}^3)$, and then we write its real part as:

$$\begin{aligned}
\mathcal{A}_R &= -i\frac{N_C}{2}\sum_{i=0}^{2}c_i\mathrm{Tr}\log\left[\partial^2 + m^2 + \Lambda^2 + g\gamma_5\left[\not{\partial}, \vec{\pi}\cdot\vec{\tau}\right] + \frac{g^2}{2m}\left[i\not{\partial}, \vec{\pi}^2\right]\right] \\
&= -i\frac{N_C}{2}\sum_{i=0}^{2}c_i\mathrm{Tr}\log\left[\partial^2 + m^2 + \Lambda_i^2 - i\epsilon\right] \\
&\quad - i\frac{N_C}{2}\sum_{i=0}^{2}c_i\mathrm{Tr}\left[\left(\partial^2 + m^2 + \Lambda_i^2 - i\epsilon\right)\left(g\gamma_5[\not{\partial}, \vec{\pi}\cdot\tau] + \frac{g^2}{2m}[i\not{\partial}, \vec{\pi}^2]\right)\right] \\
&\quad + i\frac{N_c}{4}\sum_{i=0}^{2}c_i\mathrm{Tr}\left[\partial^2 + m^2 + \Lambda_i^2 - i\epsilon\right]^{-1}g\gamma_5\left[\not{\partial}, \vec{\pi}\cdot\vec{\tau}\right]\left[\partial^2 + m^2 + \Lambda_i^2 - i\epsilon\right]^{-1}\left(g\gamma_5\left[\not{\partial}, \vec{\pi}\cdot\vec{\tau}\right]\right) + \mathcal{O}(\vec{\pi}^4).
\end{aligned} \tag{2.64}$$

The first term does not depend on $\vec{\pi}$, so it can be absorbed into the normalisation constant. The second term is zero since both $\mathrm{tr}(\gamma_\mu) = 0$ and $\mathrm{tr}(\gamma_5\gamma_\mu) = 0$. The last term is the bilinear term

$$A_R^2 = -2iN_cg^2\int_0^1 dx\int\frac{d^4q}{(2\pi)^4}\int\frac{d^4k}{(2\pi)^4}q^2\vec{\pi}(q)\cdot\vec{\pi}(-q)\left[m^2 - k^2 - q^2x(1-x) + \Lambda_i^2 - i\epsilon\right]^{-2}. \tag{2.65}$$

Putting Eqs. (2.63) and (2.65) together we find:

$$\mathcal{A}_{NJL} = g^2\int\frac{d^4q}{(2\pi)^4}\vec{\pi}(q)\cdot\vec{\pi}(-q)\left[2N_cq^2\Pi(q^2) - \frac{1}{2G}\frac{m}{m_0}\right] + \mathcal{O}(\vec{\pi}^4), \tag{2.66}$$

with the polarisation function

$$\Pi(q^2) = \int_0^1 dx\Pi(q^2, x), \tag{2.67}$$

where

$$\Pi(q^2,x) = -i\sum_{i=0}^{2} c_i \int \frac{d^4k}{(2\pi)^4}\left[-k^2 - x(1-x)q^2 + m^2 + \Lambda_i^2 - i\epsilon\right]^{-2}. \tag{2.68}$$

The square bracket term in Eq.(2.66)

$$D_\pi^{-1}(q^2) = \left[2N_c q^2 \Pi(q^2) - \frac{1}{2G}\frac{m}{m_0}\right] \tag{2.69}$$

is the inverse propagator and the on-shell condition states that the propagator has a pole at the physical mass. Hence, we have a relation for the pion mass ($m_\pi \approx 135\text{MeV}$)

$$m_\pi^2 = \frac{1}{4G}\frac{m_0}{m}\frac{1}{N_C \Pi(m_\pi^2)}. \tag{2.70}$$

Furthermore the residue of that pole must be unity. This relates the coupling constant

$$\frac{1}{g^2} = 4N_C \frac{d}{dq^2}\left[q^2\Pi(q^2)\right]|_{q^2=m_\pi^2} \tag{2.71}$$

to the pion mass.

Lastly we compute the pion decay constant. To do this, first let us consider the axial current for the NJL model. Introducing an external source for the axial current we have:

$$iD \to iD + \not{a}\gamma_5 \quad \text{and} \quad iD_5 \to iD_5 + \not{a}\gamma_5, \quad \text{where} \quad \not{a} = a_\alpha^\mu \gamma_\mu \frac{\tau^\alpha}{2}. \tag{2.72}$$

The linear coupling to this source then is the axial current:

$$A_\mu^b(x) = \frac{\delta}{\delta a_\mu^b(x)}\left\{-i\frac{N_C}{2}\sum_{i=0}^{2} c_i \text{Tr}\log(-DD_5 + \Lambda_i^2 - i\epsilon)\right\}|_{a_\mu=0}. \tag{2.73}$$

We only need the one pion matrix element of $\mathcal{A}_\mu$ so we will expand A_μ to linear order in the pion field $\pi_\mu(q)$,

$$\begin{aligned} A_\mu^b(x) &\approx -\frac{N_C}{2}\sum_i c_i \int \frac{d^4p}{(2\pi)^4}\int \frac{d^4k}{(2\pi)^4}\int_0^1 \frac{\text{tr}(g\gamma_5 p_\mu \gamma^\mu \tau^b \pi(p))(m\gamma_5\gamma_\mu\tau^b e^{-ip\cdot x})}{(-k^2+m^2-x(1-x)p^2+\Lambda_i^2-i\epsilon)^2} \\ &= 4mgN_C \int \frac{d^4p}{(2\pi)^4}\Pi(p^2)p_\mu \pi^b(p)e^{-ip\cdot x}. \end{aligned} \tag{2.74}$$

Then the axial current matrix element defines the pion decay constant f_π as

$$\langle \pi^a(q)|\, A_\mu^b(x)\,|0\rangle = f_\pi q_\mu \delta^{ab} e^{-iq\cdot x}, \tag{2.75}$$

With covariant normalisation the single pion matrix element is

$$\langle \pi^a(q)|\, \pi^b(p)\,|0\rangle = \delta_{ab}(2\pi)^4\delta^3(\vec{q}-\vec{p}), \quad q^2 = m_\pi^2 \tag{2.76}$$

so we identify

$$f_\pi = 4mgN_C\Pi(m_\pi^2). \tag{2.77}$$

The pion decay constant can be determined. To do this we start of from experimental values with the weak pion decay

$$\pi^-(q) \to \mu_-(p) + \bar{\nu}(p'), \tag{2.78}$$

with its interaction described by the Lagrangian

$$\mathcal{L}_{\text{eff}} = -\frac{G_F}{\sqrt{2}} J_\lambda^\dagger(x) J^\lambda(x) + \text{h.c.}, \tag{2.79}$$

where G_F is the Fermi coupling constant. The weak current is of the vector-minus-axial-vector structure $(V-A)$. We decompose this weak current

$$J_\lambda(x) = J_\lambda^l(x) + J_\lambda^h(x). \tag{2.80}$$

into its leptonic

$$J^l_\lambda = \bar{\nu}_\mu \gamma_\lambda (1-\gamma_5)\mu \tag{2.81}$$

and hadronic parts

$$J^h_\lambda(x) = \bar{u}\gamma_\lambda(1-\gamma_5)\cos\theta_c d, \tag{2.82}$$

where θ_c is the Cabibbo angle. With a vanishing Cabibbo angle $\theta_c \to 0$ the pion decay amplitude is of the form[30]

$$T_\pi = \frac{G_F}{\sqrt{2}} \langle \pi^a | A_\lambda | 0 \rangle l_\lambda, \tag{2.83}$$

where

$$l_\lambda = \bar{u}(p)\gamma_\lambda(1-\gamma_5)\nu(p') \tag{2.84}$$

is the lepton part of the transition matrix. This is written in terms of the electron (u) and anti-neutrino (ν) Dirac spins. Due to isospin and Lorentz invariance only axial current $A_\lambda = \bar{u}\gamma_\lambda\gamma_5 d$ contributes to the hadron matrix elements. The hadron matrix elements come to be of the form

$$\langle \pi^a(q) | A_\lambda(x) | 0 \rangle = i f_\pi q_\lambda e^{-iq\cdot x}, \tag{2.85}$$

with the observed decay width being

$$T = \frac{1}{T(\pi^- \to \mu_- + \bar{\nu})} = 2.6 \times 10^{-8}\text{sec}. \tag{2.86}$$

Using Eq. (2.83) one obtains the pion decay constant as

$$f_\pi \approx 93\text{MeV}. \tag{2.87}$$

This will be the value used in the numerical simulations.

Lastly to eliminate G we use the Gell-Mann-Renner-Oakes relation. This is obtained by solving

$$D_\pi^{-1}(q^2) = 0 \tag{2.88}$$

in the chiral limit $m_0 = 0$ by setting $q^2 = -m_\pi^2 = 0$, i.e. the pions are Goldstone bosons. This gives [20]

$$m_\pi^2 f_\pi^2 = \frac{m_0 m}{G} = 2m_0\langle\bar{q}q\rangle \frac{m}{m-m_0} \approx 2m_0\langle\bar{q}q\rangle. \tag{2.89}$$

CHAPTER 3

CONSTRUCTING THE SELF CONSISTENT SOLITON

The section describes the use of the hedgehog ansatz to numerically simulate a baryon as a soliton. It starts with a brief discussion on the hedgehog configuration and the baryon number current.

We will derive an energy functional for the hedgehog configuration. By minimising this functional we will establish an equation of motion for the hedgehog profile and solve that equation self-consistently. From this solution we obtain a mass formula for baryons using the cranking formalism to generate eigenstates of spin and isospin. Here we follow arguments from Refs. [20, 21, 24].

3.1 HEDGEHOG CONFIGURATION AND BARYON NUMBER CURRENT

This chapter will briefly go over the hedgehog configuration and a relation between the topological current of the chiral field and the baryon number current for the NJL model. We start of by defining the chiral field

$$U(\vec{x}) = \exp(i\theta(\vec{x})). \tag{3.1}$$

For two flavours, the static chiral field maps the coordinate space onto elements of this isospin group $\mathrm{SU}(2)$

$$U : \mathbb{R}^3 \to \mathrm{SU}(2). \tag{3.2}$$

Since solitons are finite energy solutions to the Euler-Lagrange equations it is required that the energy density vanishes at spatial infinity. This translates to

$$\mathrm{U}(\vec{x}) \to 1 \quad \text{as} \quad r = |\vec{x}| \to \infty. \tag{3.3}$$

This implies that all points at spatial infinity are identified thereby compactifying $\mathbb{R}^3$ to a three dimensional sphere S^3. The group manifold of $\mathrm{SU}(2)$ is also a S^3. Therefore a static chiral field configuration with boundary condition (3.3) represents a mapping

$$U : S^3 \to S^3. \tag{3.4}$$

These mappings can be distinguished by a winding number $\nu \in \mathbb{Z}$.

$$\nu[U] = \int B^0(r) d^3r. \tag{3.5}$$

Here B^μ is the topological current[31]

$$B^\mu = \frac{1}{24\pi^2}\epsilon^{\mu\nu\kappa\lambda}\mathrm{tr}(L_\nu L_\kappa L_\lambda), \tag{3.6}$$

where

$$L_\nu = U^\dagger \partial_\nu U. \tag{3.7}$$

A gradient expansion of $\langle \bar{q}\gamma_\mu q\rangle$ shows that B_μ is indeed (the leading contribution to) the baryon number current.

An example of a non-trivial mapping is the hedgehog ansatz

$$U(\vec{x}) = \exp(i\vec{\tau}\cdot\hat{x}F(r)), \tag{3.8}$$

where the isospin vector points in the radial direction. Then the winding number density becomes

$$B^0 = \frac{1}{2\pi^2}\theta'(r)\frac{\sin^2 F(r)}{r^2} \quad \text{which} \quad B^i = 0 \tag{3.9}$$

and $F(0) = -\nu\pi$ together with Eq. (3.3) produces, the desired baryon number.

3.2 The Soliton Energy

In this section we will elaborate on the soliton solution in the NJL model and compute its classical energy. In order to do so, we first consider the non-local part of the effective action $-iN_C\mathrm{Tr}_\Lambda \log iD$ and evaluate it in the presence of the hedgehog field:

$$U(\vec{x}) = \exp(i\vec{\tau}\cdot\hat{x}F(r)) \tag{3.10}$$

This is the hedgehog ansatz with the radial function $F(r)$ being the chiral angle. [1] From

$$iD = i\partial\!\!\!/ - (MP_R + M^\dagger P_L) = \beta(i\partial_t - h) \text{ where } \beta = \gamma^0 \tag{3.11}$$

we identify the single particle Dirac Hamiltonian

$$h = -i\beta\vec{\gamma}\cdot\vec{\partial} + \beta m\{U(\vec{x})\}^{\gamma_5}, \tag{3.12}$$

with

$$\{U(\vec{x})\}^{\gamma_5} = \exp(i\gamma_5\vec{\tau}\cdot\hat{x}F(r)) = \cos F(r) + i\gamma_5\hat{x}\cdot\vec{\tau}\sin F(r).$$

Without the soliton we have $F \equiv 0$ and thus $h^0 = -i\beta\vec{\gamma}\cdot\vec{\partial} + \beta m$.

To calculate the non-local part of the action we first write $\mathrm{Tr}\log(iD) = \log\mathrm{Det}(iD)$ and

$$\mathrm{Det}(iD) = \mathrm{Det}(i\partial_t - h), \text{ since } \det\beta = 1. \tag{3.13}$$

We calculate this determinant as the product over all the eigenvalues of $i\partial_t - h$. The chiral field is static so $i\partial_t$ and h commute, and we can determine the eigenvalues of $i\partial_t - h$ by the eigenvalues of the two separate operators $i\partial_t$ and h.

For $i\partial_t$ we first note that we have anti-periodic boundary conditions for the fermionic quark wave function

$$q(t+T,\vec{x}) = -q(t,\vec{x}), \tag{3.14}$$

where T is the time interval. So the eigenvalues for $i\partial_t$ are the Matsubara frequencies for fermions

$$\Omega_n = \frac{(2n+1)\pi}{T}, n = 0, \pm1, \pm2, \ldots. \tag{3.15}$$

The eigenvalues for the Dirac Hamiltonian are discretised by imposing spatial boundary conditions which will be specified and discussed later. Then we write the eigenvalue equation

$$h\Psi_\alpha = \epsilon_\alpha\Psi_\alpha \tag{3.16}$$

with ϵ_α and Ψ_α being the energy eigenvalues and the corresponding quark wave functions, respectively. They are functionals of the chiral angle. The corresponding formula for $F = 0$ is $(-i\vec{\alpha}\cdot\vec{\partial} - m)\Psi_\alpha^{(0)} = \epsilon_\alpha^{(0)}\Psi_\alpha^{(0)}$.

With these eigenvalues the functional determinant is formally, i.e. without any regularisation given as [32,

[1] This anzats has the particular feature that the isovector of the pion field points in radial direction.

33]

$$\mathrm{Det}(i\partial_t - h) = \prod_\alpha \prod_n (\Omega_n - \epsilon_\alpha) = \mathcal{C} \prod_\alpha \prod_{\Omega_n > 0} \left(1 - \left(\frac{\epsilon_\alpha}{\Omega_n}\right)^2\right) \tag{3.17}$$

$$\mathcal{C} = \prod_\alpha \prod_{n \geq 0} (-\Omega_n^2). \tag{3.18}$$

The constant does not depend on ϵ_α and thus not on the chiral angle. It is merely an additive constant in $\ln \mathrm{Det}(iD)$ and may be ignored. The sum over the Matsubara frequencies can be expressed in closed form [2]

$$\begin{aligned} \prod_\alpha \prod_{\Omega_n > 0} \left(1 - \left(\frac{\epsilon_\alpha}{\Omega_n}\right)^2\right) &= \prod_\alpha \cos\left(\frac{\epsilon_\alpha T}{2}\right) \\ &= \left[\prod_\alpha [1 + \exp(-i|\epsilon_\alpha|T)]\right] \exp\left(\frac{i}{2}\sum_\alpha |\epsilon_\alpha| T\right) \\ &= \sum_{\{\eta_\alpha\}} \exp\left(-i\sum_\alpha \eta_\alpha |\epsilon_\alpha| T\right) \exp\left(\frac{i}{2}\sum_\alpha \{\epsilon_\alpha\} T\right). \end{aligned} \tag{3.19}$$

Hence the functional determinant is

$$\mathrm{Det}(iD) = \mathcal{C} \sum_{\{\eta_\alpha\}} \exp\left[i\mathcal{A}_{\mathrm{v}}^{\{\eta_\alpha\}}\right] \exp[i\mathcal{A}_{\mathrm{s}}] \tag{3.20}$$

Above, the η_α are occupation numbers for the quark eigenstates. The first summation goes over all the possible sets of η_α's, where each η_α can be zero or one. In Eq. (3.20), we have

$$\mathcal{A}_{\mathrm{s}} = T\frac{N_C}{2}\sum_\alpha |\epsilon_\alpha|, \tag{3.21}$$

$$\mathcal{A}_{\mathrm{v}}^{\{\eta_\alpha\}} = -TN_C \sum_\alpha \eta_\alpha |\epsilon_\alpha|. \tag{3.22}$$

These are the vacuum and valence contributions to the action, respectively. The sum over the colour degrees of freedom merely results in the overall factor N_C because the model does not have colour interactions.

For a large time interval $T \to \infty$ only the vacuum state contributes to the integral since only the term with all $\eta_\alpha = 0$ survives: The Feynman boundary conditions, as for example reflected by the "$-i\epsilon$ " prescription in (2.50), can be realised by a Wick rotation to Euclidian space, where all contributions with $\eta_\alpha \neq 0$ are exponentially suppressed as $T \to \infty$. [3] For static configurations the action is $(-T)$ times the energy. For a particular set of occupation number we thus identify the energy

$$E_{\eta_\alpha} = N_C \sum_\alpha (-\frac{1}{2}|\epsilon_\alpha| + \eta_\alpha |\epsilon_\alpha|). \tag{3.23}$$

It is advantageous to separate the valence contribution

$$E_{\mathrm{val}} = N_C \sum_\alpha \eta_\alpha |\epsilon_\alpha| \tag{3.24}$$

and vacuum contribution

$$E_{\mathrm{s}} = -\frac{1}{2} N_C \sum_\alpha |\epsilon_\alpha| \tag{3.25}$$

components. The latter carries the label 's' for the Dirac "sea". The free vacuum energy $(F \equiv 0)$ is $E_s^{(0)} = -\frac{1}{2}N_C \sum_\alpha |\epsilon^{(0)}|$. Sometimes the difference $E_s - E_s^{(0)}$ is called the vacuum polarisation energy (VPE).

We can now relate the set of particle occupation numbers to the baryon number. To do this we first consider the baryon number current

$$j^\mu(x) = \frac{1}{N_C}\langle \bar{q}(x)\gamma^\mu q(x)\rangle = \frac{1}{N_C}\frac{i\delta}{\delta \nu_\mu} \log \mathrm{Det}(iD - \not{\nu})|_{\nu_\mu(x)=0} \tag{3.26}$$

[2] The Ω_n product and the trigonometrical function on the right hand side agree for $\epsilon_\alpha = 0$ and have the same roots.

[3] Projection onto the vacuum is the construction principle for the "$-i\epsilon$" prescription.

The reason for the $\frac{1}{N_C}$ is due to the quarks carrying the baryon number $1/N_C$. When we apply this functional derivative we find the baryon number current to be

$$j^\mu(x) = \sum_{\{\eta_\alpha\}} j^\mu_{\{\eta_\alpha\}}(x) = j^\mu_{\rm v}(x) + j^\mu_s(x). \tag{3.27}$$

In this equation $j^\mu_{\rm v}$ and j^μ_s are the valence and vacuum part of the baryon current respectively. To derive the explicit expression for these currents we apply the Feynman Hellmann theorem [34] to

$$\epsilon_\alpha[J_\mu] = -\int d^3x \Psi^\dagger_\alpha(x)(i\partial_t - h - \beta\not{\nu})\Psi_\alpha(x) \tag{3.28}$$

and find that

$$\frac{\delta\epsilon_\alpha}{\delta\nu_\mu(x)}\Big|_{\nu_\mu(x)=0} = \Psi^\dagger_\alpha(x)\beta\gamma^\mu\Psi_\alpha(x).$$

From this and Eq. (3.26) we can calculate the valence baryon number current and the vacuum baryon number current.

$$j^\mu_{\rm s}(x) = -\frac{1}{2}\sum_\alpha {\rm sgn}(\epsilon_\alpha)\bar\Psi_\alpha(x)\gamma^\mu\Psi_\alpha(x), \tag{3.29}$$

$$j^\mu_{\rm v}(x) = \sum_\alpha \eta_\alpha {\rm sgn}(\epsilon_\alpha)\bar\Psi_\alpha(x)\gamma^\mu\Psi_\alpha(x). \tag{3.30}$$

Using this and assuming proper normalisation ($\int d^3x\Psi^\dagger_\alpha(x)\Psi_\beta(x) = \delta_{\alpha\beta}$) we calculate the baryon number to be

$$B(\{\eta_\alpha\}) = \int d^3x j^0(x) = \sum_\alpha(\eta_\alpha - \frac{1}{2}){\rm sgn}(\eta_\alpha). \tag{3.31}$$

For a prescribed baryon number we choose the η_α to minimise E_{η_α}. This determines η_α uniquely, unless degenerate ϵ_α are involved.

Above we have computed the vacuum contribution to the energy formally, (3.25). However, we need to do so for the regularised bosonized action. With this in mind we will also require the operator iD_5 to introduce a single particle Hamiltonian with the hedgehog configuration.

$$iD_5 = (-i\partial_t - h)\beta, \tag{3.32}$$

$$-DD_5 = \beta(\partial_t^2 + h^2)\beta. \tag{3.33}$$

Using the above eigenvalues for $i\partial_t$ and h the real part of the action, (2.50) becomes

$$\mathcal{A}_{\rm R} = -i\frac{N_C}{2}\sum_{i=0}^{2} c_i \sum_{\alpha,n}(\log[-\Omega_n^2 + \epsilon_\alpha^2 + \Lambda_i^2 - i\epsilon] - \log[-\Omega_n^2 + (\epsilon_\alpha^{(0)})^2 + \Lambda_i^2 - i\epsilon]), \tag{3.34}$$

where we have subtracted the $F \equiv 0$ counterpart. This part is not dynamical as it is not a functional of the chiral angle. As before we extract the vacuum part by taking $T \to \infty$. Then the sum on the Matsubara frequencies turns into an integral over a continuous variable $\sum_n(\Omega_n) \to T\int \frac{dz}{2\pi} f(z)$. Applying this to (3.34) we have that

$$\mathcal{A}_{\rm R} = -iT\frac{N_C}{2}\sum_{i=0}^{2} c_i \sum_\alpha \int \frac{dz}{2\pi}(\log[-z^2 + \epsilon_\alpha^2 + \Lambda_i^2 - i\epsilon] - \log[-z^2 + (\epsilon_\alpha^{(0)})^2 + \Lambda_i^2 - i\epsilon]). \tag{3.35}$$

To compute this integral we first use a Wick rotation with $z \to iz$ followed by an integration by parts. The non-integral term in the integration by parts is cancelled out by the vacuum part which has the same non-

integral term contribution. The explicit calculation is

$$\begin{aligned}
&\int_{-\infty}^{\infty} dz \log[-z^2+\epsilon_\alpha^2+\Lambda_i^2-i\epsilon] = \frac{i}{2\pi}\int_{-\infty}^{\infty} dz \log[z^2+\epsilon_\alpha^2+\Lambda_i^2] \\
&= \frac{-i}{\pi}\int_{-\infty}^{\infty} dz \frac{z^2}{z^2+\epsilon_\alpha^2+\Lambda_i^2} = \frac{i}{\pi}\int_{-\infty}^{\infty} dz \left[-1+\frac{\epsilon_\alpha^2+\Lambda_i^2}{z^2+(\epsilon_\alpha^2+\Lambda_i^2)}\right] \\
&= \frac{i}{\pi}\int_{-\infty}^{\infty} dz \left[\frac{1}{(z-i\sqrt{\epsilon_\alpha^2+\Lambda_i^2})(z+i\sqrt{\epsilon_\alpha^2+\Lambda_i^2})}\right](\epsilon_\alpha^2+\Lambda_i^2) \\
&= \sqrt{\epsilon_\alpha^2+\Lambda_i^2}.
\end{aligned} \tag{3.36}$$

The -1 in the third line drops out because $\sum_{i=0}^{2} c_i = 0$. Hence the vacuum part of the action is given as

$$\mathcal{A}_{\mathrm{R}} = T\frac{N_C}{2}\sum_{i=0}^{2} c_i \sum_\alpha \left\{\sqrt{\epsilon_\alpha^2+\Lambda_i^2} - \sqrt{(\epsilon_\alpha^{(0)})^2+\Lambda_i^2}\right\}. \tag{3.37}$$

Finally we obtain the fully regularised vacuum energy functional

$$E_S = -\frac{N_C}{2}\sum_{i=0}^{2} c_i \sum_\alpha \left\{\sqrt{\epsilon_\alpha^2+\Lambda_i^2} - \sqrt{(\epsilon_\alpha^{(0)})^2+\Lambda_i^2}\right\}. \tag{3.38}$$

With the single cut-off prescription, (2.54) the total energy is

$$\begin{aligned}
E[F(r)] = N_C\sum_\alpha \eta_\alpha|\epsilon_\alpha| - \frac{N_C}{2}\sum_\alpha \Bigg\{&\left[|\epsilon_\alpha| - \sqrt{\epsilon_\alpha^2-\Lambda^2} + \frac{1}{2}\frac{\Lambda^2}{\sqrt{\epsilon_\alpha^2-\Lambda^2}}\right] \\
&- \left[|\epsilon_\alpha^{(0)}| - \sqrt{(\epsilon_\alpha^{(0)})^2-\Lambda^2} + \frac{1}{2}\frac{\Lambda^2}{\sqrt{(\epsilon_\alpha^{(0)})^2-\Lambda^2}}\right]\Bigg\} + E_m.
\end{aligned} \tag{3.39}$$

Here E_m is the contribution from the local part of the effective action. Using Eqs. (2.70) and (2.77) yields

$$E_m = -\frac{mm_0}{4G}\int d^3x \mathrm{tr}[U+U^\dagger-2] = m_\pi^2 f_\pi^2 \int d^3x(1-\cos F(r)). \tag{3.40}$$

A configuration with the boundary conditions $F(0) = -\pi$ and $F(0) = 0$ strongly binds a single Dirac level in the baryon number one sector. This single Dirac level is the so-called valence quark level, with energy eigenvalue ϵ_{v}. To minimise E, only this level may be occupied, i.e $\eta_\alpha \equiv 0$ for $\alpha \neq \mathrm{v}$. If the profile function $F(r)$ is wide, ϵ_{v} turns negative. In that case the vacuum contributes unit baryon number and this level must not be explicitly occupied. We can write this condition as

$$\eta_{\mathrm{v}} = \frac{1}{2}[1+\mathrm{sgn}(\epsilon_{\mathrm{v}})]. \tag{3.41}$$

Finally the total energy becomes

$$\begin{aligned}
E[F(r)] = \frac{N_C}{2}[1+\mathrm{sgn}(\epsilon_{\mathrm{v}})]\epsilon_{\mathrm{v}} - \frac{N_C}{2}\sum_\alpha \Bigg\{&\left[|\epsilon_\alpha| - \sqrt{\epsilon_\alpha^2+\Lambda^2} + \frac{1}{2}\frac{\Lambda}{\sqrt{\epsilon_\alpha^2+\Lambda^2}}\right] \\
&- \left[|\epsilon_\alpha^{(0)}| - \sqrt{\epsilon_\alpha^{(0)2}+\Lambda^2} + \frac{1}{2}\frac{\Lambda}{\sqrt{\epsilon_\alpha^{(0)2}+\Lambda^2}}\right]\Bigg\} + m_\pi^2 f_\pi^2 \int d^3x(1-\cos F(r)).
\end{aligned} \tag{3.42}$$

3.3 Diagonalising the Dirac Hamiltonian

In this section we will discuss the energy eigenvalues and eigenstates of the Dirac Hamiltonian. We can start off by noting that

$$[h, \vec{J}] \neq 0 \tag{3.43}$$

$$[h, \frac{\vec{\tau}}{2}] \neq 0, \tag{3.44}$$

since the hedgehog configuration is neither invariant under spatial- or isorotation Where h is our Dirac Hamiltonian (3.12), while $\vec{J}$ and $\frac{\vec{\tau}}{2}$ are the spin and the isospin operators, respectively. However, the so-called grand spin does commute

$$[h, \vec{G}] = 0 \quad \text{with} \quad \vec{G} = \vec{J} + \frac{\vec{\tau}}{2} = \vec{L} + \frac{\vec{\sigma}}{2} + \frac{\vec{\tau}}{2}. \tag{3.45}$$

Since the hedgehog configuration is invariant under the combined spatial- and isorotation. Here $\vec{\sigma}$ and $\vec{\tau}$ are the Pauli matrices for spin and isospin, respectively while $\vec{L}$ is the orbital angular momentum operator. For $\vec{G}$ we have the quantum numbers $\vec{G}^2 = G(G+1)$ and $G_3 = M$ (refer to appendix C for details) and the eigenfunctions are generalised spherical harmonics

$$\left[\mathcal{Y}^{GM}_{LJ}(\vec{x})\right]_{si} = \sum_{m,s_3,i_3,J_3} \mathcal{C}^{GM}_{JJ_3,\frac{1}{2}i_3} \mathcal{C}^{JJ_3}_{Lm,\frac{1}{2}s_3} Y_{Lm}(\hat{x}) \chi_s(s_3) \chi_i i_3, \tag{3.46}$$

where $\mathcal{C}^{GM}_{JJ_3,\frac{1}{2}i_3}$ and $\mathcal{C}^{JJ_3}_{Lm,\frac{1}{2}s_3}$ are $SU(2)$ Clebsch-Gordon coefficients. Furthermore, $Y_{Lm}(\hat{x})$ are the spherical harmonic functions and χ_s and χ_i are the two components spinors for spin and isospin, respectively. The spin matrix $\vec{\sigma}$ acts on χ_s but the isospin matrix $\vec{\tau}$ acts on χ_i.

We can now construct four component Dirac spinors. To do this, we combine two Weyl spinors $[\mathcal{Y}_{...}(\hat{x})]_{si}$ and $[\mathcal{Y}_{...}(\hat{x})]_{s'i}$. As already discussed, h commutes with $\vec{G}$, but it also commutes with parity. In the Dirac theory this is the combination of spatial reflection followed by multiplication of the spinor by γ_0: $\hat{P}\psi(\vec{x}) = \gamma_0\psi(-\vec{x})$. With this the grand spin basis is

$$\Psi^{(G,+)}_{\alpha}(\vec{x}) = \begin{pmatrix} ig^{(G,+;1)}_{\alpha}(r)\mathcal{Y}_{G,G+\frac{1}{2},G,M}(\hat{x}) \\ f^{(G,+;1)}_{\alpha}(r)\mathcal{Y}_{G+1,G+\frac{1}{2},G,M}(\hat{x}) \end{pmatrix} + \begin{pmatrix} ig^{(G,+;2)}_{\alpha}(r)\mathcal{Y}_{G,G-\frac{1}{2},G,M}(\hat{x}) \\ -f^{(G,+;2)}_{\alpha}(r)\mathcal{Y}_{G-1,G-\frac{1}{2},G,M}(\hat{x}) \end{pmatrix} \tag{3.47}$$

$$\Psi^{(G,-)}_{\alpha}(\vec{x}) = \begin{pmatrix} ig^{(G,-;1)}_{\alpha}(r)\mathcal{Y}_{G+1,G+\frac{1}{2},G,M}(\hat{x}) \\ -f^{(G,-;1)}_{\alpha}(r)\mathcal{Y}_{G,G+\frac{1}{2},G,M}(\hat{x}) \end{pmatrix} + \begin{pmatrix} ig^{(G,-;2)}_{\alpha}(r)\mathcal{Y}_{G-1,G-\frac{1}{2},G,M}(\hat{x}) \\ f^{(G,-;2)}_{\alpha}(r)\mathcal{Y}_{G,G-\frac{1}{2},G,M}(\hat{x}) \end{pmatrix} \tag{3.48}$$

Intrinsic parity $\prod_{\text{intr}} = \pm 1$ is labeled by the second of the superscripts. The parity is $\prod = (-1)^G \prod_{\text{intr}}$ since $Y_{Lm}(-\vec{x}) = (-1)^L Y_{Lm}(\vec{x})$. Furthermore, g and f are radial functions (refer to appendix C) where α refers to the energy eigenstate. These energies are descretised by demanding that there is no flux outside a ball of radius D, where D should be significantly larger than the soliton interaction range. This can be done by demanding that one of the two radial functions vanishes at $r = D$, choosing both to vanish over constrains the system. There are however various other choices that one can use to ensure this[20].

In the following we will discuss some characteristics of the Dirac energy spectrum, see Fig. 3.1. With this in mind let us characterise the length scale of the chiral angle $F(r)$ by $b \ll D$ and consider the spinors $\Psi^{(0,+)}_{\alpha}$ with $G = 0$ as this channel contains the strongly bounded mode. Since the constituent quark mass m is the only explicit parameter in the Dirac Hamiltonian we can distinguish three different regions based on the dimensionless variable bm.

The first region we can consider is for $bm \ll 1$. In this region the mesonic background interacts weakly with the quarks. The valence quark is weakly bound with positive energy slightly less than the mass threshhold.

In the second region $bm \sim 1$, this level is moderately bound. The interaction between the quarks and the mesonic background is strong. The energy of the valence quark is still positive. Summing the vacuum baryon number over all the states, both positive and negative energies, results in $B_S = 0$. This would mean that a unit baryon number requires $\eta_v = 1$.

In the last region where $bm \gg 1$ the valence quark enters the Dirac sea so the energy eigenvalue becomes negative. This time for a single bound quark we would have that $B_S = 1$, so all occupation numbers η_α must be set to zero. In this case the vacuum becomes so strongly polarised that it acquires a baryonic charge[35].

For a pion field with $B = 1$ there is one bound state. This bound state moves from the upper to the lower Dirac sea continuum as the spatial extension of the pion field increases.

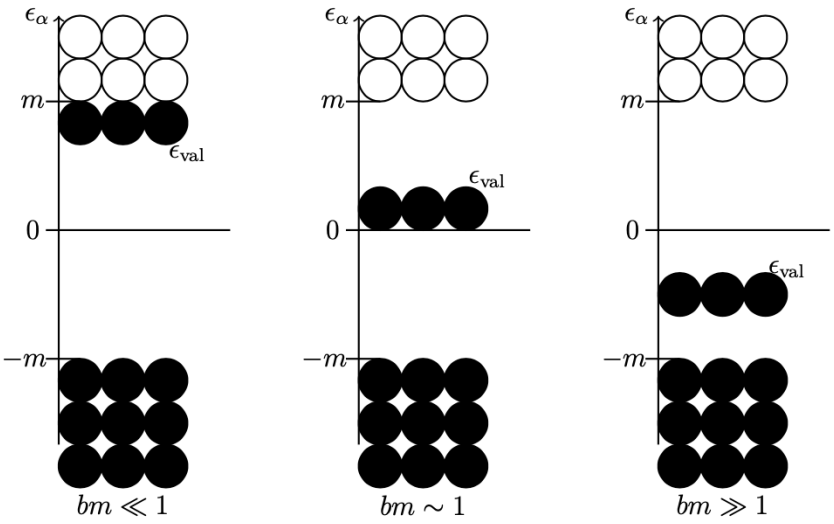

Figure 3.1: Dirac Spectrum for $G = 0$ channel for $N_C = 3$. Each circle represents an energy level, levels shown with open circles are unoccupied, whereas the levels shown with black circles are occupied. Also indicated here are the excited states with $|\epsilon| \geq 0$. Furthermore, the $\epsilon_{\rm val}$ is the energy eigenvalue of the bound valence quark level. The length b represents the width of the profile $F(r)$.

3.4 Constructing the Soliton

The chiral angle $F(r)$ and hence the soliton is obtained by extremising (3.39),

$$\frac{\delta E[F(r)]}{\delta F(r)} = \sum_\alpha \frac{\partial E_{\rm s}}{\partial \epsilon_\alpha}\frac{\delta \epsilon_\alpha}{\delta F(r)} + \frac{\partial E_{\rm v}}{\partial \epsilon_{\rm v}}\frac{\delta \epsilon_{\rm v}}{\delta F(r)} + \frac{\delta E_{\rm m}}{\delta F(r)} = 0 \tag{3.49}$$

The derivative of ϵ_α can be computed by the Feynman-Hellmann theorem $\delta\epsilon = \langle\psi|\,\delta H\,|\psi\rangle$, using the formulas (3.12) and (3.28)

$$\frac{\delta\epsilon_\alpha[F(r)]}{\delta F(r)} = \langle\psi|\,\frac{\delta h}{\delta F(r)}\,|\psi\rangle = m\int d\Omega \Psi^\dagger_\alpha(\vec{x})\beta[-\sin F(r) + i\gamma_5\vec{\tau}\cdot\hat{x}\cos F(r)]\Psi_\alpha(\vec{x}). \tag{3.50}$$

Using this, Eq. (3.49) becomes

$$\cos F(x)\mathrm{tr}\int d\Omega\rho(\vec{x},\vec{x})i\gamma_5\vec{\tau}\cdot\hat{x} = \sin F(r)\left[\mathrm{tr}\int d\Omega\rho(\vec{x},\vec{x}) - \frac{m_\pi^2 f_\pi^2}{mN_C}\right]. \tag{3.51}$$

According to Eq. (3.49) the density has valence and sea contributions:

$$\rho(\vec{x},\vec{y}) = \rho_{\rm v}(\vec{x},\vec{y}) + \rho_{\rm s}(\vec{x},\vec{y}) \tag{3.52}$$

$$\rho_{\rm s}(\vec{x},\vec{y}) = -\frac{1}{2}\sum_{i=0}^{2} c_i \sum_\alpha \Psi_\alpha(\vec{x})\frac{\epsilon_\alpha}{\sqrt{\epsilon_\alpha^2+\Lambda_i^2}}\bar{\Psi}_\alpha(\vec{y}) \tag{3.53}$$

$$\rho_{\rm v}(\vec{x},\vec{y}) = \frac{1}{2}[1+\mathrm{sgn}(\epsilon_{\rm v})]\Psi_{\rm v}(\vec{x})\Psi_{\rm v}(\vec{y}). \tag{3.54}$$

This set of equations is the radial reduction of the equation of motion for the chiral soliton.

We will follow the Hartree iteration method for the above equations [36–38], first an initial $F(r)$ shall be guessed such that obeys the boundary conditions $F(r=\infty) = 0$ and $F(r=0) = -\pi$. This chiral angle function $F(r)$ is used to construct the eigenvectors Ψ_α and energy eigenvalues ϵ_α of h from the (free) basis spinors[4]. In a first step we construct a basis for the free Dirac spinors, $\Psi^{(0)}_\alpha$. They are discretised by requiring that there is no flux through a spherical cavity of radius D which is much larger than the extension of the

[4]Free basis spinors have appropriate spherical Bessel functions for f and g in Eqs. (3.47) and (3.48)

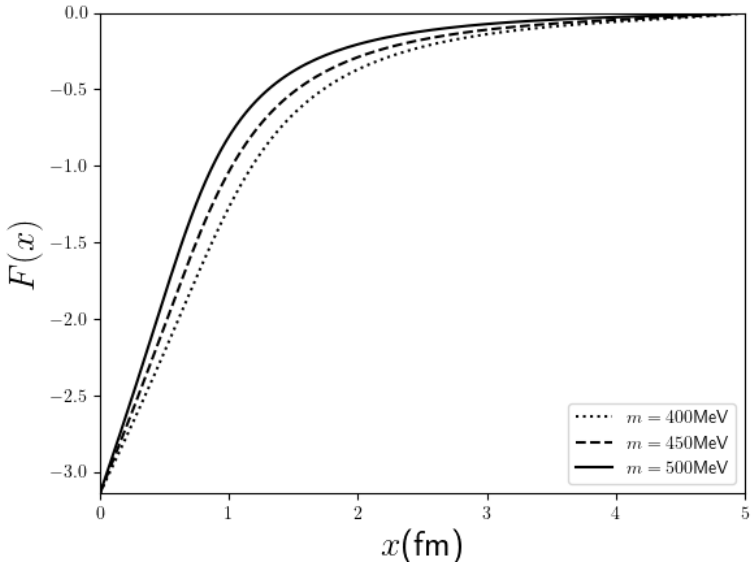

Figure 3.2: Chiral angle $F(x)$ for constituent quark masses $m = 400, 450, 500$MeV

typical soliton. This requirement can, for example, be realised by setting the upper components of the basis spinors to zero for $r = D$. To render a finite dimensional diagonalisation problem we only consider basis spinors with momenta less then $k_{\text{cut}} \gg \Lambda$. This also imposes a restriction on the grand spin since the position of the first root of a Bessel function increases with angular momentum.

We then compute the matrix elements $\left\langle \Psi_\alpha^{(0)} \middle| h \middle| \Psi_{\alpha'}^{(0)} \right\rangle$ and diagonalise these matrices in each grand spin and parity channel. The eigenvectors of these matrices $V_{\alpha n}$ lead to the eigenspinors $\Psi_\alpha = \sum_\alpha V_{\alpha n} \Psi_n^{(0)}$ that are substituted into Eqs. (3.51)-(3.54) to generate an updated chiral angle. This process is repeated until convergence has been reached; usually between 20 and 50 iterations, depending on the quality of the initial guess. We repeat the calculation for various (large) values of D and k_{cut} to ensure that the final result is not sensitive to these numerical parameters.

3.5 Cranking Corrections

We have so far attained solutions in the $B = 1$ sector by extremising the static energy. These solutions have zero grand spin; as a result, they do not have fixed eigenvalues for neither $\vec{J}$ nor $\vec{I}$ which are spin and isospin operators, respectively. Our aim now is to generate states with good spin and isospin quantum numbers. To do this, we will canonically quantise time-dependent rotations in isospace. Due to the grand spin symmetry of the hedgehog configuration they also parameterise spatial rotations. These rotations are the zero modes of the hedgehog configuration. Let us approximate the time dependent field configuration as

$$U(t, \vec{x}) = A(t) U(\vec{x}) A^\dagger(t), \tag{3.55}$$

where $A(t) \in \text{SU}(2)$ is a time dependent collective coordinate matrix which parameterises the isospin orientation of the soliton and $U(\vec{x})$ is the static hedgehog configuration (3.8). This can then be expanded and expressed in the adjoint representation

$$U(t, \vec{x}) = \exp(iA(t)\vec{\tau} \cdot \hat{x} A^\dagger(t) F(r)) = \exp(i\tau_i D_{ij}(t) \hat{x}_j F(r)), \tag{3.56}$$

where $D_{ij}(t) = \frac{1}{2}\mathrm{tr}(\tau_i A(t)\tau_j A^\dagger(t))$ is an orthogonal matrix. From the hedgehog structure we can assert the identity

$$[(\vec{x}\times\vec{\nabla})_l, U(t,\vec{x})] = i\frac{1}{2}[U(t,\vec{x}),\tau_j]D_{jl}. \tag{3.57}$$

The commutator on the left-hand side generates ordinary rotations, the one on the right does so for isorotations. Hence we have the operator identity

$$\vec{J} = -\vec{I}D, \tag{3.58}$$

which implies

$$\left|\vec{J}\right| = \left|\vec{I}\right|. \tag{3.59}$$

That is, the hedgehog soliton describes baryons with equal spin and isospin.

For the effective action (2.46) the mesonic part is time independent since it does not depend on $A(t)$. For the non-local part of the effective action we will follow discussion of Ref. [32]. We first eliminate $A(t)$ from the pseudo-scalar field by transforming the fermion field to a flavour rotating system

$$q \to q' = A(t)q. \tag{3.60}$$

This transformation produces new Dirac operators

$$\bar{q}iDq = \bar{q}'iD'q' \quad \text{and} \quad \bar{q}iD_5q = \bar{q}'iD_5'q', \tag{3.61}$$

with

$$iD' = A(t)\beta(i\partial_t - \vec{\tau}\cdot\vec{\Omega} - h)A^\dagger(t) \quad \text{and} \quad iD_5' = A(t)\beta(-i\partial_t + \vec{\tau}\cdot\vec{\Omega} - h)A^\dagger(t). \tag{3.62}$$

Here the angular velocity vector $\vec{\Omega}$ has emerged from the time dependence of the rotations

$$A^\dagger(t)\dot{A}(t) = \frac{i}{2}\vec{\Omega}\cdot\vec{\tau}. \tag{3.63}$$

This parameterisation is legitimate because $A^\dagger\dot{A}$ is anti-hermitian and traceless.

The exact eigenvalues of $h \pm \vec{\tau}\cdot\vec{\Omega}$ are unknown, so we will perform a perturbation expansion. To this end we compute the fermion determinant by a similar calculation as in section 3.2. This again separates into vacuum and valence (anti-)quark parts. Noting that due to isospin symmetry only even powers of $\vec{\Omega}$ contribute, the valence part is given by

$$\mathcal{A}_{\mathrm{v}}^{\{\eta_\alpha\}} = -N_C T E_{\mathrm{v}} + \frac{T}{2}\sum_{ij}^{3} F_{ij}^{\mathrm{v}}\Omega_i\Omega_j + \mathcal{O}(\vec{\Omega}^4), \tag{3.64}$$

with the valence contribution to the moment of inertia [32, 39]

$$F_{ij}^{\mathrm{v}} = -\frac{N_C}{2}\sum_{\alpha\neq\mathrm{v}}\eta_{\mathrm{v}}\frac{\langle\mathrm{v}|\,\tau_i\,|\alpha\rangle\langle\alpha|\,\tau_j\,|\mathrm{v}\rangle}{\epsilon_{\mathrm{v}} - \epsilon_\alpha} \tag{3.65}$$

calculated using standard time-independent perturbation theory.

Next we consider the vacuum contribution to the moment of inertia. This we extract from the real part of the effective action

$$\mathcal{A}_R = i\frac{N_C}{2}T\sum_{i=0}^{2}c_i\int\frac{dz}{2\pi}\mathrm{Tr}\log[(-z^2 + h^2 + \Lambda_i^2 - i\epsilon) + \frac{1}{2}z\vec{\Omega}\cdot\vec{\tau} + [\vec{\Omega}\cdot\vec{\tau}, h] - \frac{1}{2}(\vec{\Omega}\cdot\vec{\tau})^2]. \tag{3.66}$$

After a few calculations we simplify this expression and then evaluate the traces in the eigenbasis of h Eq. (3.12). Again we introduce a moment of inertia tensor and write

$$\mathcal{A}_R = -TE_{\mathrm{s}} + \frac{T}{2}\sum_{ij}F_{ij}^{\mathrm{s}}\Omega_i\Omega_j + \mathcal{O}(\vec{\Omega}^4), \tag{3.67}$$

where

$$F_{ij}^{\mathrm{s}} = \frac{N_C}{2}\sum_{\alpha\neq\beta}\sum_{i=0}^{2}c_i\int\frac{dz}{2\pi}\frac{(z^2 - \epsilon_\alpha\epsilon_\beta + \Lambda_i^2)\langle\alpha|\,\tau_i\,|\beta\rangle\langle\beta|\,\tau_j\,|\alpha\rangle}{(z^2 + \epsilon_\alpha^2 + \Lambda_i^2 - i\epsilon)(z^2 + \epsilon_\beta^2 + \Lambda_i^2 - i\epsilon)}. \tag{3.68}$$

Using a Wick rotation followed by Cauchy's residue theorem and finally taking the single cut-off limit the vacuum contribution to the moment of inertia becomes [32]

$$
\begin{aligned}
F^{\mathrm{s}}_{ij} &= \frac{N_C}{4}\sum_{\alpha\neq\beta}\frac{\langle\alpha|\,\tau_i\,|\beta\rangle\,\langle\beta|\,\tau_j\,|\alpha\rangle}{(\epsilon_\alpha^2-\epsilon_\beta^2)} \\
&\times\Bigg(\Big\{\Big[\,|\epsilon_\alpha|-\sqrt{\epsilon_\alpha^2+\Lambda^2}+\frac{1}{2}\frac{\Lambda^2}{\sqrt{\epsilon_\alpha^2+\Lambda^2}}\Big]-\Big[\,|\epsilon_\beta|-\sqrt{\epsilon_\beta^2+\Lambda^2}+\frac{1}{2}\frac{\Lambda^2}{\sqrt{\epsilon_\beta^2+\Lambda^2}}\Big]\Big\} \\
&+\epsilon_\alpha\epsilon_\beta\Big\{\frac{|\epsilon_\alpha|-|\epsilon_\beta|}{|\epsilon_\alpha|\,|\epsilon_\beta|}-\frac{\sqrt{\epsilon_\alpha^2+\Lambda^2}-\sqrt{\epsilon_\beta^2+\Lambda^2}}{\sqrt{\epsilon_\alpha^2+\Lambda^2}\sqrt{\epsilon_\beta^2+\Lambda^2}}\Big\}-(\epsilon_\alpha\epsilon_\beta-\Lambda^2)\frac{\Lambda^2}{2}\frac{\sqrt[3]{\epsilon_\alpha^2+\Lambda^2}-\sqrt[3]{\epsilon_\beta^2+\Lambda^2}}{\sqrt[3]{\epsilon_\alpha^2+\Lambda^2}\sqrt[3]{\epsilon_\beta^2+\Lambda^2}}\Bigg).
\end{aligned}
\tag{3.69}
$$

Both, F^{v}_i and F^{s}_i are iso-singlets, and we can write

$$
F^{\mathrm{v}}_{ij}+F^{\mathrm{s}}_{ij}=\alpha^2\delta_{ij} \tag{3.70}
$$

yielding the Lagrange function

$$
L=-E+\frac{1}{2}\alpha^2\vec{\Omega}^2+\mathcal{O}(\Omega^2) \tag{3.71}
$$

It is straight forward to show that

$$
\dot{U}=\frac{i}{2}[A\vec{\tau}\cdot\vec{\Omega}A^\dagger,U] \tag{3.72}
$$

so that

$$
\frac{\partial\dot{U}}{\partial\Omega_j}=\frac{i}{2}[\tau_i,U]D_{ij}=-[(\vec{x}\times\vec{\nabla})_j,U]. \tag{3.73}
$$

That is, $\frac{\partial\dot{U}}{\partial\Omega_j}$ produces infinitesimal rotations.

Hence, we obtain the spin as the Noether charge

$$
\vec{J}=\int d^3r\,\mathrm{tr}\Big\{\frac{\partial L}{\partial\dot{U}}\frac{\partial\dot{U}}{\partial\vec{\Omega}}+\frac{\partial L}{\partial\dot{U}^\dagger}\frac{\partial\dot{U}^\dagger}{\partial\vec{\Omega}}\Big\}=\frac{\partial L}{\partial\vec{\Omega}}=\alpha^2\vec{\Omega} \tag{3.74}
$$

and the Hamiltonian becomes

$$
H=\vec{J}\cdot\frac{\partial L}{\partial\vec{\Omega}}-L=E+\frac{1}{2\alpha^2}\vec{J}^2. \tag{3.75}
$$

The collective coordinate quantisation is that of a SU(2) rigid top [40]. The eigenfunctions are the Wigner-D functions of Euler angles representing $A(t)$. The eigenvalue equations are

$$
\vec{J}^2D^{J=I}_{m,m'}(A)=\vec{I}^2D^{J=I}_{m,m'}=J(J+1)D^{J=I}_{m,m'}(A), \tag{3.76}
$$

$$
J_3D^{J=I}_{m,m'}(A)=-m'D^{J=I}_{m,m'}(A), \tag{3.77}
$$

and

$$
I_3D^{I=J}_{m,m'}(A)=m'D^{I=J}_{m,m'}(A). \tag{3.78}
$$

The left index of D_{ij} behaves like an isovector and the right index like the angular momentum vector. Hence, we can write $\langle D_{ij}\rangle=K\langle I_iJ_j\rangle$ where K is the reduced matrix element. Using Eq. (3.58) we see that $K=\frac{-1}{I(I-1)}=\frac{-1}{J(J+1)}$. Thus,

$$
\langle N|\,D_{ij}\,|N\rangle=-\frac{4}{3}\,\langle N|\,I_iJ_j\,|N\rangle\,, \tag{3.79}
$$

where $|N\rangle$ is the nucleon state with $I=J=\frac{1}{2}$.

There is more to say about the cranking procedure. Fortunately, all we need for the exploration of the iso-singlet unpolarised structure function is the nucleon matrix element in Eq. (3.79).

CHAPTER 4

NUCLEON STRUCTURE FUNCTIONS

In this chapter we will derive a formal expression for the unpolarised nucleon structure functions in the regularised NJL model. We will then manipulate these expressions such that they are accessible to numerical simulations. To this end we will adopt the Pauli-Villars subtraction regularisation scheme and use the Compton tensor as a starting point. Subsequently, the optical theorem relates the hadronic tensor to the imaginary (absorptive) part of the Compton scattering amplitude

$$W_{\mu\nu}(p,q) = \frac{1}{2\pi}\mathrm{Im}[T_{\mu\nu}(p,q)]. \tag{4.1}$$

The Compton tensor is the matrix element of a time-ordered product of the electromagnetic currents

$$T_{\mu\nu}(p,q) = \int d^3\xi e^{iq\cdot\xi} \langle p,s|\, T(J_\mu(\xi)J_\nu(0))\,|p,s\rangle \tag{4.2}$$

rather than their commutators. This has the advantage that the time-ordered product is obtained from the regularised action of the NJL model by functional differentiation

$$T(J_\mu(\xi)J_\nu(0)) = \frac{-i\delta^2}{\delta v_\mu(\xi)\delta v_\nu(0)}\mathrm{Tr}_\Lambda \log[i\partial\!\!\!/ - (MP_R + M^\dagger P_L) + \mathcal{Q}v\!\!\!/]\Big|_{v_\mu=0}, \tag{4.3}$$

where $Q = \mathrm{diag}(\frac{2}{3}, -\frac{1}{3})$ is the quark charge generator. Once the Compton tensor has been obtained, Cutkosky's rules relate the result to the hadronic tensor and thus provide the structure functions. Some formal analysis of this method can be found in Ref. [24].

To set up the model calculations we will first analyse the simpler case of the pion structure function.

4.1 PION STRUCTURE FUNCTION

In this section we consider deep inelastic scattering (DIS) for pions in the NJL model. This will motivate and support simplifications for the calculation of the nucleon structure function in the same model.

We write the hadronic current operator in Eq. (1.18) as

$$J_\mu(\xi) = \bar{q}(\xi)\mathcal{Q}\gamma_\mu q(\xi). \tag{4.4}$$

This current sets the framework for computing DIS properties of the pion and the nucleon. Its correlation functions are computed by introducing an external photon-like vector source in the effective action as

$$iD \to iD + \mathcal{Q}v\!\!\!/ \quad \text{and} \quad iD_5 \to iD_5 - \mathcal{Q}v\!\!\!/. \tag{4.5}$$

This allows us to write the (connected part of the) time ordered current-current product as

$$T(J_\mu(\xi)J_\nu(0)) = -iN_C\frac{\delta^2}{\delta v_\mu(\xi)\delta v_\nu(0)}\mathrm{Tr}_\Lambda \log[i\partial\!\!\!/ - (MP_R + MP_L) + \mathcal{Q}v\!\!\!/]|_{v_\mu=0}, \tag{4.6}$$

specific to the NJL model as the colour trace has been taken yielding the factor N_C.

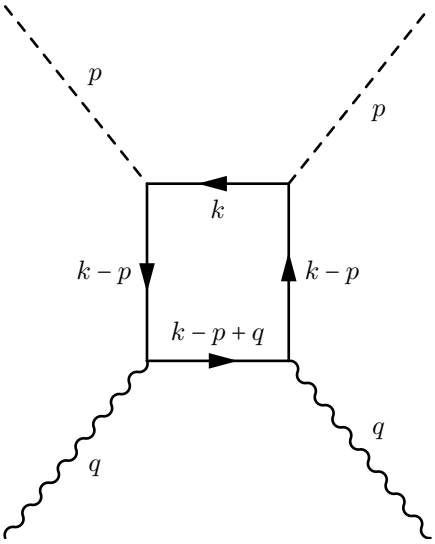

Figure 4.1: Graphical representation of the handbag diagram, with p being the momentum of the pion, q being that of the photon and k being the momentum of the looping quark.

To explore off-shell photon pion scattering $\gamma^*\pi \to \gamma^*\pi$ we write

$$iD = i\not{\partial} + m + ig\gamma_5\vec{\pi}\cdot\vec{\tau} \text{ and } iD_5 = -i\not{\partial} + m - ig\gamma_5\vec{\pi}\cdot\vec{\tau} \tag{4.7}$$

and expand to $\mathcal{O}(\vec{\pi}^2)$. With $|p,a\rangle$ being the state vector of a pion with momentum p and isospin a such that $\vec{\tau}\cdot\vec{\pi}\,|p,a\rangle = \tau^a e^{-ipx}\,|p,a\rangle$ the Compton amplitude in the Bjorken limit is [24, 41]

$$\begin{aligned} T^{\mu\nu} &= \lim_{|q^2|\to\infty}\int d^3\xi e^{iq\cdot\xi}\,\langle p,a|\,T(J^\mu(\xi)J^\nu(0))\,|p,a\rangle \\ &= \sum_{i=0}^{2} c_i\Bigg\{(4N_C g^2)\frac{5}{9}\int\frac{d^4k}{(2\pi)^4}\frac{\mathrm{tr}(\not{k}-\not{p}+\not{q}+m)\gamma^\mu(\not{k}-\not{p}+m)\gamma^\mu}{[-(k-p+q)^2+m^2+\Lambda_i^2-i\epsilon][-(k-p)^2+m^2+\Lambda_i^2-i\epsilon]^2} \\ &\times\frac{\gamma^5(\not{k}+m)\gamma^5(\not{k}-\not{p}+m)\gamma^\nu}{(-k^2+m^2+\Lambda_i^2-i\epsilon)}\Bigg\}. \end{aligned} \tag{4.8}$$

The factor $(4N_C g^2)\frac{5}{9}$ is due to the trace of the photon $\mathrm{tr}(\tau_a\tau_a\mathcal{Q}\mathcal{Q}) = \frac{10}{9}$. The momenta q_μ and p_μ are for the external photon and pion respectively, while k_μ is the momentum of the looping quark. The full calculation has a few more terms; in particular those with the trace structure $\mathrm{tr}(\tau_a\mathcal{Q}\tau_b\mathcal{Q})$. Fortunately they become irrelevant in the Bjorken limit. This finding is consistent with the fact that $T^{\mu\nu}$ should not depend on the charge of the pion.

Figure 4.1 shows the Feynman diagram representation for $T^{\mu\nu}$ (The effect of regularisation is not displayed). This is a standard handbag diagram[41]. The aim now is to extract the imaginary (absorptive) part in the Bjorken limit.

Applying Cutkosky's rules we obtain the imaginary part by replacing the propagators with the indicated cut in figure 4.1 by their pole terms:

$$\frac{1}{(-k^2+m^2+\Lambda_i^2-i\epsilon)} \to -2\pi i\delta(k^2-m^2-\Lambda_i^2) \tag{4.9}$$

$$\frac{1}{(-(k\pm q-p)^2+m^2+\Lambda_i^2-i\epsilon)} \to -2\pi i\delta((k\pm q-p)^2-m^2-\Lambda_i^2). \tag{4.10}$$

We introduce light cone coordinates $q^\pm = \frac{1}{\sqrt{2}}(q^0\pm p^3) = \frac{1}{\sqrt{2}}(q_0\mp p_3)$ etc. Then the Bjorken limit amounts to $q^-\to\infty$ and $q^+\to xp^+ = Mx$, where Bjorken x is defined in Eq. (1.35). To leading order in $\frac{1}{q^-}$

$$\delta((k\pm q-p)^2-m^2-\Lambda_i^2) \sim \frac{1}{2q^-}\delta(k^+-p^+\pm q^+). \tag{4.11}$$

The importance of Eq. (4.11) should not be underestimated: The cut-off has disappeared on the right-hand

side; so has the mass term. That is, the same result would have been obtained if we had taken the quark propagator carrying the large momentum q as a free massless propagator. Stated otherwise, functional differentiating

$$A^{2,v}_{\Lambda,\mathrm{R}} = -i\frac{N_C}{4}\sum_{i=0}^{2} c_i \mathrm{Tr}\{(-DD_5+\Lambda_i^2)^{-1}[\mathcal{Q}^2\not{v}(\not{\partial})^{-1}\not{v}D_5 - D(\not{v}(\not{\partial})^{-1}\not{v})_5\mathcal{Q}^2]\} \tag{4.12}$$

yields the same result for the structure function in the Bjorken limit [42]. The disappearance of the cut-off in the propagator is an important feature of the Pauli-Villars regularisation; it is not guaranteed in other regularisation prescriptions. Later we will adopt Eq. (4.12) as the starting point for computing nucleon structure functions.

Collecting pieces, the hadronic tensor becomes

$$\begin{aligned} W^{\mu\nu} =& \mathrm{Im}T^{\mu\nu} \\ =&(2N_Cg^2)\frac{5}{9}\sum_{i=0}^{2}c_i\int\frac{d^4k}{(2\pi)^4}\frac{\mathrm{tr}(-\not{k}+m)(\not{k}-\not{p}+m)\gamma^\mu\gamma^\rho q_\rho\gamma^\nu(\not{k}-\not{p}+m)}{(-k^2+m^2+\Lambda_i^2-i\epsilon)_{\mathrm{pole}}[-(k-p)^2+m^2+\Lambda_i^2-i\epsilon]^2} \\ &\times\frac{\delta(k^+-p^+q^+)}{q^-}, \end{aligned} \tag{4.13}$$

here the 'pole' subscript denotes the pole contribution Eq.(4.9) of the relevant term in the parenthesis. We can now evaluate the Dirac trace

$$\gamma^\mu\gamma^\rho\gamma^\nu = S^{\mu\rho\nu\sigma}\gamma_\sigma - i\epsilon^{\mu\rho\nu\sigma}\gamma_\sigma\gamma_5, \tag{4.14}$$

where

$$S^{\mu\rho\nu\sigma} = g^{\mu\rho}g^{\nu\sigma}+g^{\mu\sigma}g^{\rho\nu}-g^{\mu\nu}g^{\rho\sigma}. \tag{4.15}$$

Let $\mu=\nu=i$ with $i=1,2$ as the transverse directions. This gives

$$S^{i+i\sigma} = g^{i+}g^{i\sigma}+g^{i\sigma}g^{i+}-g^{ii}g^{+\sigma}. \tag{4.16}$$

The none vanishing elements of the metric tensor of light cone coordinates are

$$g^{+-}=g^{-+}=1 \text{ and } g^{11}=g^{22}=-1, \tag{4.17}$$

from this it follows that $g^{i+}=g^{i\sigma}=0$ with $\sigma=-$, $S^{i+i-}=1$ and therefore

$$\sum_{i=1}^{2}W^{ii} = 2N_Cg^2\frac{5}{9}\sum_{i=0}^{2}c_i\int\frac{d^4k}{(2\pi)^4}\frac{\delta(k^++q^+-p^+)\mathrm{tr}(-\not{k}+m)(\not{k}-\not{p}+m)\gamma^+(\not{k}-\not{p}+m)}{(-k^2+m^2+\Lambda_i^2-i\epsilon)_{\mathrm{pole}}[-(k-p)^2+m^2+\Lambda_i^2-i\epsilon]^2}. \tag{4.18}$$

By substituting the pole term, two of the momentum integrals can be evaluated. This just leaves the integration over the transverse momenta.

The pion DIS is described by the form factor decomposition of the hadronic tensor

$$W_{\mu\nu} = G(x,Q^2)\left[-g_{\mu\nu}+\frac{q_\mu q_\nu}{q^2}-\frac{1}{q^2}(p_\mu-\frac{q_\mu}{2x})(p_\nu-\frac{q_\nu}{2x})\right], \tag{4.19}$$

and in Bjorken limit this turns into the structure function

$$F(x) = \lim_{\substack{Q^2\to\infty \\ x \text{ fixed}}} G(x,Q^2). \tag{4.20}$$

Next we apply this limit to Eq. (4.18) and extract, cf. also Ref. [41]

$$F(x) = (2N_Cg^2)\frac{5}{9}\sum_{i=0}^{2}c_i\int\frac{d^2k_\perp}{(2\pi)^3}\left\{\frac{1}{m^2+k_\perp^2+\Lambda_i^2-x(1-x)m_\pi^2}+\frac{m_\pi^2x(1-x)}{[m^2+k_\perp^2+\Lambda_i^2-x(1-x)m_\pi^2]^2}\right\}. \tag{4.21}$$

We recall the polarisation function Eq. (2.68) and write it as a Feynman parameter integral

$$\Pi(q^2) = \int_0^1 dx \Pi(q^2, x), \tag{4.22}$$

$$\Pi(q^2, x) = -i\sum_{i=0}^{2} c_i \int \frac{d^4k}{(2\pi)^4} \frac{1}{[m^2 - k^2 - x(1-x)q^2 + \Lambda_i^2 - i\epsilon]^2}. \tag{4.23}$$

Integrating over the longitudinal momenta gives the polarisation function as [42, 43]

$$\Pi(q^2, x) = \frac{1}{2}\sum_{i=0}^{2} c_i \int \frac{d^2k_\perp}{(2\pi)^3} \frac{1}{m^2 + \vec{k}_\perp^2 + \Lambda_i^2 - x(1-x)q^2}. \tag{4.24}$$

Following from this, the structure function is calculated to be

$$\begin{aligned} F(x) &= \frac{5}{9}(4N_C g^2)\{\Pi(q^2, x) + q^2 \frac{d}{dq^2}\Pi(q^2, x)\}\big|_{q^2=m_\pi^2} \\ &= \frac{5}{9}(4N_C g^2)\frac{d}{dq^2}[q^2\Pi(q^2, x)]\big|_{q^2=m_\pi^2}, \end{aligned} \tag{4.25}$$

Two important observations can be made. First a comparison with Eq. (2.71) shows that

$$\int_0^1 dx F(x) = \frac{5}{9} = \sum_i e_i^2 \tag{4.26}$$

the structure function is normalised to summed square of the quark charges. Second, in the chiral limit $(m_\pi = 0), F(x) = \frac{5}{9}$ for $0 \le x \le 1$ and zero otherwise.

We also recognise that the same result could have been obtained by ignoring the issue of regularisation and computing the 'handbag' diagram, Fig. 4.1 and subsequently enforcing the Pauli-Villars regularisation on the polarisation function $\Pi(q^2)$.

4.2 Nucleon Structure Function

We are now prepared to compute the nucleon structure functions. To do this we will reintroduce the charge matrix factors

$$\mathcal{A}^{(2,v)}_{\Lambda,R} = -i\frac{N_C}{4}\sum_{i=0}^{2} c_i \mathrm{Tr}\{(-DD_5 + \Lambda_i^2)^{-1}[\mathcal{Q}^2 \not{\nu}(\not{\partial})^{-1}\not{\nu}D_5 - D(\not{\nu}(\not{\partial})^{-1}\not{\nu})_5\mathcal{Q}^2]\} \tag{4.27}$$

$$\mathcal{A}^{(2,v)}_{\Lambda,I} = -i\frac{N_C}{4}\mathrm{Tr}\{(-DD_5)^{-1}[\mathcal{Q}^2 \not{\nu}(\not{\partial})^{-1}\not{\nu}D_5 + D(\not{\nu}(\not{\partial})^{-1}\not{\nu})_5\mathcal{Q}^2]\}. \tag{4.28}$$

As mentioned above the large photon momentum runs through the propagators in the square brackets. These propagators have thus been replaced by those of a free massless fermion. The subscript "5" in Eqs. (4.27) and (4.28) defines

$$(\gamma^\mu\gamma^\rho\gamma^\nu)_5 = S^{\mu\rho\nu\sigma}\gamma_\sigma + i\epsilon^{\mu\rho\nu\sigma}\gamma_\sigma\gamma_5. \tag{4.29}$$

The unconventional sign of the ϵ-term is required because axial sources appear with opposite signs in iD and iD_5. It is a necessary change for the regularisation of the structure functions to be consistent with the sum rules[24]. However, this prescription only affects the polarised structure functions, and we are no longer concerned.

We now define the hadronic tensor for localised field configurations. This, among other things, demands the restoration of translational invariance. To do this we introduce the collective coordinate $\vec{R}$ for the centre of the soliton. Its conjugate momentum is $\vec{p}$ such that $\langle \vec{R}|\vec{p}\rangle = 2\sqrt{M}e^{i\vec{R}\cdot\vec{p}}$. Averaging over the position of the soliton, turns the Compton tensor into

$$\begin{aligned} T_{\mu\nu} &= 2iM_N \int d^4\xi \int d^3R e^{iq\cdot\xi} \langle p, s|T\{J_\mu(\xi - \vec{R})J_\nu(-\vec{R})\}|p, s\rangle \\ &= 2iM_N \int d^4\xi_1 \int d^3\xi_2 e^{iq\cdot(\xi_1-\xi_2)} \langle s|T\{J_\mu(\xi_1)J_\nu(\xi_2)\}|s\rangle. \end{aligned} \tag{4.30}$$

We consider ξ_2 as a four-vector with $\xi_2^0 = 0$. The factor $2M_N$ arises from the normalisation of the eigenstates of the momentum $\vec{p}$. Before moving on we note that:

- The functional trace of the operator in the square brackets that appears in the action functional $\mathcal{A}^{(2,v)}_{\Lambda,R}$ and $\mathcal{A}^{(2,v)}_{\Lambda,I}$ is computed using the plane-wave basis. The matrix elements of the operators in Eqs. (2.47) and (2.48) are evaluated by using the eigenfunctions Ψ_α of the Dirac Hamiltonian (3.12).
- Next, the action is expanded to leading order in $\frac{1}{N_C}$ by rotating the charge matrix $\mathcal{Q}^2 \to \mathcal{Q}_A^2 = A^\dagger(\xi_1^0)\mathcal{Q}^2 A(\xi_2^0)$. In the computation of the nucleon structure function, we make use of the identity

$$A^\dagger(\xi_1^0)\tau_i A(\xi_2^0) = \frac{1}{2}\mathrm{Tr}(A^\dagger(\xi_1^0)\tau_i A(\xi_2^0)\tau_j)\tau_j + \mathcal{O}(\xi_1^0 - \xi_2^0), \tag{4.31}$$

  whenever the rotated quark charge matrix contains an isospin factor. Considering the time evolution of the collective coordinate $A(t)$, one can write[44]

$$A(\xi_1^0) = \exp(-i(\xi_1^0 - \xi_2^0)\frac{\vec{J}^2}{2\alpha^2})A(\xi_2^0)\exp(i(\xi_1^0 - \xi_2^0)\frac{\vec{J}^2}{2\alpha^2}), \tag{4.32}$$

  where $\vec{J}$ is the spin operator and α is the moment of inertia. Since $\alpha^2 \sim N_C$ we observe that the effects from $\xi_1^0 \neq \xi_2^0 = 0$ are subleading in $\frac{1}{N_C}$. Taking traces of the time-dependent collective coordinate matrix $A(t)$ in the plane wave basis gives

$$\langle t, \vec{\xi}| A(t) |\omega, \alpha\rangle = A(t)e^{-i\omega t}\Psi_\alpha(\vec{\xi}). \tag{4.33}$$

- Lastly, the matrix elements of the operators in Eqs. (2.47) and (2.48) are also taken at leading order in $\frac{1}{N_C}$

$$\langle\omega,\alpha|\,(-DD_5 + \Lambda_i^2)^{-1}\,|\omega,\beta\rangle = \frac{\delta_{\alpha\beta}}{\omega^2 - \epsilon_\alpha^2 - \Lambda_i^2} + \mathcal{O}(\frac{1}{N_C}). \tag{4.34}$$

With these remarks, we write leading order in $\frac{1}{N_C}$ of the gauged action explicitly

$$\begin{aligned}\mathcal{A}^{(2,\nu)}_{\Lambda} &= \mathcal{A}^{(2,\nu)}_{\Lambda,R} + \mathcal{A}^{(2,\nu)}_{\Lambda,L} \\ &= -i\frac{N_C}{2}\int\frac{d\omega}{2\pi}\sum_\alpha\{\langle\omega,\alpha|\,\mathcal{Q}_A^2\gamma^0\not{\nu}(i\not{\partial})^{-1}\not{\nu}\,|\omega,\alpha\rangle\, f_\alpha^+(\omega) \\ &+ \langle\omega,\alpha|\,\mathcal{Q}_A^2[\not{\nu}(i\not{\partial})^{-1}\not{\nu}]_5\gamma^0\,|\omega,\alpha\rangle\, f_\alpha^-(\omega)\} + \mathcal{O}(\frac{1}{N_C}).\end{aligned} \tag{4.35}$$

The frequency integral results from summing over the eigenvalues of $i\partial_t$ contained in the operators iD and iD_5. The Dirac matrix γ^0 appearing in the action $\mathcal{A}^{(2,\nu)}_{\Lambda}$ is a result of the definitions of the operators iD and iD_5. The spectral functions

$$f_\alpha^\pm(\omega) = \sum_{i=0}^{2} c_i\frac{\omega \pm \epsilon_\alpha}{\omega^2 - \epsilon_\alpha^2 - \Lambda_i^2 + i\epsilon} \pm \frac{\omega \pm \epsilon_\alpha}{\omega^2 - \epsilon_\alpha^2 + i\epsilon} \tag{4.36}$$

emerge from the expansion in (4.34), with and without regularising (DD_5^{-1}).

Taking the functional derivative of $\mathcal{A}^{(2,v)}_{\Lambda}$ gives the Compton amplitude in leading order of $\frac{1}{N_C}$

$$\begin{aligned}T_{\mu\nu}(q) = -M_N\frac{N_C}{2}\int\frac{d\omega}{2\pi}\sum_\alpha\int dt\int d^3\xi_1\int d^3\xi_2\int\frac{d^4k}{(2\pi)^4}e^{i(q_0+k_0)t}e^{-i(\vec{q}+\vec{k})\cdot(\vec{\xi}_1-\vec{\xi}_2)}\frac{1}{k^2+i\epsilon} \\ \langle N|\,\{[\Psi_\alpha^\dagger(\vec{\xi}_1)\gamma^0\mathcal{Q}_A^2\gamma_\mu\not{k}\gamma_\nu\Psi_\alpha(\vec{\xi}_2)e^{i\omega t} - \Psi_\alpha^\dagger(\vec{\xi}_2)\gamma^0\mathcal{Q}_A^2\gamma_\nu\not{k}\gamma_\mu\Psi_\alpha(\vec{\xi}_1)e^{-i\omega t}]f_\alpha^+(\omega) \\ +[\Psi_\alpha^\dagger(\vec{\xi}_1)\mathcal{Q}_A^2(\gamma_\mu\not{k}\gamma_\nu)_5\gamma^0\Psi_\alpha(\vec{\xi}_2)e^{i\omega t} - \Psi_\alpha^\dagger(\vec{\xi}_2)\mathcal{Q}_A^2(\gamma_\mu\not{k}\gamma_\nu)_5\gamma^0\Psi_\alpha(\vec{\xi}_1)e^{-i\omega t}]f_\alpha^-(\omega)\}\,|N\rangle\,,\end{aligned} \tag{4.37}$$

with the time coordinate $t = \xi_1^0$. Recall that the quark wave functions are localised which means that the coordinate space integrals gather most support when $\vec{\xi}_1 \sim \vec{\xi}_2$. Hence, the only region of the k-integral that will be relevant has $k_\sigma \sim -q_\sigma$, i.e. the loop momentum should be of the order of the infinitely large photon momentum. With that in mind we can now apply Cutkosky's rules to access the hadronic tensor. The temporal integral yields $k_0 = q_0 \pm \omega$, this fixes the spatial part of the loop momentum due to $\delta(k^2)$ in $\frac{1}{k^2+i\epsilon}\,\text{pole} = i\delta(k^2)$.

To further exploit the Bjorken limit we define the Fourier transform of the quark wave-functions

$$\tilde{\Psi}_\alpha(\vec{p}) = \int \frac{d^3x}{4\pi}\Psi_\alpha(\vec{x})e^{i\vec{x}\cdot\vec{p}} \tag{4.38}$$

and make use of the fact that the eigenstates of the Dirac Hamiltonian carry definite parity. The latter property allows us to compensate spatial reflections by factors of the Dirac matrix β. With these preliminaries the spatial integrals can be performed

$$\begin{aligned} W_{\mu\nu}(q) = iM_N\frac{N_C}{2}(4\pi)^2\int\frac{d\omega}{2\pi}\sum_\alpha\int\frac{d^3k}{(2\pi)^2}\frac{1}{2|\vec{k}|} \\ \times\langle N|\{[\tilde{\Psi}^\dagger_\alpha((\vec{q})+\vec{k})\mathcal{Q}_A^2\gamma^0\gamma_\mu\not{k}\gamma_\nu\tilde{\Psi}_\alpha(\vec{q}+\vec{k})\delta(|k|-q_0-\omega_0) \\ -\tilde{\Psi}^\dagger_\alpha(\vec{q}+\vec{k})\mathcal{Q}_A^2\gamma_\nu\not{k}\gamma_\mu\gamma^0\tilde{\Psi}_\alpha(\vec{q}+\vec{k})\delta(|k|-q_0+\omega_0)]f^+_\alpha(\omega)|_{\text{pole}} \\ +[\tilde{\Psi}^\dagger_\alpha(\vec{q}+\vec{k})\mathcal{Q}_A^2(\gamma_\mu\not{k}\gamma_\nu)_5\gamma^0\tilde{\Psi}_\alpha(\vec{q}+\vec{k})\delta(|k|-q_0-\omega_0) \\ -\tilde{\Psi}^\dagger_\alpha(\vec{q}+\vec{k})\mathcal{Q}_A^2\gamma^0(\gamma_\nu\not{k}\gamma_\mu)_5\tilde{\Psi}_\alpha(\vec{q}+\vec{k})\delta(|k|-q_0+\omega_0)]f^-_\alpha(\omega)|_{\text{pole}}\}|N\rangle\,. \end{aligned} \tag{4.39}$$

The 'pole' subscript prescribes that the spectral function in Eq (4.36) are truncated to their δ-function component. Hence, the spectral integral is restricted to those values of ω which cause the respective denominators of the spectral functions to vanish.

We choose the coordinate system so that the photon moves along the z-axis. This introduces the Bjorken scaling variable

$$q_0 = q_3 - M_N x. \tag{4.40}$$

We change the integration variable $\vec{k}\to\vec{p}=\vec{q}+\vec{k}$, and take into account the Jacobian of the transformation, which becomes feasible because only the $|\vec{p}|=0$ regime contributes to the integral [45–47]. Then the hadronic tensor becomes

$$\begin{aligned} W_{\mu\nu}(q) = i\frac{N_C}{4}\int\frac{d\omega}{2\pi}\sum_\alpha\int d^3p\,\langle N|\{[\tilde{\Psi}^\dagger_\alpha(\vec{p})\mathcal{Q}_A^2\gamma^0\gamma_\mu\not{n}\gamma_\nu\tilde{\Psi}_\alpha(\vec{p})f^+_\alpha(\omega)|_{\text{pole}} \\ +\tilde{\Psi}^\dagger_\alpha(\vec{p})\mathcal{Q}_A^2(\gamma_\mu\not{n}\gamma_\nu)_5\gamma^0\tilde{\Psi}_\alpha(\vec{p})f^-_\alpha(\omega)|_{\text{pole}}]\delta(p_3-M_Nx+\omega) \\ -[\tilde{\Psi}^\dagger_\alpha(\vec{p})\mathcal{Q}_A^2\gamma_\nu\not{n}\gamma_\mu\gamma^0\tilde{\Psi}_\alpha(\vec{p})f^+_\alpha(\omega)|_{\text{pole}} \\ +\tilde{\Psi}^\dagger_\alpha(\vec{p})\mathcal{Q}_A^2(\gamma_\nu\not{n}\gamma_\mu)_5\gamma^0\tilde{\Psi}_\alpha(\vec{p})f^-_\alpha(\omega)|_{\text{pole}}]\delta(p_3-M_Nx-\omega)\}|N\rangle\,, \end{aligned} \tag{4.41}$$

where the light cone vector $n^\mu=(1,0,0,1)^\mu$ has been introduced. The exponential representation for the δ-function allows us to switch to a coordinate space representation

$$\begin{aligned} W_{\mu\nu}(q) = -iM_N\frac{N_C}{4}\int\frac{d\omega}{4\pi}\sum_\alpha\int d^3\xi\int\frac{d\lambda}{2\pi}e^{iM_Nx\lambda} \\ \times\{[\bar{\Psi}_\alpha(\vec{\xi})\mathcal{Q}_A^2\gamma_\mu\not{n}\gamma_\nu\Psi_\alpha(\vec{\xi}+\lambda\hat{e}_3)e^{-i\lambda\omega}-\bar{\Psi}_\alpha(\vec{\xi})\mathcal{Q}_A^2\gamma_\nu\not{n}\gamma_\mu\Psi_\alpha(\vec{\xi}-\lambda\hat{e}_3)e^{i\lambda\omega}]f^+_\alpha(\omega)|_{\text{pole}} \\ +[\bar{\Psi}_\alpha(\vec{\xi})\mathcal{Q}_A^2(\gamma_\mu\not{n}\gamma_\nu)_5\Psi_\alpha(\vec{\xi}+\lambda\hat{e}_3)e^{-i\lambda\omega}-\bar{\Psi}_\alpha(\vec{\xi})\mathcal{Q}_A^2(\gamma_\nu\not{n}\gamma_\mu)_5\Psi_\alpha(\vec{\xi}-\lambda\hat{e}_3)e^{i\lambda\omega}]f^-_\alpha(\omega)|_{\text{pole}}. \end{aligned} \tag{4.42}$$

The terms with $\Psi_\alpha(\vec{\xi}+\lambda\hat{e}_3)$ and $\Psi_\alpha(\vec{\xi}-\lambda\hat{e}_3)$ have opposite signs in the frequency factors, $e^{\pm i\omega\lambda}$. They are hence interpreted as quark and anti-quark contributions, respectively.

In order to get our structure functions we simply contract the hadronic tensor $W_{\mu\nu}$ with appropriate projectors. Our focus will be solely on the unpolarised structure functions F_1 and F_2, the relevant projector for this is $-\frac{1}{2}g^{\mu\nu}$. Using this projector, generalising the photon direction $\hat{e}_3$ into an arbitrary unit spherical direction $\hat{z}$ and taking its average $\int\frac{d\Omega_z}{4\pi}\ldots$ gives [24, 48]

$$\begin{aligned} F_1(x) = i\frac{5\pi}{72}MN_C\int\frac{d\Omega_z}{4\pi}\int\frac{d\omega}{2\pi}\sum_\alpha\int\frac{d\lambda}{2\pi}e^{iMx\lambda}\left(\sum_{i=0}^{2}c_i\frac{\omega+i\epsilon}{\omega^2-\epsilon_\alpha^2-\Lambda_i^2+i\epsilon}\right)_{\text{pole}} \\ \times\int d^3\xi\big\{\Psi^\dagger_\alpha(\vec{\xi})(1-\vec{\alpha}\cdot\hat{z})\Psi_\alpha(\vec{\xi}+\lambda\hat{z})e^{-i\omega\lambda}-\Psi^\dagger_\alpha(\vec{\xi})(1-\vec{\alpha}\cdot\hat{z})\Psi_\alpha(\vec{\xi}-\lambda\hat{z})e^{i\omega\lambda}\big\}. \end{aligned} \tag{4.43}$$

The Callan-Gross relation $F_2=2xF_1$ immediately yields the second unpolarised structure function. This is an identity for Dirac particles.

The aim now is to get (4.43) into a form that allows for numerical simulation. To do so we follow Ref.

[1, 2] and first take the Fourier transform of the eigenfunctions Ψ_α into momentum space

$$\begin{aligned} F_1(x) = i\frac{5\pi}{72}MN_C \int \frac{d\Omega_z}{4\pi}\int \frac{d\omega}{2\pi}\sum_\alpha \int \frac{d\lambda}{2\pi}e^{iMx\lambda}\left(\sum_{i=0}^{2}\frac{\omega+\epsilon_\alpha}{\omega^2-\epsilon_\alpha^2-\Lambda_i^2+i\epsilon}\right)_{\text{pole}} \\ \times \int \frac{d^3p}{2\pi^2}\int \frac{d^3k}{2\pi^2}\int d^3\xi\Big\{\tilde{\Psi}_\alpha^\dagger(\vec{p})(1-\vec{\alpha}\cdot\hat{z})\tilde{\Psi}_\alpha(\vec{k})e^{i\vec{\xi}\cdot(\vec{p}-\vec{k})}e^{i\lambda(Mx-\hat{z}\cdot\vec{k})}e^{-i\omega\lambda} \\ -\tilde{\Psi}_\alpha^\dagger(\vec{p})(1-\vec{\alpha}\cdot\hat{z})\tilde{\Psi}_\alpha(\vec{k})e^{i\vec{\xi}\cdot(\vec{p}-\vec{k})}e^{i\lambda(Mx+\hat{z}\cdot\vec{k})}e^{i\omega\lambda}\Big\}. \end{aligned} \tag{4.44}$$

The pole contributions are given by Dirac-δ functions

$$\left(\sum_{i=0}^{2}c_i\frac{\omega+\epsilon_\alpha}{\omega^2-\epsilon_\alpha^2-\Lambda_i^2+i\epsilon}\right)_{\text{pole}} = \sum_{i=0}^{2}c_i\frac{-i\pi}{\omega_0}[\delta(\omega+\omega_0)+\delta(\omega-\omega_0)], \tag{4.45}$$

with $\omega_0 = \sqrt{\epsilon_\alpha^2+\Lambda_i^2}$. The frequency integrals can be easily computed

$$\int\frac{d\omega}{2\pi}\left(\sum_{i=0}^{2}c_i\frac{\omega+\epsilon_\alpha}{\omega^2-\epsilon_\alpha^2-\Lambda_i^2+i\epsilon}\right)_{\text{pole}}e^{\mp i\omega\lambda} = \sum_{i=0}^{2}c_i\frac{1}{\omega_0}[\mp\omega_0\sin\omega_0\lambda - i\epsilon_\alpha\cos\omega_0\lambda]. \tag{4.46}$$

Subsequently, we can integrate over λ

$$\begin{aligned} &\int\frac{d\lambda}{2\pi}\sum_{i=0}^{2}c_i\frac{1}{\omega_0}[\mp\omega_0\sin\omega_0\lambda - i\epsilon_\alpha\cos\omega_0\lambda]e^{i\lambda(Mx\mp\hat{z}\cdot\vec{p})} \\ &= \mp\frac{\omega_0}{2}[\delta(Mx\mp\hat{z}\cdot\vec{p}+\omega_0)-\delta(Mx\mp\hat{z}\cdot\vec{p}-\omega_0)] + \frac{\epsilon_\alpha}{2}[\delta(Mx\mp\hat{z}\cdot\vec{p}+\omega_0)+\delta(Mx\mp\hat{z}\cdot\vec{p}-\omega_0)]. \end{aligned} \tag{4.47}$$

The averaging procedure over Ω_z turns these Dirac-δ functions into step functions. For example

$$\int\frac{d\Omega_z}{2\pi}\delta(Mx\mp\hat{z}\cdot\vec{p}+\omega_0) = \mp\frac{1}{2|\vec{p}|}\Theta(|\vec{p}|-|Mx+\omega_0|). \tag{4.48}$$

We now write the momentum integral in spherical coordinates

$$\int d^3p\cdots = \int_0^\infty dpp^2\int d\Omega_p\cdots. \tag{4.49}$$

This gives the sea contribution to the unpolarised structure function as

$$[F_1(x)]_s^\mp = \frac{5MN_C}{144}\sum_\alpha\sum_{i=0}^{2}c_i\int_{|Mx_\alpha^\pm|}^\infty pdp\int d\Omega_p\left\{\pm\tilde{\Psi}_\alpha^\dagger(\vec{p})\tilde{\Psi}_\alpha(\vec{p}) - \frac{\epsilon_\alpha}{\omega_0}\frac{Mx_\alpha^\pm}{p}\tilde{\Psi}_\alpha^\dagger(\vec{p})\hat{p}\cdot\alpha\tilde{\Psi}_\alpha(\vec{p})\right\}, \tag{4.50}$$

where

$$Mx_\alpha^\pm = Mx\pm\omega_0. \tag{4.51}$$

The two forms $[F_1(x)]_s^\pm$ arise from the positive (negative) frequency components typically referred to as the quark and anti-quark distributions, respectively. The total sea contribution to the unpolarised structure function is then simply

$$[F_1(x)]_s = [F_1(x)]_s^- + [F_1(x)]_s^+. \tag{4.52}$$

Details on the Fourier transform of the eigenfunction $\tilde{\Psi}_\alpha(\vec{p})$ can be found in appendix C.

When constructing the soliton solution, a particular coordinate system had to be selected. We took it to be the rest frame (RF). This (or any other) choice has non-vanishing structure functions for $|x| > 1$. This seemingly Lorentz violating effect can be cured by transforming to the infinite momentum frame (IMF) [49, 50]. We note that the parton model assumes this frame. In that model the parton masses are neglected, which is a reliable approximation when the momenta are arbitrarily large. With Eq. (4.52) identified as f_{RF} we then get the physically reliable structure function as

$$f_{\text{IMF}}(x) = \frac{\Theta(1-x)}{1-x}f_{\text{RF}}(-ln(1-x)), \tag{4.53}$$

where f_{RF} is the rest frame structure function from Eq. (4.52).

Eq. (4.43) requires us to calculate the matrix elements

$$\int d\Omega_p \tilde{\Psi}^{\dagger}_{\alpha}(\vec{p})\tilde{\Psi}_{\alpha}(\vec{p}) \quad \text{and} \tag{4.54}$$

$$\int \Omega_p \tilde{\Psi}^{\dagger}_{\alpha}(\vec{p})\hat{p}\cdot\vec{\alpha}\tilde{\Psi}_{\alpha}(\vec{p}) = \int d\Omega_p \tilde{\Psi}^{\dagger}_{\alpha}(\vec{p})\hat{p}\cdot\vec{\sigma}\gamma_5\tilde{\Psi}_{\alpha}(\vec{p}). \tag{4.55}$$

Since the spherical Bessel functions only depend on the radius and the orthogonality of the generalised spherical harmonic functions

$$\int d\Omega_p \left(\mathcal{Y}^{GM}_{JL}\right)^{\dagger}(\hat{p})\mathcal{Y}^{G'M'}_{J'L'}(\hat{p}) = \delta_{JJ'}\delta_{LL'}\delta_{GG'}\delta_{MM'}, \tag{4.56}$$

the matrix elements of (4.54) are straightforwardly calculated: For positive intrinsic parity $(+)$ we have

$$\begin{aligned}\int d\Omega_p \tilde{\Psi}^{\dagger(G,+)}_{\alpha}(\vec{p})\tilde{\Psi}^{(G,+)}_{\alpha}(\vec{p}) = (2G+1)\Big\{&\left[\tilde{g}^{(G,+;1)}_{\alpha}(p)\right]^2 + \left[\tilde{f}^{(G,+;1)}_{\alpha}(p)\right]^2 \\ &+ \left[\tilde{g}^{(G,+;2)}_{\alpha}(p)\right]^2 + \left[\tilde{f}^{(G,+;2)}_{\alpha}(p)\right]^2\Big\},\end{aligned} \tag{4.57}$$

and for negative intrinsic parity we have

$$\begin{aligned}\int d\Omega_p \tilde{\Psi}^{\dagger(G,-)}_{\alpha}(\vec{p})\tilde{\Psi}^{(G,-)}_{\alpha}(\vec{p}) = (2G+1)\Big\{&\left[\tilde{g}^{(G,-;1)}_{\alpha}(p)\right]^2 + \left[\tilde{f}^{(G,-;1)}_{\alpha}(p)\right]^2 \\ &+ \left[\tilde{g}^{(G,-;2)}_{\alpha}(p)\right]^2 + \left[\tilde{f}^{(G,-;2)}_{\alpha}(p)\right]^2\Big\},\end{aligned} \tag{4.58}$$

where $\tilde{g}^{(G,\pm;1)}_{\alpha}$, $\tilde{g}^{(G,\pm;2)}_{\alpha}$, $\tilde{f}^{(G,\pm;1)}_{\alpha}$ and $\tilde{g}^{(G,\pm;2)}_{\alpha}$ are the Fourier transforms of $g^{(G,\pm;1)}_{\alpha}$ etc., details on these are given in appendix C. The factor $(2G+1)$ arises from summing over grand spin projection in $\sum_{\alpha}$ since the eigenvalues ϵ_{α} are degenerate with respect to this quantum number. The integral (4.55) is computed from the matrix elements from table 4.1: For positive intrinsic parity we find

$$\begin{aligned}\int d\Omega_p \tilde{\Psi}^{\dagger(G,+)}_{\alpha}(\vec{p})\hat{p}\cdot\vec{\sigma}\gamma_5\tilde{\Psi}^{(G,+)}_{\alpha}(\vec{p}) = -2(2G+1)[&\tilde{g}^{(G,+;1)}_{\alpha}(p)\tilde{f}^{G,+;1}_{\alpha}(p) \\ &+ \tilde{g}^{(G,+;2)}_{\alpha}(p)\tilde{f}^{(G,+;2)}_{\alpha}(p)],\end{aligned} \tag{4.59}$$

and similarly for negative intrinsic parity we have

$$\begin{aligned}\int d\Omega_p \tilde{\Psi}^{\dagger(G,-)}_{\alpha}(\vec{p})\hat{p}\cdot\vec{\sigma}\gamma_5\tilde{\Psi}^{(G,-)}_{\alpha}(\vec{p}) = -2(2G+1)[&\tilde{g}^{(G,-;1)}_{\alpha}(p)\tilde{f}^{G,-;1}_{\alpha}(p) \\ &+ \tilde{g}^{(G,-;2)}_{\alpha}(p)\tilde{f}^{(G,-;2)}_{\alpha}(p)].\end{aligned} \tag{4.60}$$

One last thing to note is that while regularisation typically removes quadratic and logarithmic divergences, quartic divergences occur in some cases. An example is the action functional itself that includes the quartically divergent cosmological constant. Such diverges are removed by subtracting the non-solitonic counterpart, this is the same quantity but computed for chiral angle $F(r) = 0$. For example, for the action functional this enforces the subtraction of the zeroth order energies in Eq. (3.39). Since our iso-singlet unpolarised structure function is related to the soliton energy via the energy sum rule (a small derivation of this will be shown in the next chapter) it is necessary to perform a similar subtraction here

$$[F_1(x)]_{\text{vac}} = [F_1(x)]_s - [F_1^{(0)}(x)]_s, \tag{4.61}$$

where $\left[F_1^{(0)}(x)\right]_s$ is the structure function computed with $F(r) = 0$.

Finally, we need to specify the valence quark contribution $[F_1(x)]_{\text{v}}$. Substituting the valence quark level into Eq. (4.43) discarding regularisation and omitting the sum over α, as there is only one valence level yields

$$\begin{aligned}[F_1(x)]_{\text{v}} = i\frac{5\pi}{72}MN_c \int \frac{d\Omega_z}{4\pi}\int\frac{d\omega}{2\pi}\int\frac{d\Lambda}{2\pi}e^{iM_x\lambda}\left(\frac{\omega+\epsilon_{\text{v}}}{\omega^2-\epsilon_{\text{v}}^2+i\epsilon}\right)_{\text{pole}} \\ \times\int d^3\xi\Big\{\Psi^{\dagger}_{\text{v}}(\vec{\xi})(1-\vec{\alpha}\cdot\hat{z})\Psi_{\text{v}}(\vec{\xi}+\lambda\hat{z})e^{-i\omega\lambda} \\ -\Psi^{\dagger}_{\text{v}}(\vec{\xi})(1-\vec{\alpha}\cdot\hat{z})\Psi_{\text{v}}(\vec{\xi}-\lambda\hat{z})e^{i\omega\lambda}\Big\}.\end{aligned} \tag{4.62}$$

$J' = G - \frac{1}{2}$		$J' = G + \frac{1}{2}$		
$L' = G - 1$	$L' = G$	$L' = G$	$L' = G + 1$	
0	−1	0	0	$L = G - 1$
				$J = G - \frac{1}{2}$
−1	0	0	0	$L = G$
0	0	0	−1	$L = G$
				$J = G + \frac{1}{2}$
0	0	−1	0	$L = G + 1$

Table 4.1: Matrix elements of $\int d\Omega_p \mathcal{Y}^{GM}_{L'J'}(\vec{p})\hat{p}\cdot\vec{\sigma}\mathcal{Y}^{GM}_{LJ}(\vec{p})$. See appendix D for more details

Repeating the calculations, that we already carried out for the sea contribution above, to the unpolarised structure function, recalling that the valence quark has positive parity and pole contribution $f^{\pm}|_{\text{pole}} = -4i\pi\delta(\omega \mp \epsilon_{\text{v}})$ yields

$$[F_1(x)]^{\mp}_{\text{v}} = -\frac{5MN_C}{72}\int_{abs Mx^{\pm}_{\text{v}}}^{\infty} pdp \int d\Omega_p \Big\{ \pm \tilde{\Psi}^{\dagger}_{\text{v}}(\vec{p})\tilde{\Psi}_{\text{v}}(\vec{p}) - \frac{Mx^{\pm}_{\text{v}}}{p}\tilde{\Psi}^{\dagger}_{\text{v}}(p)\hat{p}\cdot\vec{\alpha}\tilde{\Psi}_{\text{v}}(p)\Big\}, \tag{4.63}$$

with $Mx^{\pm}_{\text{v}} = Mx \pm \epsilon_{\text{v}}$.

The valence quark has $G = 0$ which means that only components with $J = \frac{1}{2}$ are allowed for the eigenspinor

$$\Psi_{\text{v}}(\vec{x}) = \begin{pmatrix} ig_{\text{v}}(r)\mathcal{Y}^{0,0}_{0,\frac{1}{2}}(\hat{x}) \\ f_{\text{v}}(r)\mathcal{Y}^{0,0}_{1,\frac{1}{2}}(\hat{x}) \end{pmatrix}, \tag{4.64}$$

here $g_{\text{v}}(r) = g^{(0,+;1)}_{\alpha}(r)$ and $f_{\text{v}} = f^{(0,+;1)}_{\alpha}(r)$ for α denoting the strongly bound level. Taking the Fourier transform results in

$$\tilde{\Psi}_{\text{v}}(\vec{p}) = \begin{pmatrix} i\tilde{g}_{\text{v}}(p)\mathcal{Y}^{0,0}_{0,\frac{1}{2}}(\hat{p}) \\ i\tilde{f}_{\text{v}}(p)\mathcal{Y}^{0,0}_{1,\frac{1}{2}}(\hat{p}) \end{pmatrix}. \tag{4.65}$$

Then using the same calculations used for the matrix elements of the sea contribution gives

$$\int d\Omega_p \tilde{\Psi}^{\dagger}_{\text{v}}(\vec{p})\tilde{\Psi}_{\text{v}}(\vec{p}) = \big(\tilde{g}_{\text{v}}(p)\big)^2 + \big(\tilde{f}_{\text{v}}(p)\big)^2, \tag{4.66}$$

$$\int d\Omega_p \tilde{\Psi}^{\dagger}_{\text{v}}(\vec{p})\hat{p}\cdot\vec{\alpha}\tilde{\Psi}_{\text{v}}(\vec{p}) = -2\tilde{g}_{\text{v}}(p)\tilde{f}_{\text{v}}(p). \tag{4.67}$$

4.3 Numerical Computation of the Structure Function

Now that we have derived the iso-singlet unpolarised structure function (IUSF) for the nucleon we can go about simulating it to further analyse the results of Ref.[1, 2]. That study found unexpected results for this particular structure function. Its sea contribution was oscillating as a function of x, with large (absolute) values of the extrema that do not seem physically sound.

For all the following experiments the constituent quark mass is taken[1] as $m = 400$MeV, using this we calculate the cutoff Λ numerically via Eq. (2.71), for further details we refer to appendix B. The value is found to be $\Lambda_{\text{new}} \approx 739.096$ MeV which is slightly smaller than the value given by Takyi $\Lambda_{\text{old}} \approx 743.059$ MeV, due to a small sign error in the code on his part Ref.[51]. Once Λ has been determined the soliton can be constructed using the method mentioned in section 3.4.[2] This calculation results in the profile function of the chiral angle, the energy eigenvalues; and wavefunctions of the quarks for each energy level. We identify the valence quark wavefunction and its corresponding energy eigenvalue as the level with the largest binding energy.

These quark wavefunctions have been constructed in coordinate space, to construct the IUSF it is necessary to take the Fourier transformation of these functions; we refer to appendix C for further details on

[1] The IUSF contains numerical factors of the nucleon mass. They need to be taken at the physical value $M = 940$MeV, rather than what the model predicts.

[2] The validity of this simulation does not depend on the value of Λ and a variety of different Λ values were chosen throughout the simulations.

this Fourier transformation. Obviously these Fourier transformations cannot be computed analytically, so a numerical computation is required. In order to make such a computation two new numerical parameters are introduced, the first being the momentum cut-off for the Fourier transformation, this set to be at least 1.5 times the absolute value of the largest energy eigenvalue ϵ_α. The second parameter being the number of momentum values in the array representing the function, this was taken to be 22001 throughout all the simulations shown in this project.

Lastly we compute the sea contribution(4.50) and the valence contribution(4.63) using their respective formula derived earlier in this section. We use the single cut-off formula (2.54) to get the sea contribution as

$$\begin{aligned}[F_1]_s^{\mp}(x) = \frac{5MN_C}{144}\Big[\sum_\alpha \int_{|Mx\pm|\epsilon_\alpha||}^{\infty} dpp \int d\Omega_p \Big\{ \pm \tilde{\Psi}_\alpha^\dagger(\vec{p})\tilde{\Psi}_\alpha(\vec{p}) - \mathrm{sgn}(\epsilon_\alpha)\frac{Mx_\alpha^\pm}{p}\tilde{\Psi}_\alpha^\dagger(\vec{p})\hat{p}\cdot\vec{\alpha}\tilde{\Psi}_\alpha(\vec{p})\Big\} \\ - \int_{|Mx_\alpha^\pm|}^{\infty} dpp \int d\Omega_p \Big\{ \pm \tilde{\Psi}_\alpha^\dagger(\vec{p})\tilde{\Psi}_\alpha(\vec{p}) - \frac{\omega_0}{M}\tilde{\Psi}_\alpha^\dagger\frac{Mx_\alpha^\pm}{p}\tilde{\Psi}_\alpha^\dagger(\vec{p})\hat{p}\cdot\vec{\alpha}\tilde{\Psi}_\alpha(p)\Big\} \\ + \Lambda^2 \int_{|M\alpha_\alpha^\pm|}^{\infty} dp \int d\Omega_p \Big\{ \frac{\epsilon_\alpha}{2\omega_\alpha^3} Mx\tilde{\Psi}_\alpha^\dagger\hat{p}\cdot\vec{\alpha}\tilde{\Psi}_\alpha \Big\} \\ + \Big\{ -\frac{\Lambda^2}{2\omega_0}Mx_\alpha^\pm \int d\Omega_p \big(\tilde{\Psi}_\alpha^\dagger\tilde{\Psi}_\alpha \pm \frac{\epsilon_\alpha\Lambda^2}{2\omega_0}|Mx_\alpha^\pm|\,\tilde{\Psi}_\alpha^\dagger\hat{p}\cdot\vec{\alpha}\tilde{\Psi}_\alpha\big)\Big\}\Big|_{p=|Mx_\alpha^\pm|}\Big].\end{aligned} \tag{4.68}$$

The numerical parameters introduced for these computations include the upper limit of the Bjorken variable, set to be $D_x = 12$ unless specified otherwise, We then define an equidistant grid $x_i = \frac{i}{N_x}D_x, i = 0, 2, \ldots, N_x$ points of which we compute the structure function, unless specified otherwise this N_x is set to 3500. The numerical integration method used during these simulations is Boole's rule[52]

$$\begin{aligned}\int_{p_0}^{p_N} f(p)dp = \frac{2h}{45}\Big(7f(p_0) + 7f(p_N) + 32 \sum_{i\in\{1,3,\ldots,N-1\}} f(p_i) \\ + 12 \sum_{i\in\{2,6,\ldots,N-2\}} f(p_i) + 14 \sum_{i\in\{4,8,\ldots,N-4\}} f(p_i)\Big),\end{aligned} \tag{4.69}$$

where $N = 4k, k \in \mathbb{Z}^+$. This integration method was used throughout all the computations of both the IUSFs and the Fourier transforms. The last term in Eq. (4.68) requires us to look at values between p_i and p_{i+1}, for some $i \in \mathbb{Z}$, where p_i are discretised momentum values required for numerical integration in momentum space. In order to do so, we interpolate between these values using the formula[52]

$$y = y_i + \frac{(y_{i+1} - y_i)}{p_{i+1} - p_i}(|Mx_\alpha^\pm| - p_i). \tag{4.70}$$

In the case of Eq. (4.68) it would be the term

$$\int d\Omega_p \big(\tilde{\Psi}_\alpha^\dagger\tilde{\Psi}_\alpha \pm \frac{\epsilon_\alpha\Lambda^2}{2\omega_0}|Mx_\alpha^\pm|\,\tilde{\Psi}_\alpha^\dagger\hat{p}\cdot\vec{\alpha}\tilde{\Psi}_\alpha\big).$$

Since our grid is momentum space is very dense, this linear interpolation is sufficient.

An example of these contributions to the structure function in the RF is given in figures 4.2 and 4.3. Figure 4.4 shows that comparison between the RF and the IMF for the sea contribution.

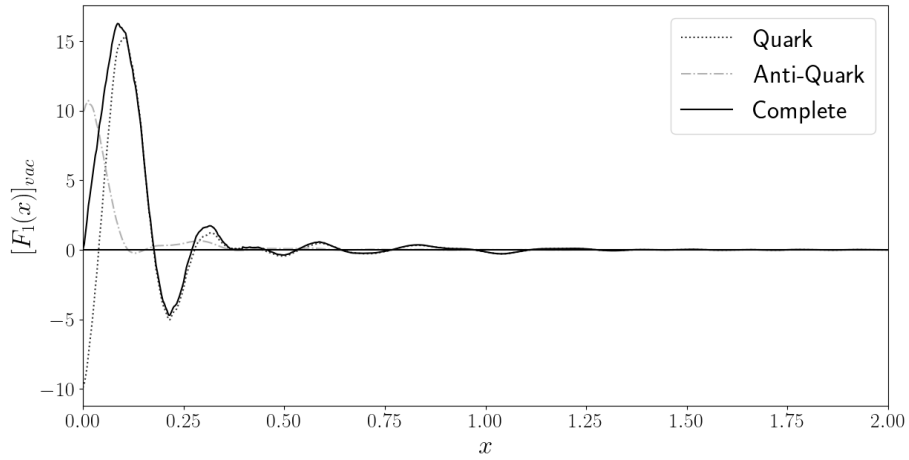

Figure 4.2: Sea contribution to an IUSF for $\Lambda = \Lambda_{\text{new}}$ and $D = 5$fm.

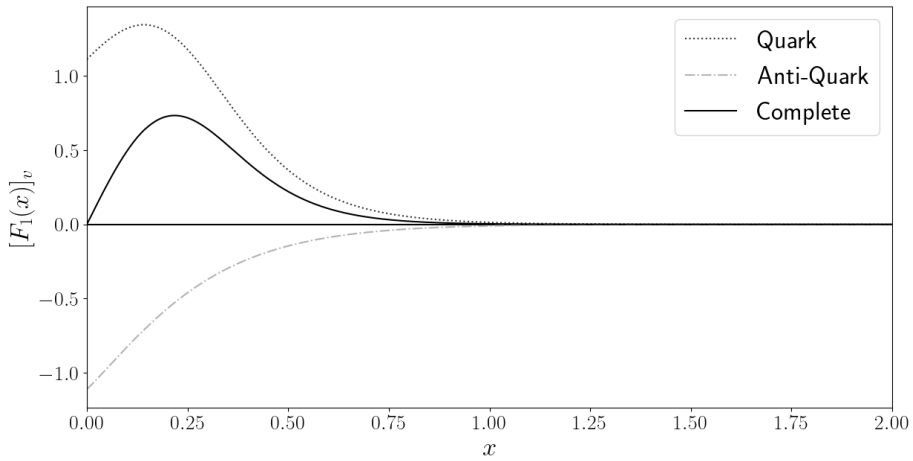

Figure 4.3: Valence contribution to an IUSF for $\Lambda = \Lambda_{\text{new}}$ and $D = 5$fm.

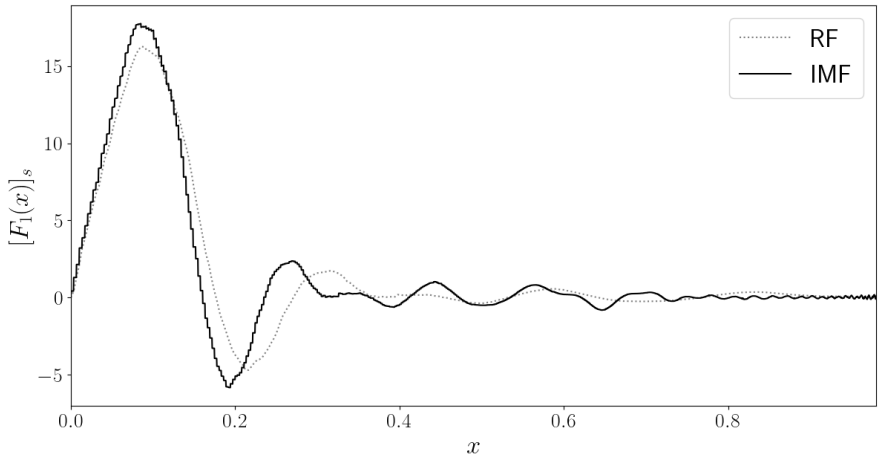

Figure 4.4: Comparison between the RF and IMF for the sea contribution to an IUSF for $\Lambda = \Lambda_{\text{new}}$ and $D = 5$fm.

CHAPTER 5

FIXING THE SUM RULE

5.1 SUM RULES

A useful method for checking the numerical accuracy of the IUSF is through the energy sum rule

$$\frac{36}{5}\int_0^\infty dx x F(x) = \frac{E_{\rm sol}[\Theta]}{M}, \tag{5.1}$$

where $E_{\rm sol}$ is the classical energy of the soliton Eq. (3.39) omitting the local piece, Eq. (3.40). We will exclusively investigate the sea contribution of the energy sum rule as the valence contribution has already proven to be reliable. The sea contribution can be written as the sum of local

$$[F_1(x)]^{\mp}_{s,1} = \frac{5N_C M}{144}\sum_{i=0}^{2}\sum_{\alpha}\int_{|Mx^{\pm}_{\alpha}|}^{\infty} dp \int d\Omega_p(\pm)\tilde{\Psi}^{\dagger}_{\alpha}(\vec{p})\tilde{\Psi}_{\alpha}(\vec{p}) \tag{5.2}$$

and non-local

$$[F_1(x)]^{\mp}_{s,2} = -\frac{5N_C M}{144}\sum_{i=0}^{2}\sum_{\alpha}\int_{|Mx^{\pm}_{\alpha}|}^{\infty} dp \int d\Omega_p \frac{\epsilon_\alpha}{\omega_0}\frac{Mx^{\pm}_{\alpha}}{p}\tilde{\Psi}^{\dagger}_{\alpha}(\vec{p})\hat{p}\cdot\vec{\alpha}\tilde{\Psi}_{\alpha}(\vec{p}) \tag{5.3}$$

terms. It is apt to give a short derivation of the sum rule for these terms as this will allow us to take note of and investigate a few things later in this chapter. We start by integrating the local term as

$$\begin{aligned}
S_{1,s} :=& \frac{36}{5}\int_0^\infty dx x[F_1(x)]_{s,1} \\
=& S^-_{1,s} + S^+_{1,s} := \frac{36}{5}\int_0^\infty dx x([F_1(x)]^-_{s,1} + [F_1(x)]^+_{s,1}) \\
=& \frac{MN_C}{4}\sum_{i=0}^{2}\sum_{\alpha} c_i \int_0^\infty dx x \int d\Omega_p \Big\{\Big[\int_{|Mx^+_\alpha|}^\infty dp p \tilde{\Psi}^{\dagger}_{\alpha}(\vec{p})\tilde{\Psi}_{\alpha}(\vec{p}) \\
& - \int_{|Mx^-_\alpha|}^\infty dp p \tilde{\Psi}^{\dagger}_{\alpha}(\vec{p})\tilde{\Psi}_{\alpha}(\vec{p})\Big] \\
=& \frac{MN_C}{4}\sum_{i=0}^{2}\sum_{\alpha} c_i \int d\Omega_p \Big[\int_0^\infty dx x \int_{|Mx^+_\alpha|}^\infty dp p \tilde{\Psi}^{\dagger}_{\alpha}(\vec{p})\tilde{\Psi}_{\alpha}(\vec{p})\Big] \\
& - \Big[\int_0^\infty dx x \int_{|Mx^-_\alpha|}^\infty dp p \tilde{\Psi}^{\dagger}_{\alpha}(\vec{p})\tilde{\Psi}_{\alpha}(\vec{p})\Big]\Big\}.
\end{aligned} \tag{5.4}$$

Next we perform a variable substitution in the x integrals, $y = x \pm \frac{\omega_0}{M}$

$$\begin{aligned}
&\frac{36}{5}\int_0^\infty dxx[F_1(x)]_{s,1} = M_{1,s} = M_{1,s}^- + M_{1,s}^+ \\
&:= \frac{MN_C}{4}\sum_{i=0}^{2}\sum_\alpha c_i \int d\Omega_p \Big\{\Big[\int_{\frac{\omega_0}{M}}^\infty dy(y-\frac{\omega_0}{M})\int_{|My|}^\infty dpp\tilde{\Psi}_\alpha^\dagger(\vec{p})\tilde{\Psi}_\alpha(\vec{p})\Big] \\
&\quad -\Big[\int_{-\frac{\omega_0}{M}}^\infty dy(y+\frac{\omega_0}{M})\int_{|My|}^\infty dpp\tilde{\Psi}_\alpha^\dagger(\vec{p})\tilde{\Psi}_\alpha(\vec{p})\Big]\Big\}.
\end{aligned} \tag{5.5}$$

The terms linear in y cancel, and it is simple to complete the calculation

$$\begin{aligned}
\frac{36}{5}\int_0^\infty dxx[F_1(x)]_{s,1} &= -\frac{N_C}{2}\sum_{i=0}^{2}\sum_\alpha c_i\omega_0\int_0^\infty dy\int_{|My|}^\infty dpp\Big[\int d\Omega_p\tilde{\Psi}_\alpha^\dagger(\vec{p})\tilde{\Psi}_\alpha(\vec{p})\Big] \\
&= \frac{N_C}{2}\sum_{i=0}^{2}\sum_\alpha c_i\omega_0\int_0^\infty dyy\frac{d}{dy}\int_{|My|}^\infty\Big[\int d\Omega_p\tilde{\Psi}_\alpha^\dagger(\vec{p})\tilde{\Psi}_\alpha(\vec{p})\Big] \\
&= -\frac{N_C}{2M}\sum_{i=0}^{2}\sum_\alpha c_i\omega_0\int_0^\infty dzz^2\Big[\int\Omega_p\tilde{\Psi}_\alpha^\dagger(\vec{p})\tilde{\Psi}_\alpha(\vec{p})\Big] \\
&= -\frac{N_C}{2M}\sum_{i=0}^{2}\sum_\alpha c_i\sqrt{\epsilon_\alpha^2+\Lambda_i^2} = \frac{E_s}{M}.
\end{aligned} \tag{5.6}$$

In the second line we wrote $1 = \frac{d}{dy}y$ and integrated by parts, obviously there is no boundary contribution. This formula shows that this part of the sum rule should work level-by-level i.e. for each individual α in the sum it should hold true. The numerical simulations will include the subtraction of the $F(r) = 0$ terms, see Eq. (4.61). We will also find it necessary to look at the simulation of the term just after the variable substitution (5.5), which we will call the mid point result $M_{1,s}$. This can be calculated numerically by using the single cut-off formula (2.54),

$$M_{1,s}^- = \Big[\int_{\frac{|\epsilon_\alpha|}{M}}^\infty dy(y-\frac{|\epsilon_\alpha|}{M})f_\alpha(y)\Big] - \Big[\int_{\frac{\omega_0}{M}}^\infty dy(y-\frac{\omega_0}{M})f_\alpha(y)\Big] - \frac{\Lambda^2}{2M\omega_0}\int_{\frac{\omega_0}{M}}^\infty f_\alpha(y)dy, \tag{5.7}$$

and

$$\begin{aligned}
M_{1,s}^+ = -\Big[&\int_0^\infty dy(y+\frac{|\epsilon_\alpha|}{M})f_\alpha(y) + \int_0^{\frac{|\epsilon_\alpha|}{M}} dy(\frac{|\epsilon_\alpha|}{M}-y)f_\alpha(y) \\
&- \int_0^\infty dy(y+\frac{\omega_0}{M})f_\alpha(y) - \int_0^{\frac{\omega_0}{M}} dy(\frac{\omega_0}{M}-y)f_\alpha(y) \\
&+ \frac{\Lambda^2}{2\omega_0 M}\int_0^\infty dyf_\alpha(y) + \frac{\Lambda^2}{2\omega_0 M}\int_0^{\frac{\omega_0}{M}} dyf_\alpha(y)\Big],
\end{aligned} \tag{5.8}$$

where the notation

$$f_\alpha(y) = \int_{|My|}^\infty dpp\int d\Omega_p\tilde{\Psi}_\alpha^\dagger(\vec{p})\tilde{\Psi}_\alpha(\vec{p}) \tag{5.9}$$

is used for brevity. In the above we have used that $f_\alpha(-y) = f_\alpha(y)$. One last thing to note is that the sum rule still needs to include its non-solitonic subtraction

$$S_{1,\text{vac}} = S_{1,s} - S_{1,s}^{(0)} \tag{5.10}$$

$$M_{1,\text{vac}} = M_{1,s} - M_{1,s}^{(0)} \tag{5.11}$$

$$\frac{E_{\text{vac}}}{M} = \frac{E_s}{M} - \frac{E_s^{(0)}}{M}. \tag{5.12}$$

To derive the sum rule for the non-local term we start again through its integration [1, 2]

$$\begin{aligned}
S_{2,s} :=& \frac{36}{5}\int_0^\infty dx x[F_1(x)]_{s,2} \\
=& -\frac{MN_C}{4}\sum_\alpha\sum_{i=0}^{2} c_i\frac{\epsilon_\alpha}{\omega}\int_0^\infty dx\Big[\int_{|Mx+\omega_0|}^\infty dp(Mx+\omega_0)\int d\Omega_p\tilde{\Psi}_\alpha^\dagger\hat{p}\cdot\vec{\alpha}\tilde{\Psi}_\alpha \\
&+\int_{|Mx-\omega_0|}^\infty dp(Mx-\omega_0)\int d\Omega_p\tilde{\Psi}_\alpha^\dagger\hat{p}\cdot\vec{\alpha}\tilde{\Psi}_\alpha\Big] \\
=&\frac{MN_C}{4}\sum_\alpha\sum_{c_1=0}^{2} c_i\frac{\epsilon_\alpha}{\omega_0}\Big[\int_{\frac{\omega_0}{M}}^\infty dy(y-\frac{\omega_0}{M})My\int_{|My|}^\infty dp\int d\Omega_p\tilde{\Psi}_\alpha^\dagger\hat{p}\cdot\vec{\alpha}\tilde{\Psi}_\alpha \\
&+\int_{-\frac{\omega_0}{M}}^\infty dy(y+\frac{\omega_0}{M})\int_{|My|}^\infty dp\int d\Omega_p\tilde{\Psi}_\alpha^\dagger\hat{p}\cdot\vec{\alpha}\tilde{\Psi}_\alpha\Big] \\
=& -\frac{M^2N_C}{2}\sum_\alpha\sum_{i=0}^{2} c_i\frac{\epsilon_\alpha}{\omega_0}\int_0^\infty dyy^2\int_{|My|}^\infty dp\int\Omega_p\tilde{\Psi}_\alpha^\dagger\hat{p}\cdot\vec{\alpha}\tilde{\Psi}_\alpha \\
=& -\frac{M^3N_C}{6}\sum_\alpha\sum_{i=0}^{2} c_i\frac{\epsilon_\alpha}{\sqrt{\epsilon_\alpha^2+\Lambda_i^2}}\int_0^\infty dyy^3\Big[\int_{|My|}^\infty dp\int\Omega_p\tilde{\Psi}_\alpha^\dagger\hat{p}\cdot\vec{\alpha}\tilde{\Psi}_\alpha\Big]\Big|_{p=My} \\
=& -\frac{N_C}{6M}\sum_\alpha\sum_{i=0}^{2} c_i\frac{\epsilon_\alpha}{\sqrt{\epsilon_\alpha^2+\Lambda_i^2}}\int_0^\infty dpp^2\int\Omega_p\tilde{\Psi}_\alpha^\dagger\vec{\alpha}\cdot\vec{p}\tilde{\Psi}_\alpha \\
=& M_{2,s} := -\frac{N_C}{6M}\sum_\alpha\sum_{i=0}^{2} c_i\frac{\epsilon_\alpha}{\sqrt{\epsilon_\alpha^2+\Lambda_i^2}}\langle\alpha|\vec{\alpha}\cdot\vec{\partial}|\alpha\rangle .
\end{aligned} \tag{5.13}$$

We relate the last matrix element to the soliton via Eq. (3.12) so that

$$\begin{aligned}
0 = \langle\alpha|[\vec{x}\cdot\vec{\partial},h]|\alpha\rangle = \langle\alpha|[\vec{x}\cdot\vec{\partial}]|\alpha\rangle + \langle\alpha|\beta m(\vec{x}\cdot\vec{\partial}U_5)|\alpha\rangle \\
\implies \langle\alpha|\beta m(\vec{x}\cdot\vec{\partial}U_5)|\alpha\rangle = -\langle\alpha|[x_i,\alpha_j p_j]\partial_i|\alpha\rangle = \langle\alpha|-i\vec{\alpha}\cdot\vec{\partial}|\alpha\rangle
\end{aligned} \tag{5.14}$$

This shows that

$$M_{2,s} \sim \sum_\alpha\langle\alpha|\left(\beta m(\vec{x}\cdot\vec{\partial}\{U(\vec{x})\}^{\gamma_5})\right)|\alpha\rangle . \tag{5.15}$$

The valence part has a similar contribution

$$M_{2,\mathrm{v}} \sim \langle\mathrm{v}|\left(\beta m(\vec{x}\cdot\vec{\partial}\{U(\vec{x})\}^{\gamma_5})\right)|\mathrm{v}\rangle . \tag{5.16}$$

In total $M_{2,s}+M_{2,v}$ is the coefficient of $s-1$ in the expansion

$$E(s) = E[U(s\vec{x})] = E_0 + (1-s)E_1 + \cdots(1-s)^n E_n + \cdots \tag{5.17}$$

of the classical energy. Since $U(\vec{x})$ minimises the energy functional we have $\frac{\partial E(s)}{\partial s}|_{s=1} = 0$ and thus $E_1 = 0$ thereby verifying the sum rule. Note that the integral of the non-local part does not vanish level by level. Rather it emerges, along with the non-local part of the valence contribution, from the variation of the total energy under the scaling transformation of the hedgehog field. Again we need to subtract the non-solitonic part

$$S_{2,\mathrm{vac}} = S_{2,s} - S_{2,s}^{(0)}, \tag{5.18}$$

$$M_{2,\mathrm{vac}} = M_{2,s} - M_{2,s}^{(0)}. \tag{5.19}$$

We will verify the accuracy of the non-local term of the IUSF by comparing its sum rule to $M_{2,s}$, note that this comparison is valid level-by-level.

As already mentioned, it was found that a small miscalculation was made for Λ. After correcting this calculation, we discovered that the numerical values for $S_{1,\mathrm{vac}}$ and $\frac{E_{\mathrm{vac}}}{M}$ of the sum rule did not match (see Table 5.2). A naive approach to solving this problem was to simply increase the momentum cut-off k_{cut} or to increase the size of the spherical box D, as shown in Table 5.1. This should act as a suitable cure since it brings the simulation closer to the continuum limit, however, as can be seen on the table 5.1 it did not prove to be as effective as one would have hoped. We note that stability has already been reached for the soliton energy as it is invariant under the changes of the distance D and the momentum cut-off k_{cut}.

After this another approach was attempted; before Fourier transforming the quark wavefunctions in po-

D	k_{cut}	k_{dist}	D_x	Renormalised	$S_{1,\text{vac}}$	$M_{1,\text{vac}}$	$\frac{E_{\text{vac}}}{M}$
5fm	2956.3MeV	4434.5MeV	12	No	0.22115	0.63514	0.63512
6fm	2956.3MeV	4434.5MeV	12	No	0.88231	0.63321	0.63324
4fm	2956.3MeV	4434.5MeV	12	No	0.20141	0.63399	0.63414
3fm	2956.3MeV	4434.5MeV	12	No	0.20141	0.63398	0.63415
5fm	4434.5MeV	6651.8MeV	12	No	1.4908	0.63232	0.63241
5fm	2217.2MeV	3325.9MeV	12	No	0.67527	0.63584	0.63589
5fm	1847.7MeV	2771.6MeV	12	No	0.65256	0.64141	0.64147
5fm	2956.3MeV	4434.5MeV	12	Yes	0.21909	0.63513	0.63513

Table 5.1: Simulations for $\Lambda = \Lambda_{\text{new}}$ with varying k_{cut}, D and renormalisation, see Eqs. (5.20) and (5.21).

Λ	$S_{1,s}$	$M_{1,s}$	$\frac{E_{\text{vac}}}{M}$
$\Lambda = \Lambda_{\text{old}}$	0.61601	0.63535	0.63538
$\Lambda = \Lambda_{\text{new}}$	0.22090	0.63511	0.63514
Λ = 720.0MeV	0.63530	0.63358	0.63360
Λ = 760.0MeV	0.62803	0.63585	0.63587

Table 5.2: Table of the local term contributions for D = 5fm, D_x = 12 and k_{cut} = 7.390964.

sition space are normalised as $\int_0^D dx \int d\Omega x^2 \Psi_\alpha^\dagger(\vec{x})\Psi_\alpha(\vec{x}) = 1$, the computation of this was correct to very high accuracy. After the Fourier transformation the normalisation $\int_0^{k_{\text{dist}}} dp \int d\Omega_p p^2 \tilde{\Psi}_\alpha^\dagger(\vec{p})\tilde{\Psi}_\alpha(\vec{p}) = 1$ was only correct up to the 2nd or 3rd decimal place, being better for levels with small energy eigenvalues. It was then conjectured that this could be causing the issue. Unfortunately increasing the number of momentum grid points, from 22001 to 33001, for the Fourier transform, did not increase the accuracy of the normalisation. Therefore, we attempted to "renormalise" these wavefunctions. This involved simply taking the inner product of the quark wavefunction after the Fourier transformation

$$\int_0^\infty dp \int d\Omega_p p^2 \tilde{\Psi}_\alpha^\dagger(\vec{p})\tilde{\Psi}_\alpha(\vec{p}) = c, \tag{5.20}$$

and creating a new quark wavefunction

$$\tilde{\Psi}_{\alpha,\text{new}}(\vec{p}) = \frac{1}{\sqrt{c}}\tilde{\Psi}_\alpha(\vec{p}), \tag{5.21}$$

which is properly normalised. The sum rules resulting from these wavefunctions are also listed in table 5.1.

Ultimately none of these previously mentioned attempts solved the problem. On the contrary, as the momentum cut-off k_{cut} decreased, we observed an increase in the accuracy of the sum rules.[1] This warranted further investigation. Since the sum rules for $[F_1(x)]$ are true level-by-level, plots can be produced for each level; Figure 5.1 shows graphs for each side of the sum rule, including the mid point $M_{1,s}$ values, for each quark level of the vacuum contribution for both the local and non-local terms restricted to $G = 0$. This demonstrates that the sum rule for this case is satisfactorily accurate for Λ_{old}.

Following this, we produce similar graphs for grand spins $G = 1$ and $G = 5$, as shown in Figs. 5.2 and 5.3 respectively. These figures lead us to conclude that as the grand spin number increases, the level-by-level sum rules stay accurate especially at lower grand spins where the contributions of each energy level are more significant. Contrary to this is the sum rule for $\Lambda = \Lambda_{\text{new}}$ with identical numerical parameters, see Figs. 5.4 and 5.5. The summation of these terms as given in table 5.2 show this sum rule is far less accurate for the correct cut-off at higher grand spins. This information shows that the accuracy for the sum rule for Λ_{old} may very well have been a welcome accident.

Figs. 5.6 and 5.7 show contributions to the sum rule for a reduced k_{cut}. As seen in table 5.1 this reduced k_{cut} resulted in higher accuracy sum rules. This was also particularly peculiar.

[1] Accuracy is measured through the difference of the term being evaluated (in this case, the left-hand side ($S_{1,s}$ for the local and $S_{2,s}$ for the non-local) of the sum rule) and a base term, which is the right-hand side ($\frac{E_S}{M}$ for the local and $M_{2,s}$ for the non-local) of the sum rule.

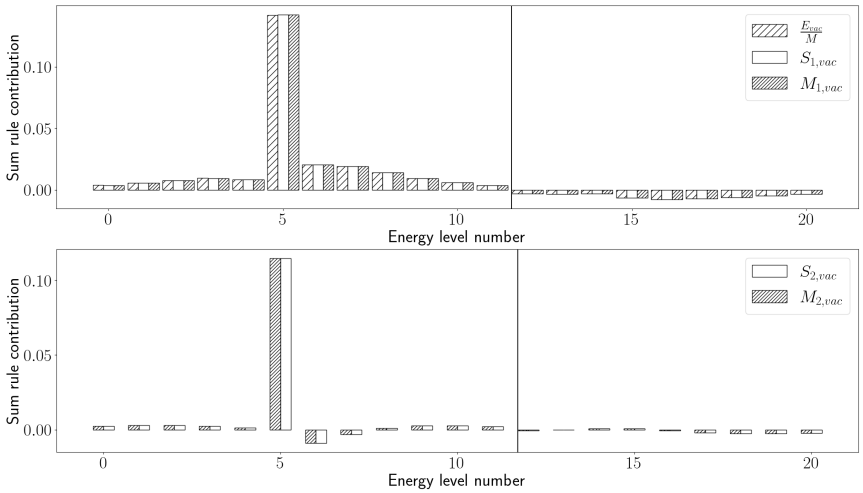

Figure 5.1: Comparison of the contributions to the sum rule given by $S_{1,s}$, $S_{2,s}$, $M_{1,s}$, $M_{2,s}$ and $\frac{E_S}{M}$ for each energy level for $\Lambda = \Lambda_{\text{old}}$, grand spin $G = 0$ and $k_{\text{cut}} = 2956.3$MeV. These contributions are seperated into graphs for the local (top) and non-local (bottom) parts. The horizontal axis counts the states and the vertical axis is the amount contributed to the sum rule. The highest contribution comes from the valence level. A black line seperates the positive intrinsic parity states (on the left) and the negative intrinsic parity states (on the left). The quark energy levels that contribute less than 2% than that of the largest contribution are not displayed, this is in order to make the graphs more readable.

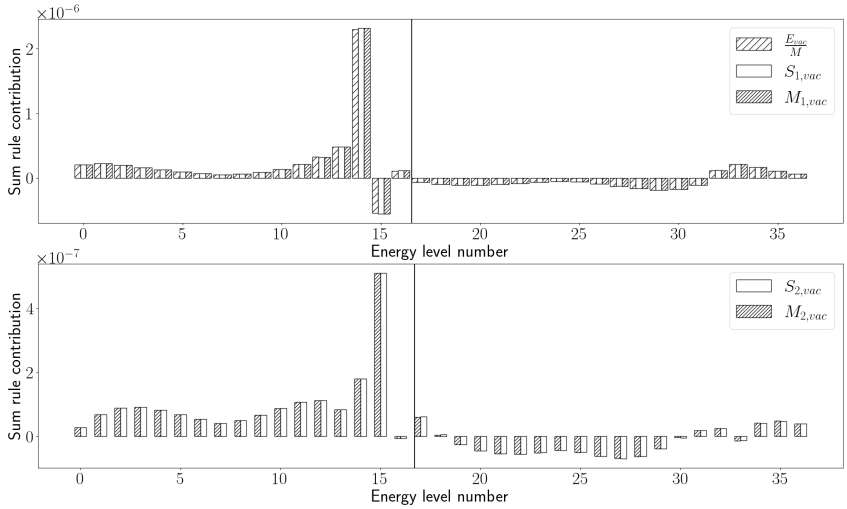

Figure 5.2: Comparison of sum rule contributions by energy level for $\Lambda = \Lambda_{\text{old}}$, grand spin $G = 1$ and $k_{\text{cut}} = 2956.3$MeV. For further details see Fig. 5.1.

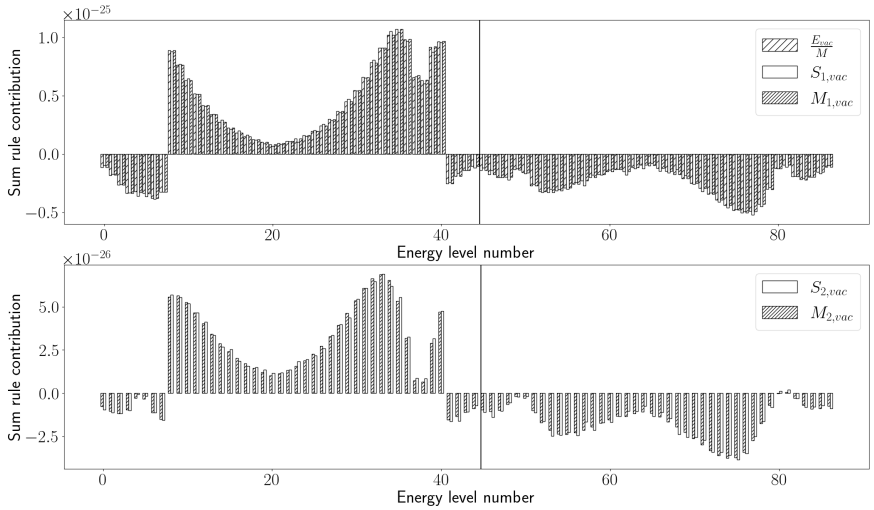

Figure 5.3: Comparison of sum rule contributions by energy level for $\Lambda = \Lambda_{\text{old}}$, grand spin $G = 5$ and $k_{\text{cut}} = 2956.3\text{MeV}$. The quark energy levels that contribute less than 10% than that of the largest contribution are not displayed. For further details see Fig. 5.1.

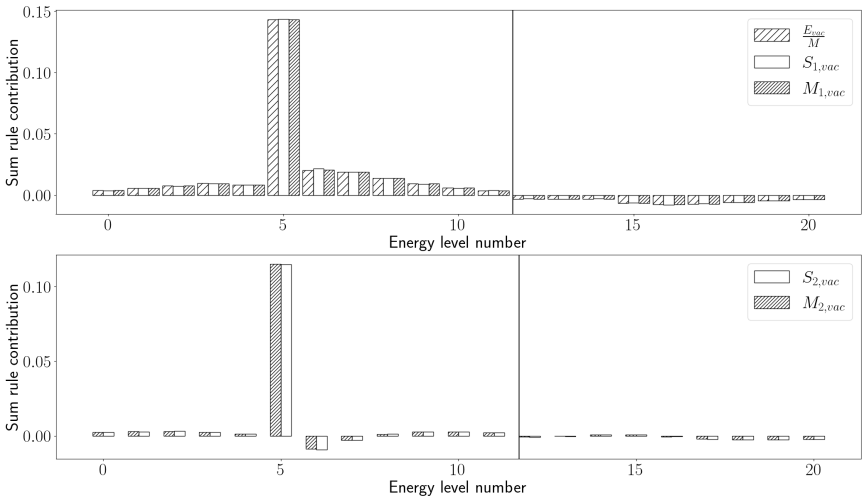

Figure 5.4: Comparison of sum rule contributions by energy level for $\Lambda = \Lambda_{\text{new}}$, grand spin $G = 0$ and $k_{\text{cut}} = 2956.3\text{MeV}$. For further details see Fig. 5.1.

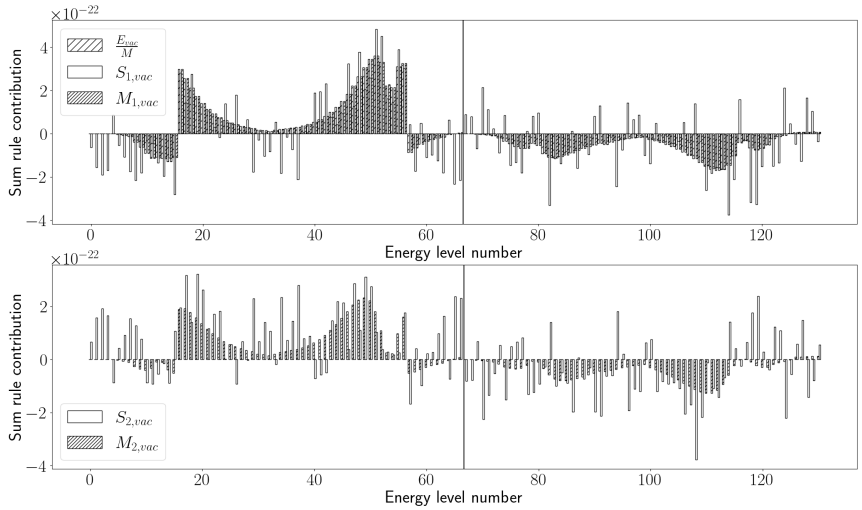

Figure 5.5: Comparison of sum rule contributions by energy level for $\Lambda = \Lambda_{\text{new}}$, grand spin $G = 5$ and $k_{\text{cut}} = 2956.3$MeV. The quark energy levels that contribute less than 10% than that of the largest contribution are not displayed. For further details see Fig. 5.1.

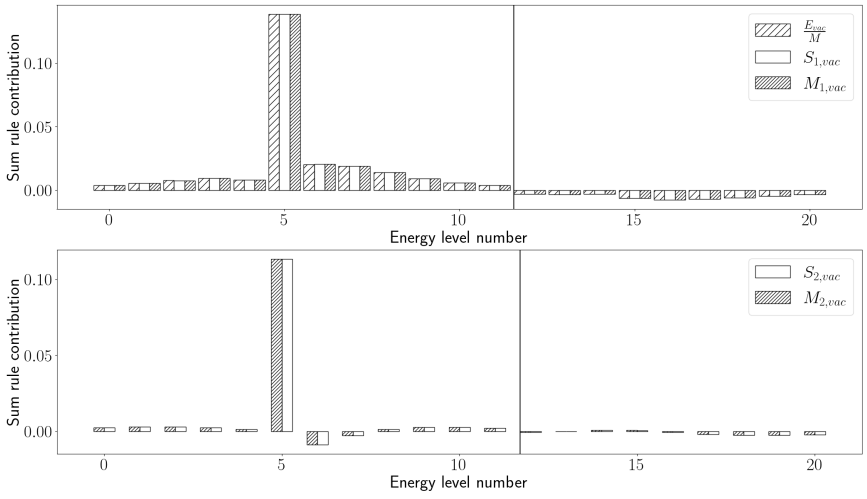

Figure 5.6: Comparison of sum rule contributions by energy level for $\Lambda = \Lambda_{\text{new}}$, grand spin $G = 0$ and $k_{\text{cut}} = 2217.2$MeV. For further details see Fig. 5.1.

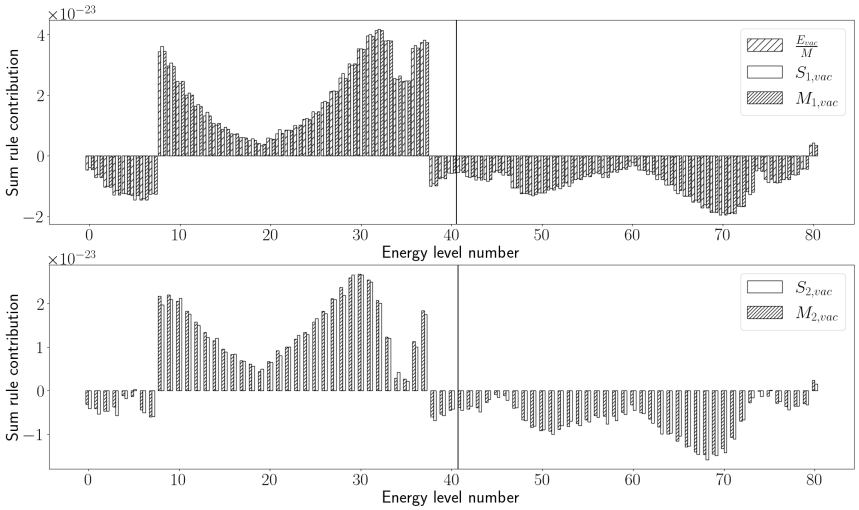

Figure 5.7: Comparison of sum rule contributions by energy level for $\Lambda = \Lambda_{\text{new}}$, grand spin $G = 5$ and $k_{\text{cut}} = 2217.2$MeV. The quark energy levels that contribute less than 10% than that of the largest contribution are not displayed. For further details see Fig. 5.1.

In all graphs we recognise that the mid point results agree with the relevant contribution to the classical energy. However the left-hand side of the sum rule, $S_{1,\text{vac}}$ does not. This means that the integration over the Bjorken x with its endpoint involving absolute values generates the problem. It is now prudent to ask which term(s) in these equations is causing such a discrepancy. To do so, we look at Eqs. (5.7) and (5.8). These are the anti-quark and quark contributions, respectively. Figure 5.8 show these contributions after the non-solitonic subtraction plotted against their sum rule counterparts $S^{-}_{1,\text{vac}}$ and $S^{+}_{1,\text{vac}}$ for $G = 0$. The contributions for $G = 5$ are given in figure 5.9. This shows that with increasing grand spin the discrepancy between the two expressions in the sum rule grows. Furthermore, the discrepancies are far more prevalent for the quark contributions than for the anti-quark ones.

Since the inaccuracy of the sum rule was for the most part coming from the quark contribution which included an absolute value term in the integration boundary, it is likely that a smaller step size should remedy the issue. This is because absolute values can be very sensitive towards to large a step size. In addition, all contributions are effectively zero when $x \geq 3$. Given this information another change in the numerical parameters can be made. New simulations are performed with lowering the Bjorken variable cut-off to $D_x = 4$. Since we keep the total number of points for $x \in [0, D_x]$ fixed, decreasing D_x amounts to even smaller step sizes. These smaller step size should allow the simulation to properly integrate the IUSF. And indeed, this fixes the problem. Note that the earlier value $\Delta x = \frac{12}{3500} = 0.003$ was already quite small which is why it was previously considered appropriate. Following this additional simulations were done where D_x was increased and the number of steps N_x was increased appropriately. For information on these simulations consider table 5.3. The data for $S_{1,\text{vac}}$ and the corresponding contribution to $\frac{E_{vac}}{M}$ agree to a much better accuracy than in tables 5.2 and 5.1. Figures 5.10, 5.11, show a few plots for these new simulations for Λ_{new}. Since these simulations also had sum rules within a reasonable degree of accuracy the problem can be considered solved. Figure 5.12 shows the IUSF sea contribution with the decreased step size. The graph in this figure exhibits a large number of smaller oscillations about the function's path as it decays. Originally these were not seen or accounted for. If we were to increase D_x then a smaller step size would also be needed, this would be due to higher frequency oscillations of the IUSF contributions at larger x values.

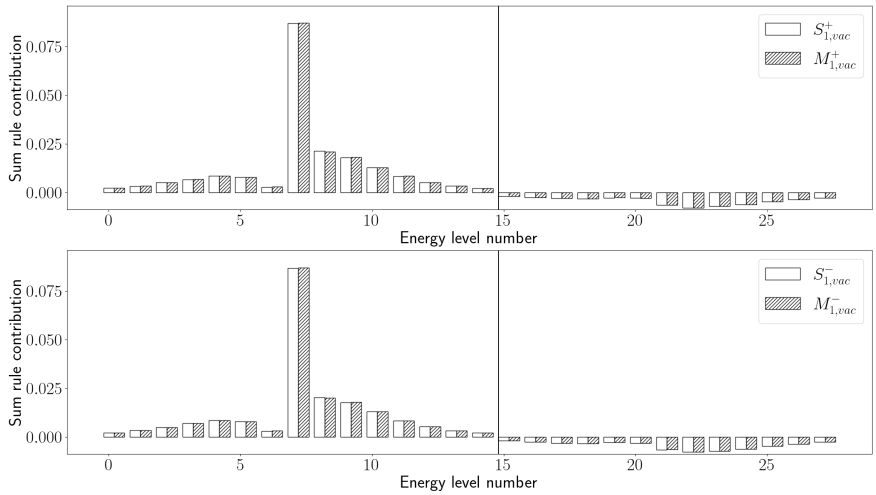

Figure 5.8: Sum rule (anti-)quark contributions for $\Lambda = \Lambda_{\text{new}}$, $k_{\text{cut}} = 2956.3\text{MeV}$ and grand spin $G = 0$. The quark contribution is displayed at the top and the anti-quark contribution is displayed at the bottom. The black line separates the positive intrinsic parity contributions (left side) from the negative intrinsic parity contributions (right side). The quark energy levels that contribute less than 2% than that of the largest contribution are not displayed, this is in order to make the graphs more readable.

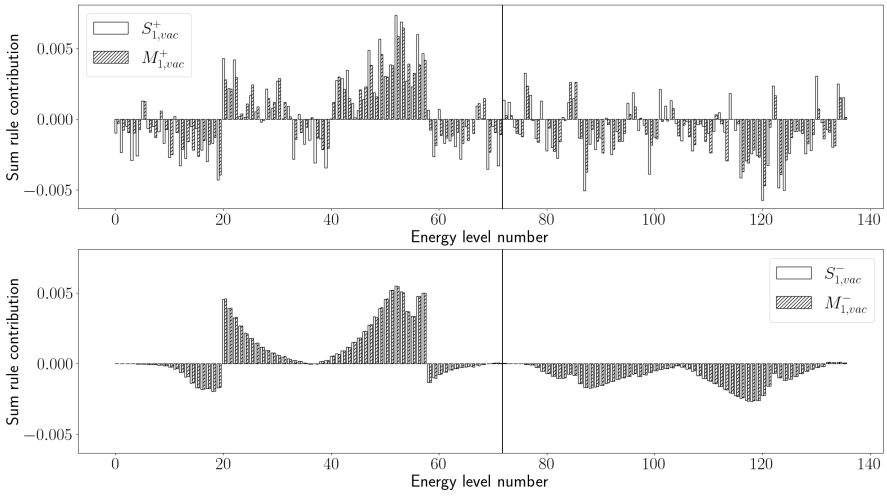

Figure 5.9: Sum rule (anti-)quark contributions for $\Lambda = \Lambda_{\text{new}}$, $k_{\text{cut}} = 2956.3\text{MeV}$ and grand spin $G = 5$. The quark energy levels that contribute less than 10% than that of the largest contribution are not displayed. For further details see Fig. 5.8.

Λ	D	D_x	N_x	$S_{1,s}$	$M_{1,s}$	$\frac{E_{\text{sol}}}{M}$
Λ_{new}	5fm	4.0	3500	0.65617	0.63511	0.63513
Λ_{new}	5fm	5.0	5000	0.66155	0.63511	0.63513
Λ_{new}	6fm	4.0	3500	0.67651	0.63665	0.63666
Λ_{new}	7.5fm	4.0	3500	0.61009	0.63746	0.63744
Λ_{old}	5fm	4.0	3500	0.62941	0.63535	0.63537
Λ_{old}	5fm	5.0	5000	0.66138	0.63535	0.63537
720MeV	5fm	4.0	3500	0.63565	0.63357	0.63360
720MeV	5fm	5.0	5000	0.64603	0.63357	0.63360
760MeV	5fm	4.0	3500	0.62934	0.63585	0.63587
760MeV	5fm	5.0	5000	0.64693	0.63585	0.63587

Table 5.3: Table of the local term contribution for $k_{\text{cut}} = 2956.3$, for the mid point $M_{1,s}$, the $S_{1,s}$ and $\frac{E_s}{M}$.

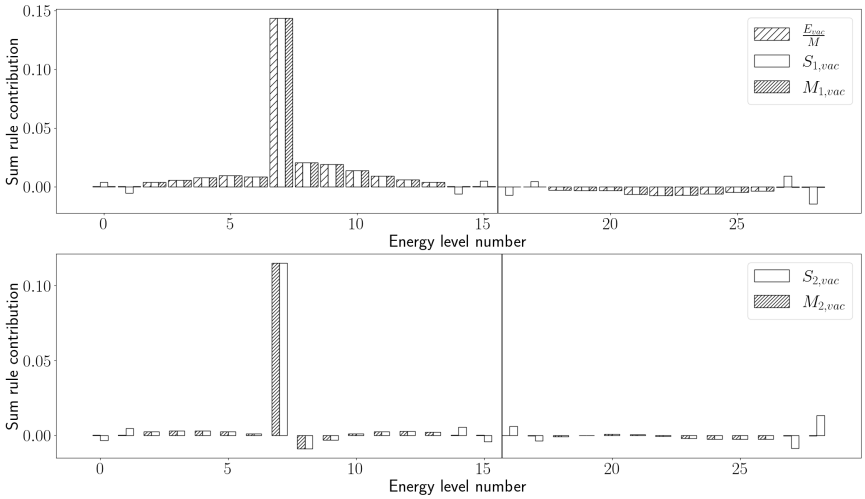

Figure 5.10: Comparison of sum rule contributions by energy level for $\Lambda = \Lambda_{\text{new}}$, grand spin $G = 0$, $k_{\text{cut}} = 2956.3$MeV, $D = 10$fm, $D_x = 4.0$ and $N_x = 3500$. These contributions are separated into graphs for the local and non-local parts. The quark energy levels that contribute less than 2% than that of the largest contribution are not displayed, this is in order to make the graphs more readable.

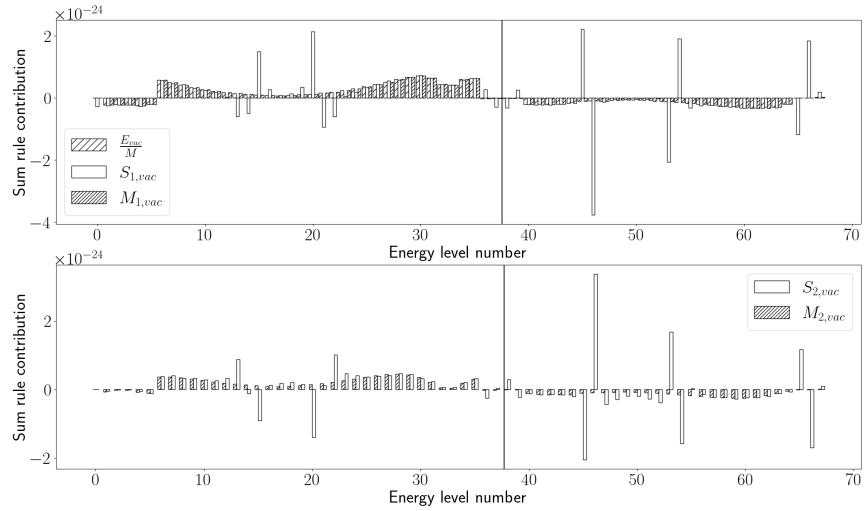

Figure 5.11: Comparison of sum rule contributions by energy level for grand spin $G = 5$. The quark energy levels that contribute less than 5% than that of the largest contribution are not displayed. For further details see Fig. 5.10.

5.2 The Regularisation of the Iso-singlet Unpolarised Nucleon Structure Function

With the issue of the sum rules resolved, some investigation into the unusual nature of the sea contribution to the IUSF can now take place. Despite the improvement in the accuracy of the function no great change in the behaviour of the functions can be noticed, see figures 5.12 and 5.13. Figure 5.13 shows the IUSF in both the IMF and RF. Note that unless explicitly stated all the graphs are in the RF of the nucleon.

Separating the IUSF into its grand spin contributions the unusual nature of the decay of the function at all grand spins is still visible, see Fig. 5.14 and 5.15. Meaning that the unusual decay is not due to a certain grand spin contribution. However, more insight may be gained by exploring the role of individual energy levels for a given grand spin. Figures 5.16, 5.17 and 5.18 show the contributions of three different energy levels to the IUSF, note the difference in scale between each graph. As is to be expected the level whose energy eigenvalue is closer to the threshold i.e. the constituent quark mass, has a more significant contribution to the behaviour of the IUSF. Additionally, the behaviours of the energy level contributions are also unusual. So the possibility of it being an emergent property of the summation of the individual energy levels is also quite unlikely.

The aim now is to alter the behaviour of the sea contribution such that the sum rule still holds and the IUSF shows a behaviour that fits experimental results, empirical results for deep inelastic lepton-nucleon scattering of a low renormalisation (as this model corresponds to) are shown in Ref.[15]. The simplest alteration that can be made is to alter the box size D, as mentioned previously, increasing this would bring the simulation closer to the continuum limit, possibly leading to a change in the behaviour of the IUSF. If the IUSF is shown to be sensitive to the box boundary at the size it is now $D = 10$fm it would mean that despite the soliton behaviour being stable at this limit the IUSF may still need it increased. Through figures 5.19, 5.20, 5.21 and 5.22 it can be seen that the IUSF does change when one changes the box size D. The change, however, is not so much as the change in the structure function behaviour as it is in the values of the extrema. This does not seem to come close to resolving the problem, but it does show that the IUSF is sensitive to the numerical parameters of the simulation. Note that as we change the box size D the sum rules is maintained, see table 5.3. To give some further information the contribution from solely grand spin $G = 0$ can also be shown, see figure 5.23.

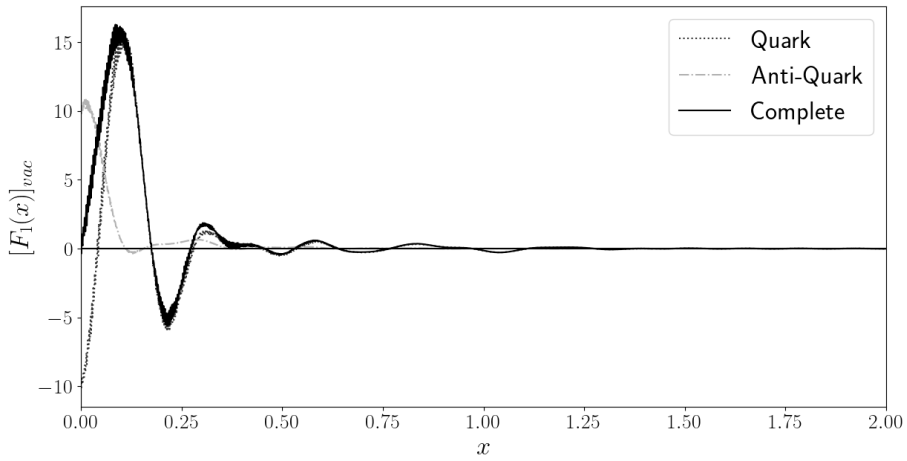

Figure 5.12: Sea contribution to the IUSF for $\Lambda = \Lambda_{\text{new}}$, $k_{\text{cut}} = 2956.3$MeV, $D = 5$fm and $D_x = 4.0$. It has been separated into its quark and anti-quark contributions.

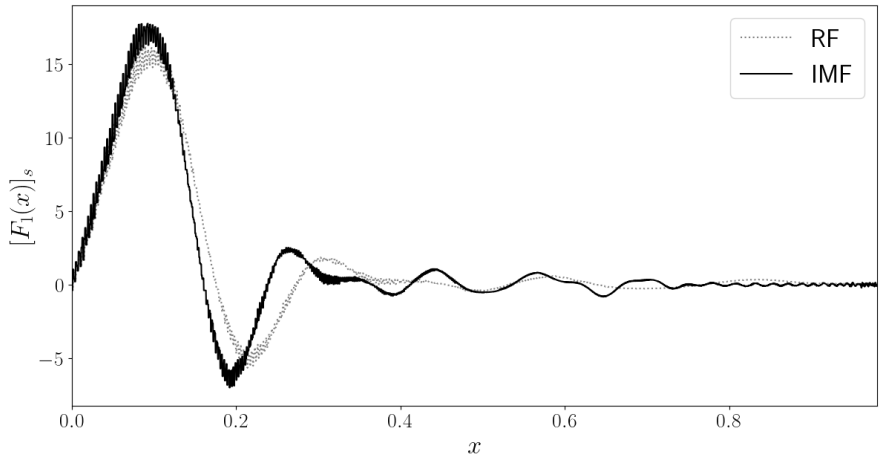

Figure 5.13: Sea contribution to the IUSF for $\Lambda = \Lambda_{\text{new}}$, $k_{\text{cut}} = 2956.3$MeV, $D = 5$fm and $D_x = 4.0$. Displayed in the rest frame(RF) and infinite momentum frame.

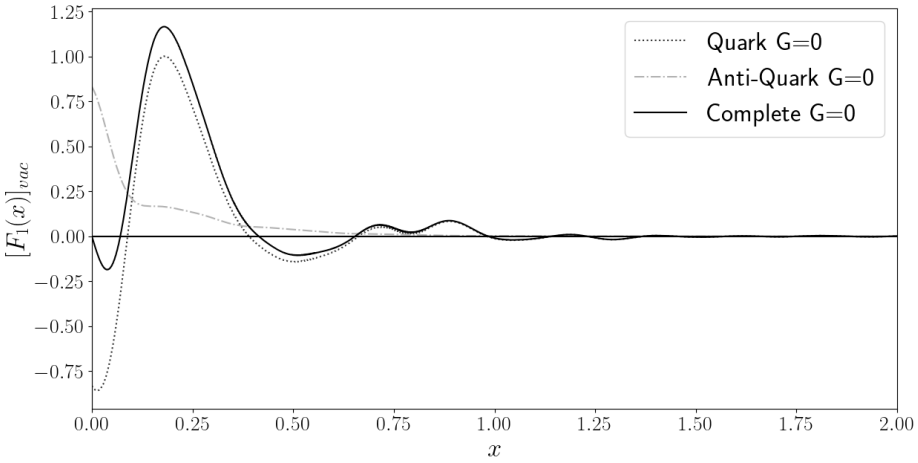

Figure 5.14: Sea contribution to the IUSF for grand spin $G = 0$. For further details see Fig. 5.12.

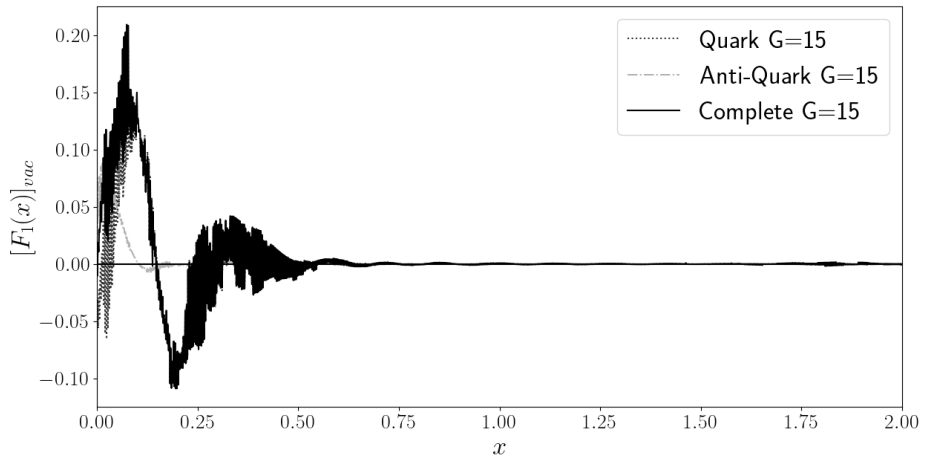

Figure 5.15: Sea contribution to the IUSF for grand spin $G = 15$. For further details see Fig. 5.12.

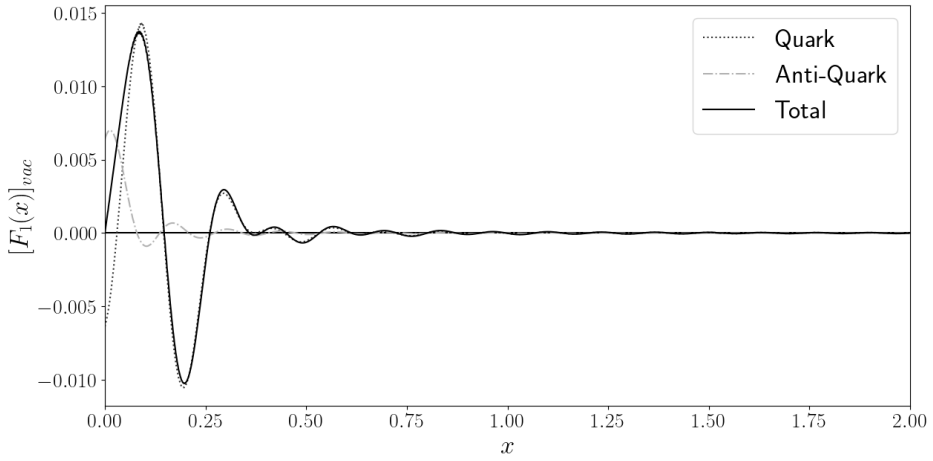

Figure 5.16: Sea contribution to the IUSF for grand spin $G = 0$ and energy eigenvalue $\epsilon = -2902.4$MeV. For further details see Fig. 5.12.

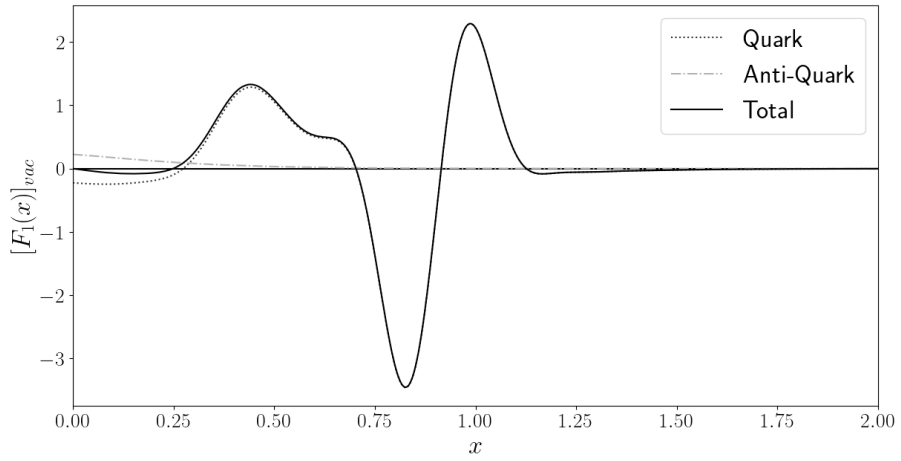

Figure 5.17: Sea contribution to the IUSF for grand spin $G = 0$ and energy eigenvalue $\epsilon = 216.78$MeV. For further details see Fig. 5.12.

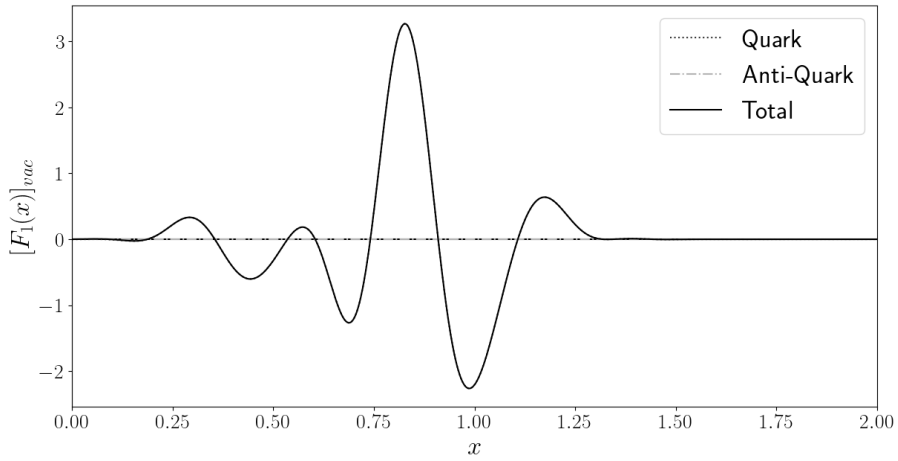

Figure 5.18: Sea contribution to the IUSF for grand spin $G = 0$ and energy eigenvalue $\epsilon = 428.37$MeV. For further details see Fig. 5.12.

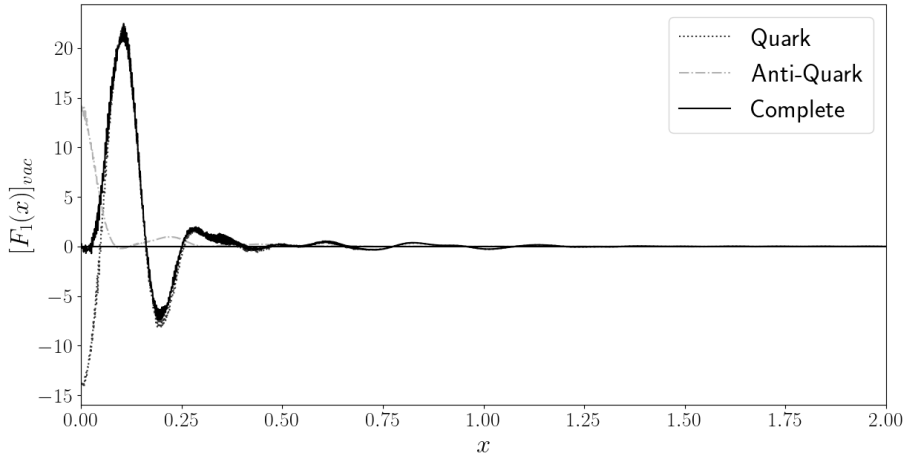

Figure 5.19: Sea contribution to the IUSF for $D = 4$fm. For further details see Fig. 5.12.

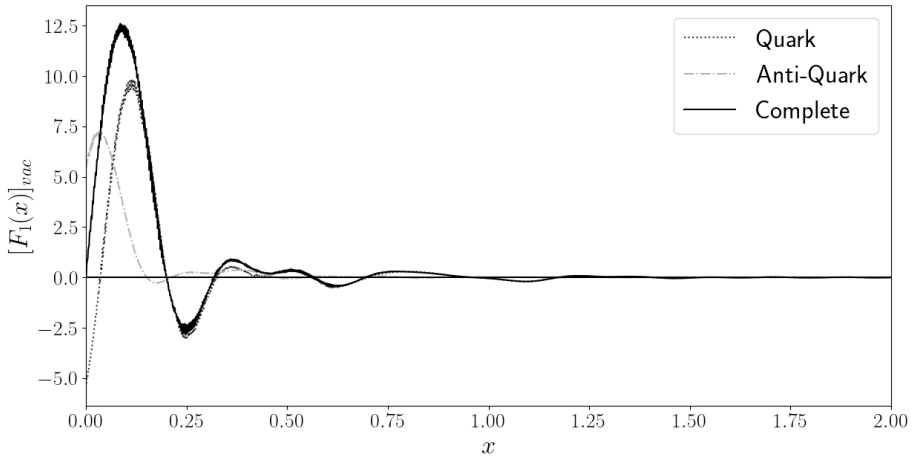

Figure 5.20: Sea contribution to the IUSF for $D = 6$fm. For further details see Fig. 5.12.

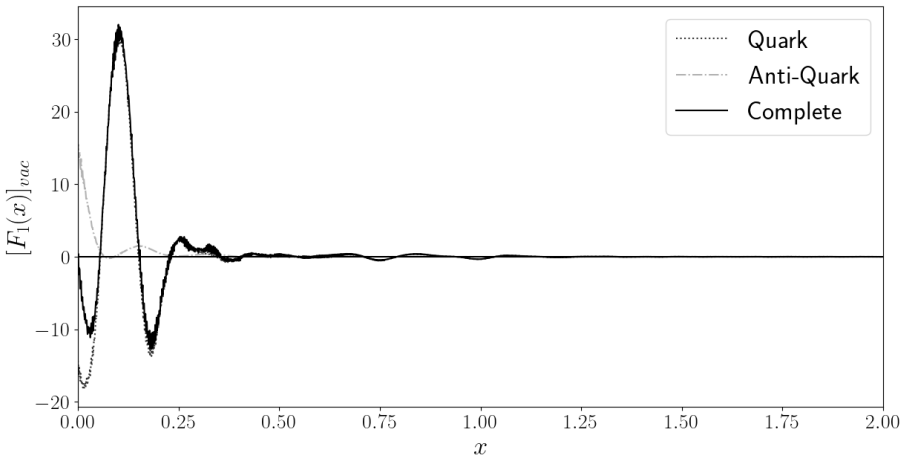

Figure 5.21: Sea contribution to the IUSF for $D = 7.5$fm. For further details see Fig. 5.12.

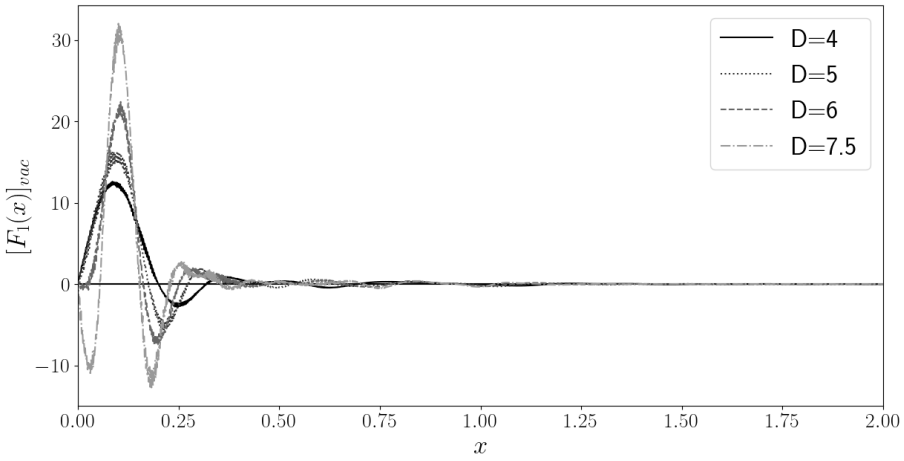

Figure 5.22: Sea contribution to the IUSF for $D = 4\text{fm}, 5\text{fm}, 6\text{fm}, 7.5\text{fm}$. For further details see Fig. 5.12.

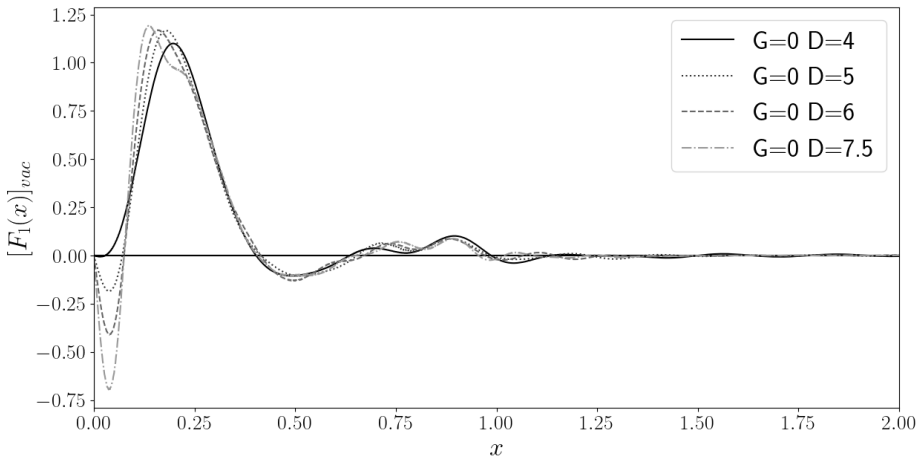

Figure 5.23: Sea contribution of $G = 0$ IUSF for $D = 4\text{fm}, 5\text{fm}, 6\text{fm}, 7.5\text{fm}$. For further details see Fig. 5.12.

The second attempt made during this investigation was just as simple. Since the non-soliton(vacuum) sector has no structure it should be invariant under changes in x. Hence, it would make sense for the vacuum contribution to the IUSF to be a constant, or rather a summation of constants of each of the different energy levels

$$[F_1^{(0)}]'_s(x) = \sum_\alpha C_\alpha, \tag{5.22}$$

such that the sum rule still holds level-by-level

$$\int_0^{D_x} dx C_\alpha = \sum_{c_i=0}^{2} \int_0^{D_x} dx \int_{|Mx_\alpha^\pm|}^{\infty} pdp \int d\Omega_p \left\{ \pm (\tilde{\Psi}_\alpha^{(0)})^\dagger(\vec{p}) \tilde{\Psi}_\alpha^{(0)}(\vec{p}) - \frac{\epsilon_\alpha}{\omega_0} \frac{M x_\alpha^\pm}{p} (\tilde{\Psi}_\alpha^{(0)})^\dagger(\vec{p}) \hat{p} \cdot \alpha \tilde{\Psi}_\alpha^{(0)}(\vec{p}) \right\}. \tag{5.23}$$

The figures 5.24, 5.25 and 5.26 show the changes to the IUSF contributions as a result of this change to the vacuum subtraction. What immediately grabs our attention is the large increase in scale, for the original IUSF the total vacuum contribution graphs had values between -10 and 20, vastly different from the values that range between -7000 and 4000 that we see now. By looking at it solely level-by-level however shows something different, see figures 5.27, 5.28 and 5.29. The graphs are clearly on the same scale however the summations almost never cancel each other out as they do for our original IUSF, for example at around $x = 0.75$ the contributions are always positive, this is not so for our original IUSF. The result is the comparatively large values after the summation.

The figures for the constant vacuum subtraction with changed box sizes are also plotted, these are given in Fig. 5.30. One of the more clear changes in the sea contribution is the increase in the extrema of the sea contributions as the box size increases. This can be seen for both the regular vacuum subtraction and the constant one. It is peculiar that the change in the vacuum subtraction such that it is invariant under x did not work. The sum rule of this vacuum subtraction is sometimes referred to as the cosmological constant or dark energy. The current findings suggest that the boundary condition imposes a structure to this energy. This may be related to the results of Ref. [53] which observed boundary affects for the energy and momentum densities of kinks in $D = 1 + 1$.

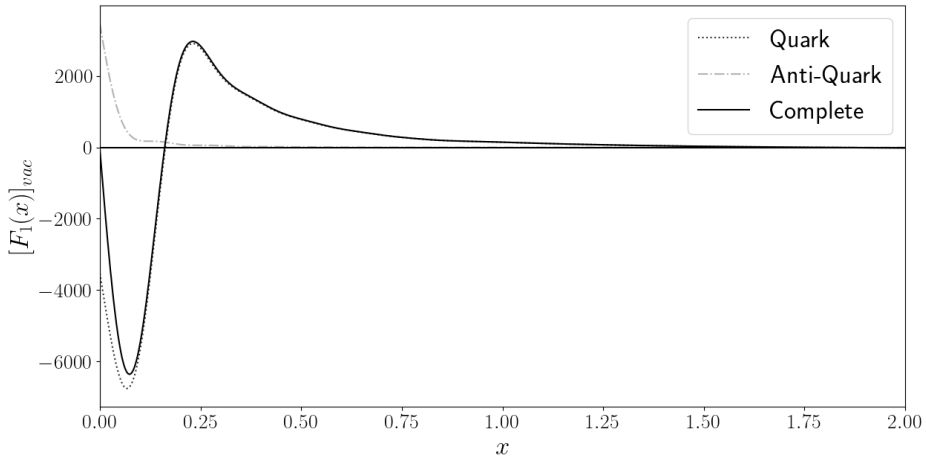

Figure 5.24: Sea contribution IUSF for $\Lambda = \Lambda_{\text{new}}$, $k_{\text{cut}} = 2956.3$MeV, $D = 5$fm and $D_x = 4.0$ with constant non-soliton sector. It has been separated into its quark and anti-quark contributions.

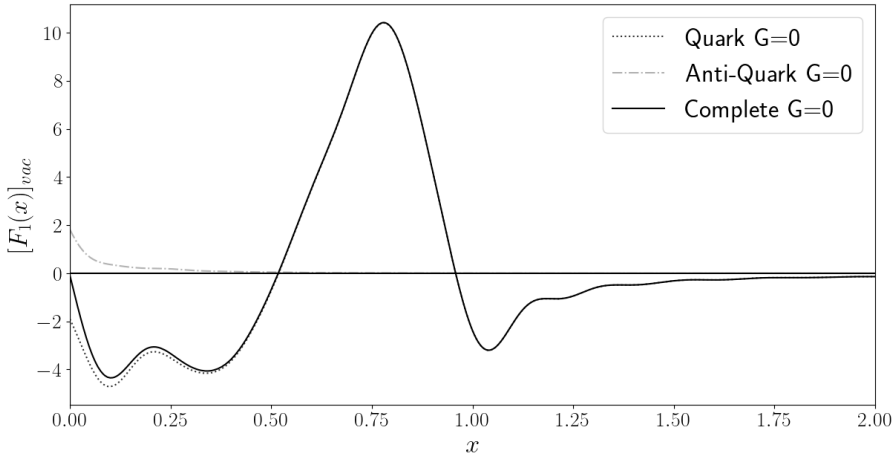

Figure 5.25: Sea contribution IUSF for grand spin $G = 0$. For further details see Fig. 5.24.

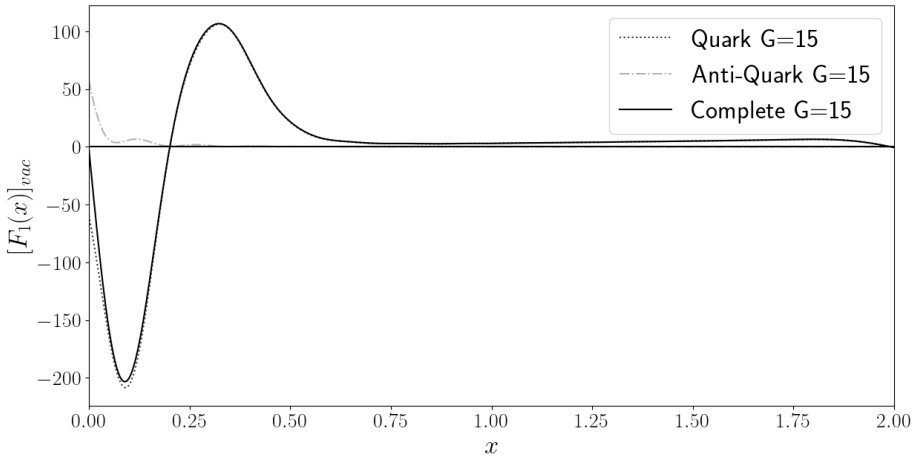

Figure 5.26: Sea contribution to the IUSF for grand spin $G = 15$. For further details see Fig. 5.24.

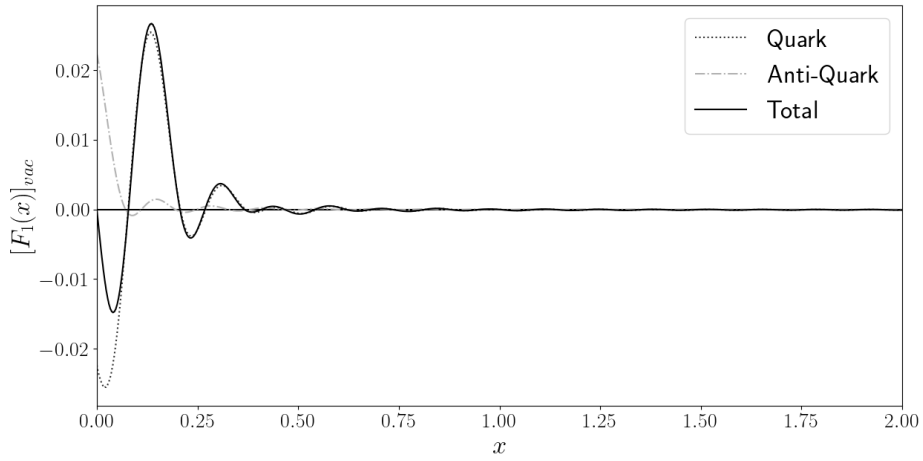

Figure 5.27: Sea contribution to the IUSF for grand spin $G = 0$ and energy eigenvalue $\epsilon = -2902.4$MeV. For further details see Fig. 5.24.

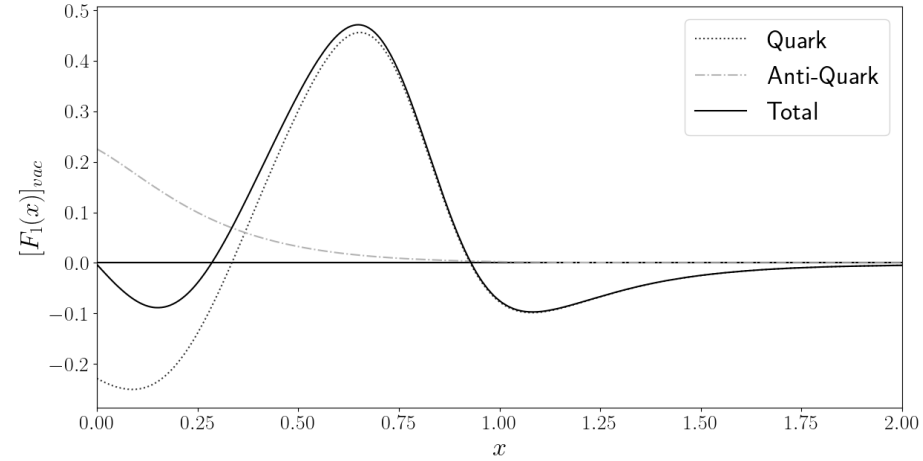

Figure 5.28: Sea contribution to the IUSF for grand spin $G = 0$ and energy eigenvalue $\epsilon = 216.78$MeV. For further details see Fig. 5.24.

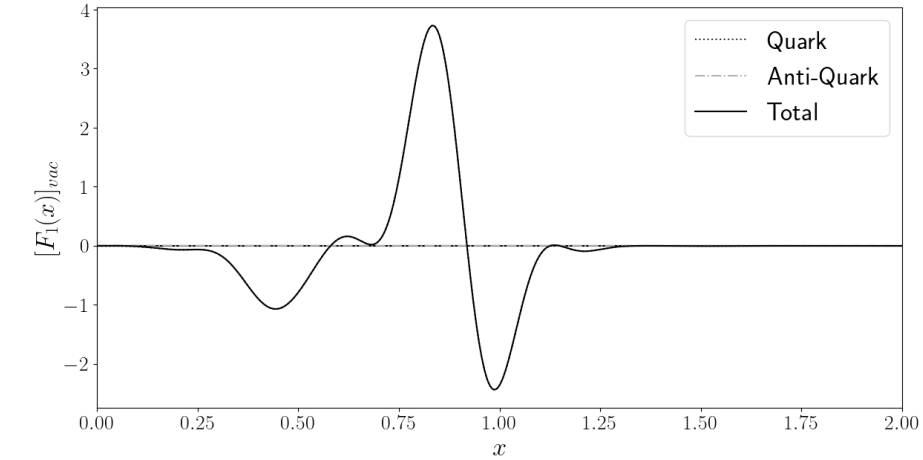

Figure 5.29: Sea contribution to the IUSF for grand spin $G = 0$ and energy eigenvalue $\epsilon = 428.37$MeV. For further details see Fig. 5.24.

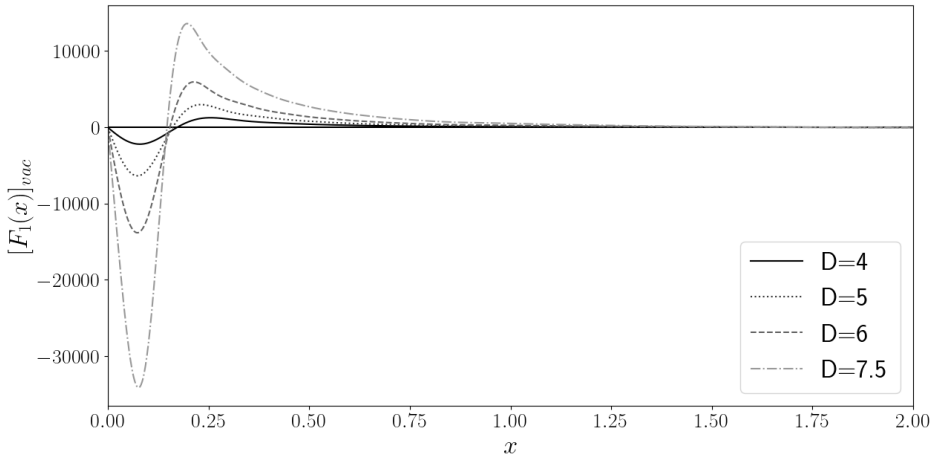

Figure 5.30: Sea contribution IUSF for D = 4fm, 5fm, 6fm, 7.5fm. For further details see Fig. 5.24.

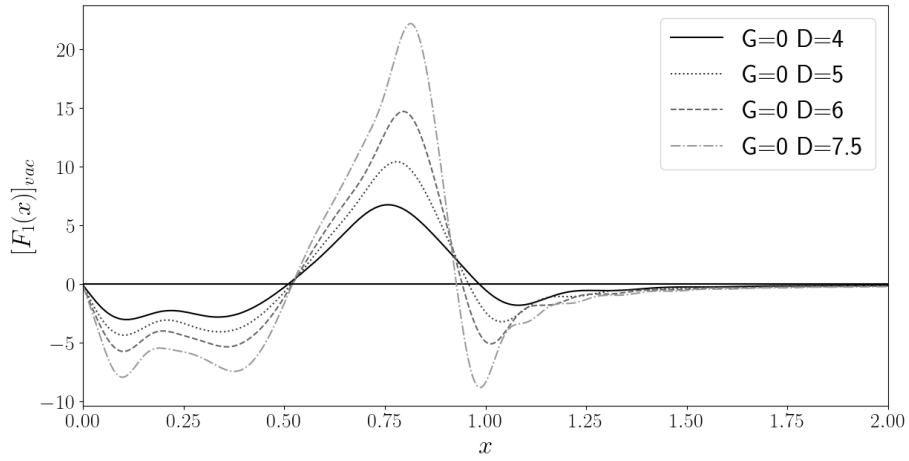

Figure 5.31: Sea contribution to the IUSF for G = 0 for D = 4fm, 5fm, 6fm, 7.5fm. For further details see Fig. 5.24.

CHAPTER 6

SUMMARY, CONCLUSIONS AND OUTLOOK

The aim of this investigation was to examine and hopefully solve the unusual behaviour of the sea contribution to the iso-singlet unpolarised nucleon structure function (IUSF) by changing the non-solitonic subtraction term in the NJL chiral soliton model. The crucial element for these changes is the energy sum rule. This sum rule relates the integrated structure function to the soliton energy. We start by attempting to reproduce the results of Ref. [1, 2]. It was soon found that the Λ cut-off used in the simulations was calculated incorrectly, with a value of $\Lambda_{\text{old}} \approx 743$ MeV[1, 2]. After correcting the value to $\Lambda_{\text{new}} \approx 739$ MeV the simulations were redone. Though this is only a small modification it resulted in the sum rule being very inaccurate. Since the sum rule is essential for any further investigation it needed to be fixed.

The first attempt to fix the sum rule was to simply increase the momentum cut-off k_{cut} or the size of the spherical box D. These numerical parameters are introduced to discretize and enumerate the quark levels and these changes should bring the simulation closer to its continuum limit. The analysis of the normalisation also showed that the Fourier transformed quark wavefunctions had significantly less accuracy than those in coordinate space. This motivated the second approach, which was to 'renormalise' the quark wavefunctions after their Fourier transformation. This was done by simply multiplying each quark wavefunction by a certain constant such that the momentum space wavefunctions would normalise to one. Unfortunately this effort did not solve the problem either.

After further investigation it was found that it was primarily the quark part to the sea contribution that lead to the inaccuracy of the sum rule. The momentum space integral entering this part of the calculation has integration boundaries with absolute values that may cause discontinuities which can affect the numerical simulation when the integration size is too large. With the knowledge that the sea contribution to the IUSF is essentialy zero at $x \geq 3$, the Bjorken x cut-off was set to $D_x = 4$ while the number of intervals remained unchanged. This fixed the problem.

Following on from this, an investigation into the unusual nature of the sea contributions behaviour was made. The sea contribution was decomposed into its seperated energy levels, and grand spins. The aim being to see if there were any particular grand spin or energy level that gave it its unusual behaviour. This, as predicted, was not fruitful. The simulations box size was then changed in order to see how the sea contribution responds. The result was a change in the extrema of the sea contribution's values, however, the overall behaviour of the structure function did not change. The next idea came in the form of altering the non-solitonic (vacuum) subtraction term, this was the initial idea in order to solve this problem. Given that our vacuum should be invariant with respect to x, the vacuum subtraction was changed to a constant such that the sum rule still held. This resulted in a large change in the scale of the structure function. Originally the structure function values ranged between -20 and 20, but with this alteration they varied between -7000 and 4000. Changing the box size D with the constant vacuum subtraction resulted in additional changes in the extrema of the sea contribution, as the box size grew so did the absolute values of the extrema. It is peculiar that making the vacuum subtraction invariant under changes in x did not get rid of the unusual behaviour of the structure function. This means that any further attempts at solving this issue would rely on the vacuum subtraction (the so called 'cosmogical constant') having a structure emerging from the box boundary conditions and a dependence thereon.

Now that the suitable parameters have been chosen, such that a reliable sum rule can be created, further changes to the vacuum subtraction can be made in an attempt to fix the sea contribution to the IUSF. Further

experiments could simply take the recorded data of the structure functions non-solitonic counter part and alter it as desired. We conjecture that only the IUSF has an unconventional box size dependence; other structure functions (isovector and/or polarised) do not contain any vacuum subtraction.

Appendices

APPENDIX A

THE SINGLE CUTOFF

We now want to find the cut-off formula with the established regularisation conditions

$$c_0 = 1, \quad \Lambda_0 = 0, \quad \sum_{i=0}^{2} c_i = 0 \quad \text{and} \quad \sum_{i=0}^{2} c_i \Lambda_i^2 = 0, \tag{A.1}$$

which yields $c_1 = \frac{\Lambda_2^2}{\Lambda_1^2 - \Lambda_2^2}$ and $c_2 = -\frac{\Lambda_1^2}{\Lambda_1^2 - \Lambda_2^2}$. For the single cut-off case $\Lambda_2 = \Lambda \to \Lambda_1$ we expand $\sum_{i=0}^{2} c_i g(\Lambda_i^2)$.

$$\begin{aligned} \sum_{i=0}^{2} c_i g(\Lambda_i^2) &= c_0 g(\Lambda_0^2) + c_1 g(\Lambda_1^2) + c_2 g(\Lambda_2^2) \\ &= g(0) + c_1 g(\Lambda_1^2) + c_2 g(\Lambda_2^2) \\ &= g(0) + \frac{\Lambda_2^2}{\Lambda_1^2 - \Lambda_1^2} g(\Lambda_1^2) - \frac{\Lambda_1^2}{\Lambda_1^2 - \Lambda_2^2} g(\Lambda_2^2) : \end{aligned} \tag{A.2}$$

Next set $\Lambda_1^2 = \Lambda_2^2 + \epsilon$ and $\Lambda_2^2 = \Lambda^2$

$$\begin{aligned} \sum_{i=0}^{2} c_i g(\Lambda_i^2) &= g(0) + \frac{\Lambda^2}{\epsilon} g(\Lambda^2 + \epsilon) - \frac{\Lambda_1^2 + \epsilon}{\epsilon} g(\Lambda) \\ &= g(0) - g(\Lambda^2) + \frac{g(\Lambda^2 + \epsilon) - g(\Lambda^2)}{\epsilon} \Lambda^2. \end{aligned} \tag{A.3}$$

Lastly take the limit $\epsilon \to 0$ which provides us with the desired single cut-off formula

$$\sum_{i=0}^{2} c_i g(\Lambda_i^2) = g(0) - g(\Lambda^2) + \Lambda^2 \frac{\partial}{\partial \Lambda^2} g(\Lambda^2). \tag{A.4}$$

APPENDIX B

DETERMINING LAMBDA

In order to numerically compute Λ, it is necessary to derive an equation for this purpose. To do so, let us first consider Eq. (2.68). We shall transform this equation into a form that can be computed numerically:

$$\Pi(q^2) = -i\sum_{i=0}^{2} c_i \int_0^1 dx \int \frac{d^4k}{(2\pi)^4}[-k^2 - x(1-x)q^2 + m^2 + \Lambda_i^2 - i\epsilon]^{-2}, \tag{B.1}$$

using a Wick rotations results in

$$\begin{aligned}\Pi(q^2) &= \sum_{i=0}^{2} c_i \int_0^1 dx \int \frac{d^4k}{(2\pi)^4}[k^2 - x(1-x)q^2 + m^2 + \Lambda_i^2 - i\epsilon]^{-2} \\ &= -\frac{1}{16\pi^2}\sum_{i=0}^{2} c_i \int_0^1 dx \log(m^2 - x(1-x)q^2 + \Lambda_i^2).\end{aligned} \tag{B.2}$$

Applying single Λ limit (2.54)

$$\Pi(q^2) = -\frac{1}{16\pi^2}\int_0^1 dx\Big\{\frac{\Lambda^2}{m^2 - x(1-x)q^2 + \Lambda} - \log\Big(\frac{m^2 - x(1-x)q^2 + \Lambda^2}{m^2 - x(1-x)q^2}\Big)\Big\}. \tag{B.3}$$

In the next step we take the derivative of Eq. (B.3)

$$\frac{d}{dq^2}\Pi(q^2) = -\frac{1}{16\pi^2}\int_0^1 dx\Big\{\frac{x(1-x)\Lambda}{(m^2 - x(1-x)q^2 + \Lambda^2)^2} + \frac{x(1-x)}{m^2 - x(1-x)q^2 + \Lambda^2} - \frac{x(1-x)}{m^2 - x(1-x)q^2}\Big\}, \tag{B.4}$$

Subsequently we use Eq. (2.71)

$$g^2 = \frac{1}{4N_C}\frac{1}{\frac{d}{dq^2}[q^2\Pi(q^2)]|_{q^2=m_\pi^2}} = \frac{1}{4N_C}\frac{1}{\Pi(m_\pi^2) + m_\pi^2\frac{d}{dq^2}\Pi(q^2)|_{q^2=m_\pi^2}}. \tag{B.5}$$

Lastly we use Eq. 2.77 to substitute the g^2

$$(\frac{f_\pi}{m})^2 = 4N_C\frac{\Pi^2(m_\pi^2)}{\Pi(m_\pi^2) + m_\pi^2\frac{d}{dq^2}\Pi(q^2)|_{q^2=m_\pi^2}} \tag{B.6}$$

Once the physical parameters—the pion decay constant $f_\pi = 93$MeV, the pion mass $m_\pi = 135$MeV, and the constituent quark mass m—have been specified, we can use Eq. (B.6) to compute Λ numerically. In this way we single out m as the only model parameter.

APPENDIX C

CONTRUCTING THE QUARK WAVEFUNCTIONS

For the effective chirally invariant meson field theory, the soliton is given by

$$U_{\mathrm{H}}(\vec{x}) = e^{i\vec{\tau}\cdot\vec{x}F(r)} \quad \text{where} \quad r = |x|. \tag{C.1}$$

Here $F(x)$ is called the soliton profile or the chiral angle. In the presence of the soliton configuration the single particle Dirac Hamiltonian is

$$h = \vec{\alpha}\cdot\vec{p} + m\beta e^{i\gamma_5\vec{\tau}\cdot\vec{x}F(r)}. \tag{C.2}$$

This Hamiltonian commutes with the grand spin operator

$$[h, \vec{G}] = 0, \tag{C.3}$$

$$\vec{G} = \vec{J} + \frac{\vec{\tau}}{2} = \vec{L} + \frac{\vec{\sigma}}{2} + \frac{\vec{\tau}}{2}, \tag{C.4}$$

which is the sum of the total spin operator $\vec{J}$ and the isospin $\frac{\vec{\tau}}{2}$. The total spin $\vec{J}$ is the sum of the angular momentum $\vec{L}$ and the intrinsic spin $\frac{\vec{\sigma}}{2}$.

The Dirac Hamiltonian is diagonalised as

$$h\Psi_\alpha = \epsilon_\alpha\Psi_\alpha. \tag{C.5}$$

This gives us eigenstates Ψ_α and real energy eigenvalues ϵ_α. Due to the Dirac Hamiltonian h commuting with the grand spin $\vec{G}$ the eigenstates Ψ_α are also eigenstates of $\vec{G}^2$ and $G_3 = M$. These eigenstates can be constructed as linear combination of the eigenstates of the free Hamiltonian ($F \equiv 0$).

$$\begin{aligned} &\left|1, n, j = G + \frac{1}{2}, M\right\rangle = \mathcal{N}_n^G \begin{pmatrix} i\omega^+_{nG} j_G(k_{nG}r)\mathcal{Y}^{GM}_{GG+\frac{1}{2}}(\hat{x}) \\ \omega^-_{nG} j_{G+1}(k_{nG}r)\mathcal{Y}^{GM}_{G+1G+\frac{1}{2}}(\hat{x}) \end{pmatrix}, \\ &e^0 = E_{nG} = \pm\sqrt{k^2_{nG} = m^2}, \prod = (-)^G, \end{aligned} \tag{C.6}$$

$$\begin{aligned} &\left|2, n, j = G - \frac{1}{2}, M\right\rangle = \mathcal{N}_n^G \begin{pmatrix} i\omega^+_{nG} j_G(k_{nG}r)\mathcal{Y}^{GM}_{GG-\frac{1}{2}}(\hat{x}) \\ -\omega^-_{nG} j_{G-1}(k_{nG}r)\mathcal{Y}^{GM}_{G-1G-\frac{1}{2}}(\hat{x}) \end{pmatrix}, \\ &e^0 = E_{nG} = \pm\sqrt{k^2_{nG} = m^2}, \prod = (-)^G, \end{aligned} \tag{C.7}$$

$$\begin{aligned} &\left|3, n, j = G + \frac{1}{2}, M\right\rangle = \mathcal{N}_n^{G+1} \begin{pmatrix} i\omega^+_{nG+1} j_{G+1}(k_{nG+1}r)\mathcal{Y}^{GM}_{G+1G+\frac{1}{2}}(\hat{x}) \\ -\omega^-_{nG+1} j_G(k_{nG+1}r)\mathcal{Y}^{GM}_{GG+\frac{1}{2}}(\hat{x}) \end{pmatrix}, \\ &e^0 = E_{nG+1} = \pm\sqrt{k^2_{nG+1} = m^2}, \prod = (-)^{G+1}, \end{aligned} \tag{C.8}$$

$$\left|4, n, j = G - \frac{1}{2}, M\right\rangle = \mathcal{N}_n^{G-1} \begin{pmatrix} i\omega^+_{nG-1} j_{G-1}(k_{nG-1}r)\mathcal{Y}^{GM}_{G-1G-\frac{1}{2}}(\hat{x}) \\ \omega^-_{nG-1} j_G(k_{nG-1}r)\mathcal{Y}^{GM}_{GG-\frac{1}{2}}(\hat{x}) \end{pmatrix},$$
$$e^0 = E_{nG-1} = \pm\sqrt{k^2_{nG-1} = m^2}, \prod = (-)^{G-1}. \tag{C.9}$$

Here j_G are the spherical Bessel functions of order G. e^0 are the energy eigenvalues of the free Dirac Hamiltonian and $\prod$ are the parity quantum numbers. $|L, J, G, M\rangle$ are the grand spin states, this is given by the coupling of $\frac{\vec{\sigma}}{2}$ and $\vec{L}$ to $\vec{J}$, which is in turn coupled with $\frac{\vec{\tau}}{2}$ to G, with M as the projection of the grand spin. Due to this coupling scheme the projection rules are

$$J = \begin{matrix} G+\frac{1}{2}, L= G+1, \\ G-\frac{1}{2}, L= G, \end{matrix} \quad \begin{matrix} \\ G-1. \end{matrix} \tag{C.10}$$

The coordinate representation $\mathcal{Y}^{GM}_{LJ}(\hat{x}) = \langle\hat{x}|LJGM\rangle$ is given in Eq. (3.46) using the conventional spherical harmonic functions $Y_{Lm}(\hat{x})$. The boundary conditions discretise the momenta k_{nG}, by demanding that the Bessel functions $j_L(k_{nL}r)$ vanish at the boundary, i.e.

$$j_L(k_{nL}D) = 0, \tag{C.11}$$

where D is the radius of the spherical cavity such that D is much larger than the range of the soliton. The kinematical factors are defined as

$$\omega^+_{nl} = \sqrt{1 + \frac{m}{E_{nl}}} \text{ and } \omega^-_{nl} = \text{sgn}(E_{nl})\sqrt{1 - \frac{m}{E_{nl}}}. \tag{C.12}$$

The normalisation factor is given by

$$\mathcal{N}^l_n = \left[D^{3/2}|j_{l+1}(k_{nl}D)|\right] \tag{C.13}$$

The numerical diagonalisation of the Dirac Hamiltonian h requires an upper bound, k_{cut} for the momenta k_{nl}. This means there is a specified number of momentum states $N(l) : k_{1l}, \cdots, k_{N(l)l}$. Taking into that for each momentum there are two energy eigenvalues $\pm e^0$, we have $2N(l)$ eigenfunctions of $h(F \equiv 0)$ for each grand spinor in equation (C.9). From this as a basis matrix elements of the Dirac Hamiltonian are constructed, then the matrix is diagonalised in each grand spin and parity sector.

The diagonalisation of this Hamiltonian yields the energies eigenvalues $\epsilon^{\pm}_G(\mu)$ and the corresponding eigenvectors $V^{(\pm)}_G(n, \mu)$. The latter are used to define the radial functions for positive intrinsic parity

$$g^{(G,+;1)}_\alpha(r) = \sum_{n=1}^{2N(G)} V^{(+)}_G(n, \alpha)\mathcal{N}^G_n \omega^+_{nG} j_G(k_{nG}r),$$
$$g^{(G,+;2)}_\alpha(r) = \sum_{n=1}^{2N(G)} V^{(+)}_G(n + 2N(G), \alpha)\mathcal{N}^G_n \omega^+_{nG} j_G(k_{nG}r),$$
$$f^{(G,+;1)}_\alpha(r) = \sum_{n=1}^{2N(G)} V^{(+)}_G(n, \alpha)\mathcal{N}^G_n \omega^-_{nG} j_{G+1}(k_{nG}r),$$
$$f^{(G,+;2)}_\alpha(r) = \sum_{n=1}^{2N(G)} V^{(+)}_G(n + 2N(G), \alpha)\mathcal{N}^G_n \omega^-_{nG} j_{G-1}(k_{nG}r),$$

and for negative intrinsic parity

$$g_\alpha^{(G,-;1)}(r) = \sum_{n=1}^{2N(G+1)} V_G^{(-)}(n,\alpha)\mathcal{N}_n^{G+1}\omega_{nG+1}^{+} j_{G+1}(k_{nG+1}r),$$
$$g_\alpha^{(G,-;2)}(r) = \sum_{n=1}^{2N(G-1)} V_G^{(-)}(n+2N(G+1),\alpha)\mathcal{N}_n^{G-1}\omega_{nG-1}^{+} j_{G-1}(k_{nG-1}r),$$
$$f_\alpha^{(G,-;1)}(r) = \sum_{n=1}^{2N(G+1)} V_G^{(-)}(n,\alpha)\mathcal{N}_n^{G}\omega_{nG+1}^{-} j_{G}(k_{nG}r),$$
$$f_\alpha^{(G,-;2)}(r) = \sum_{n=1}^{2N(G-1)} V_G^{(-)}(n+2N(G+1),\alpha)\mathcal{N}_n^{G-1}\omega_{nG-1}^{-} j_{G}(k_{nG}r).$$

These radial function are then used to define the eigenstates of the Dirac Hamiltonian h in coordinate space

$$\Psi_\alpha^{(G,+)}(\vec{x}) = \begin{pmatrix} ig_\alpha^{(G,+;1)}(r)\mathcal{Y}^{GM}_{G,G+\frac{1}{2}}(\hat{x}) \\ f_\alpha^{(G,+;1)}(r)\mathcal{Y}^{GM}_{G+1G+\frac{1}{2}}(\hat{x}) \end{pmatrix} + \begin{pmatrix} ig_\alpha^{(G,+;2)}(r)\mathcal{Y}^{GM}_{GG-\frac{1}{2}}(\hat{x}) \\ -f_\alpha^{(G,+;2)}(r)\mathcal{Y}^{GM}_{G-1G-\frac{1}{2}}(\hat{x}) \end{pmatrix} \tag{C.14}$$

$$\Psi_\alpha^{(G,-)}(\vec{x}) = \begin{pmatrix} ig_\alpha^{(G,-;1)}(r)\mathcal{Y}^{GM}_{G+1G+\frac{1}{2}}(\hat{x}) \\ -f_\alpha^{(G,-;1)}(r)\mathcal{Y}^{GM}_{GG+\frac{1}{2}}(\hat{x}) \end{pmatrix} + \begin{pmatrix} ig_\alpha^{(G,-;2)}(r)\mathcal{Y}^{GM}_{G-1G-\frac{1}{2}}(\hat{x}) \\ f_\alpha^{(G,-;2)}(r)\mathcal{Y}^{GM}_{GG-\frac{1}{2}}(\vec{x}) \end{pmatrix}. \tag{C.15}$$

Next we can take the Fourier transform of these eigenstates

$$\tilde{\Psi}_\alpha(\vec{p}) = \int \frac{d^3x}{4\pi} e^{i\vec{p}\cdot\vec{x}}\Psi_\alpha(\vec{x}) \tag{C.16}$$

Since this involves the generalised spherical harmonics and radial functions it can be written as

$$\begin{aligned}\tilde{\Psi}_\alpha(\vec{p}) &= \int \frac{d^3x}{4\pi} e^{i\vec{p}\cdot\vec{x}}\phi_\alpha(r)\mathcal{Y}^{GM}_{L_\alpha J}(\hat{x}) \\ &= \sum_{m_\alpha,s_3,i_3,J_3} C^{GM}_{JJ_3,\frac{1}{2}i_3} C^{JJ_3}_{L_\alpha m_\alpha,\frac{1}{2}s_3}\chi_s(s_3)\chi_i(i_3)\int \frac{d^3x}{4\pi} e^{i\vec{p}\cdot\vec{x}}\phi_\alpha(r)Y_{L_\alpha m_\alpha}(\vec{x})\end{aligned} \tag{C.17}$$

where $\phi_\alpha(r)$ is any of the radial functions and $Y_{L_\alpha m_\alpha}(\hat{x})$ is the spherical harmonic function. We expand the plane wave function in terms of spherical Bessel function as

$$e^{i\vec{p}\cdot\vec{x}} = 4\pi\sum_{Lm}(i)^L j_L(pr)Y^*_{Lm}(\hat{x})Y_{Lm}(\hat{p}). \tag{C.18}$$

This gives

$$\begin{aligned}\tilde{\Psi}_\alpha(\vec{p}) = &\sum_{m_\alpha,s_3,i_3,J_3} C^{GM}_{JJ_3,\frac{1}{2}i_3} C^{JJ_3}_{L_\alpha m_\alpha,\frac{1}{2}s_3}\chi_s(s_3)\chi_i(i_3) \\ &\times\sum_{Lm}(i)^L\int d^3x j_L(pr)Y^*_{Lm}(\hat{x})Y_{Lm}(\vec{p})\phi_\alpha(r)Y_{L_\alpha m_\alpha}(\vec{x}).\end{aligned} \tag{C.19}$$

Expressing the integral variable in spherical coordinates as

$$\int d^3x = \int_0^\infty dx x^2\int d\Omega_x, \tag{C.20}$$

where Ω_r is the solid angle and using the orthogonal identity

$$\int d\Omega_r Y^*_{Lm}(\hat{x})Y_{L'm'}(\hat{x}) = \delta_{LL'}\delta_{mm'} \tag{C.21}$$

gives

$$\begin{aligned}\tilde{\Psi}_\alpha(\vec{p}) =& \sum_{m_\alpha,s_3,i_3,J_3} C^{GM}_{JJ_3,\frac{1}{2}i_3} C^{JJ_3}_{L_\alpha m_\alpha,\frac{1}{2}s_3}\chi_s(s_3)\chi_i(i_3)\\ &\times\sum_{Lm}(i)^L\int drr^2 j_L(pr)\phi_\alpha(r)Y_{Lm}(\hat{p})\delta_{LL_\alpha}\delta_{mm_\alpha},\\ =&(i)^{L_\alpha}\tilde{\phi}_\alpha(p)\mathcal{Y}^{GM}_{L_\alpha J}(\hat{p}),\end{aligned} \tag{C.22}$$

where

$$\mathcal{Y}^{GM}_{LJ}(\hat{p}) = \sum_{m,s_3,i_3,J_3} \mathcal{C}^{GM}_{JJ_3,\frac{1}{2}i_3}\mathcal{C}^{JJ_3}_{Lm,\frac{1}{2}s_3}Y_{LM}(\hat{p})\xi_s(s_3)\xi_i(i_3) \tag{C.23}$$

is a generalised spherical harmonic function in momentum space and

$$\tilde{\phi}_\alpha(p) = \int drr^2 j_{L_\alpha}(pr)\phi_\alpha(r) \tag{C.24}$$

is the radial function in momentum space. Using the above results, we have the two eigenfunctions in momentum space: For $(-)^L = (-)^G$ (positive intrinsic parity) as

$$\tilde{\Psi}^{(G,+)}_\alpha(\vec{p}) = \begin{pmatrix}(i)^{G+1}\tilde{g}^{(G,+;1)}_\alpha(p)\mathcal{Y}^{GM}_{GG+\frac{1}{2}}(\hat{p})\\ (i)^{G+1}\tilde{f}^{(G,+;1)}_\alpha(p)\mathcal{Y}^{GM}_{G+1G+\frac{1}{2}}(\hat{p})\end{pmatrix} + \begin{pmatrix}(i)^{G+1}\tilde{g}^{(G,+;2)}_\alpha(p)\mathcal{Y}^{GM}_{GG-\frac{1}{2}}(\hat{p})\\ -(i)^{G-1}\tilde{f}^{(G,+;2)}_\alpha(p)\mathcal{Y}^{GM}_{G-1G-\frac{1}{2}}(\hat{p})\end{pmatrix}. \tag{C.25}$$

For $(-)^L = (-)^{G+1}$ (negative intrinsic parity) the momentum space wavefunctions are

$$\Psi^{(G,-)}_\alpha(\vec{p}) = \begin{pmatrix}(i)^{G+2}\tilde{g}^{(G,-;1)}_\alpha(p)\mathcal{Y}^{GM}_{G+1G+\frac{1}{2}}(\hat{p})\\ -(i)^{G}\tilde{f}^{(G,-;1)}_\alpha(p)\mathcal{Y}^{GM}_{GG+\frac{1}{2}}(\hat{p})\end{pmatrix} + \begin{pmatrix}(i)^{G}\tilde{g}^{(G,-;2)}_\alpha(p)\mathcal{Y}^{GM}_{G-1G-\frac{1}{2}}(\hat{x})\\ \tilde{f}^{(G,-;2)}_\alpha(p)\mathcal{Y}^{GM}_{GG-\frac{1}{2}}(\hat{p})\end{pmatrix}. \tag{C.26}$$

The radial functions are expressed as

$$\begin{aligned}\tilde{g}^{(G,+;1)}_\alpha(p) &= \int_0^D drr^2\sum_{n=1}^{2N(G)} V^{(+)}_G(n,\alpha)\mathcal{N}^G_n\omega^+_{nG}j_G(k_{nG}r)j_G(pr),\\ \tilde{g}^{(G,+;2)}_\alpha(p) &= \int_0^D drr^2\sum_{n=1}^{2N(G)} V^{(+)}_G(n+2N(G),\alpha)\mathcal{N}^G_n\omega^+_{nG}j_G(k_{nG}r)j_G(pr),\\ \tilde{f}^{(G,+;1)}_\alpha(p) &= \int_0^D drr^2\sum_{n=1}^{2N(G)} V^{(+)}_G(n,\alpha)\mathcal{N}^G_n\omega^-_{nG}j_{G+1}(k_{nG}r)j_{G+1}(pr),\\ \tilde{f}^{(G,+;2)}_\alpha(p) &= \int_0^D drr^2\sum_{n=1}^{2N(G)} V^{(+)}_G(n+2N(G),\alpha)\mathcal{N}^G_n\omega^-_{nG}j_{G-1}(k_{nG}r)j_{G-1}(pr),\end{aligned}$$

for positive intrinsic parity.

For negative intrinsic parity they are

$$\begin{aligned}\tilde{g}^{(G,-;1)}_\alpha(p) &= \int_0^D drr^2\sum_{n=1}^{2N(G+1)} V^{(-)}_G(n,\alpha)\mathcal{N}^{G+1}_n\omega^+_{nG+1}j_{G+1}(k_{nG+1}r)j_{G+1}(pr),\\ \tilde{g}^{(G,-;2)}_\alpha(p) &= \int_0^D drr^2\sum_{n=1}^{2N(G-1)} V^{(-)}_G(n+2N(G+1),\alpha)\mathcal{N}^{G-1}_n\omega^+_{nG-1}j_{G-1}(k_{nG-1}r)j_{G-1}(pr),\\ \tilde{f}^{(G,-;1)}_\alpha(p) &= \int_0^D drr^2\sum_{n=1}^{2N(G+1)} V^{(-)}_G(n,\alpha)\mathcal{N}^G_n\omega^-_{nG+1}j_G(k_{nG}r)j_G(pr),\\ \tilde{f}^{(G,-;2)}_\alpha(p) &= \int_0^D drr^2\sum_{n=1}^{2N(G-1)} V^{(-)}_G(n+2N(G+1),\alpha)\mathcal{N}^{G-1}_n\omega^-_{nG-1}j_G(k_{nG}r)j_G(pr).\end{aligned}$$

APPENDIX D

THE MATRIX ELEMENTS OF DIRAC OPERATORS

D.1 CALCULATION OF $\hat{r}\cdot\vec{\tau}$

To determine the matrix of $\int d\Omega_p(\mathcal{Y}^{GM}_{L'J'})^\dagger(\hat{r})\hat{r}\cdot\vec{\tau}\mathcal{Y}^{GM}_{LJ}(\hat{r})$ first let us first describe our relevant generalised spherical harmonic functions in position space[1]

$$\mathcal{Y}^{G,G}_{G-\frac{1}{2},G-1} = Y_{G-1G-1}\chi^{(I)}_{\frac{1}{2}}\chi^{(S)}_{\frac{1}{2}} \tag{D.1}$$

$$\mathcal{Y}^{GG}_{G-\frac{1}{2}G} = -\sqrt{\frac{1}{2G+1}}Y_{GG-1}\chi^{I}_{\frac{1}{2}}\chi^{(S)}_{\frac{1}{2}} + \sqrt{\frac{2G}{2G+1}}Y_{GG}\chi^{I}_{\frac{1}{2}}\chi^{(S)}_{-\frac{1}{2}} \tag{D.2}$$

$$\begin{aligned}\mathcal{Y}^{GG}_{G+\frac{1}{2}G} = &-\sqrt{\frac{1}{2G+2}}\left[\sqrt{\frac{2G}{2G+1}}Y_{GG-1}\chi^{(S)}_{\frac{1}{2}} + \sqrt{\frac{1}{2G+1}}Y_{GG}\chi^{(S)}_{-\frac{1}{2}}\right]\chi^{(I)}_{\frac{1}{2}}\\ &+\sqrt{\frac{2G+1}{2G+2}}Y_{GG}\chi^{(S)}_{\frac{1}{2}}\chi^{(I)}_{-\frac{1}{2}}\end{aligned} \tag{D.3}$$

$$\begin{aligned}\mathcal{Y}^{GG}_{G+\frac{1}{2}G+1} = &-\sqrt{\frac{1}{2G+2}}\left[-\sqrt{\frac{2}{2G+3}}Y_{G+1G-1}\chi^{(S)}_{\frac{1}{2}} + \sqrt{\frac{2G+1}{2G+3}}Y_{G+1G}\chi^{(S)}_{-\frac{1}{2}}\right]\chi^{(I)}_{\frac{1}{2}}\\ &+\sqrt{\frac{2G+1}{2G+2}}\left[-\sqrt{\frac{1}{2G+3}}Y_{G+1G}\chi^{(S)}_{\frac{1}{2}} + \sqrt{\frac{2G+2}{2G+3}}Y_{G+1G+1}\chi^{(S)}_{-\frac{1}{2}}\right]\chi^{(I)}_{-\frac{1}{2}}\end{aligned} \tag{D.4}$$

The spatial parity of the eigenstates is $(-1)^l$ and the $\hat{r}\cdot\vec{\tau}$ operators parity is -1. In order for a matrix element $\langle J'l'GG|\,\hat{r}\cdot\vec{\tau}\,|JlGG\rangle$ to be non-zero we will need that l and l' are separated by an odd number of integers in order to produce a non-antisymmetric parity. The scalar product $\hat{r}\cdot\vec{\tau}$ can be rewritten as:

$$\hat{r}\cdot\vec{\tau} = \sqrt{\frac{4\pi}{3}}\begin{pmatrix} Y_{10} & \sqrt{2}Y_{1-1} \\ -\sqrt{2}Y_{11} & -Y_{10}\end{pmatrix}, \tag{D.5}$$

where each of these matrices are chosen based on the isospin of the bra and ket vectors. Additionally, the identity [54]

$$Y_{l_1m_1}(\hat{r})Y_{l_2m_2}(\hat{r}) = \sum_l\sqrt{\frac{(2l_1+1)(2l_2+1)}{4\pi(2l+1)}}C^{l,0}_{l_1,0;l_2,0}C^{l,m}_{l_1,m_1;l_2,m_2}Y_{lm}(\hat{r}) \tag{D.6}$$

[1] We need only use $G = M$ as this is the simplest case and our operators are degenerate with respect to M.

can be used to calculate the integral

$$\begin{aligned}\int d\Omega Y^*_{l_1m_1}Y_{l_2m_2}Y_{l_3m_3} &= \sum_{l=|l_2-l_3|}^{l_2+l_3}\sum_{m=-l}^{l}\frac{\sqrt{(2l_2+1)(2l_3+1)}}{\sqrt{4\pi(2l+1)}}\mathcal{C}^{l,0}_{l_2,0;l_3,0}\mathcal{C}^{l,m}_{l_2,m_2;l_3,m_3}\int d\Omega Y_{l_1m_1}(\hat{r})Y_{lm}(\hat{r})\\ &=\frac{\sqrt{(2l_2+1)(2l_3+1)}}{\sqrt{4\pi(2l_1+1)}}\mathcal{C}^{l_1,0}_{l_2,0;l_3,0}\mathcal{C}^{l_1,m_1}_{l_2,m_2;l_3,m_3}.\end{aligned} \tag{D.7}$$

Using these identities the non-zero matrix elements are calculated to be

$$\begin{aligned}\int d\Omega(\mathcal{Y}^{GG}_{G-\frac{1}{2}G-1})^\dagger(\hat{r})\hat{r}\cdot\vec{\tau}\mathcal{Y}^{GG}_{G-\frac{1}{2}G}(\hat{r}) &= -\int d\Omega\sqrt{\frac{1}{2G+1}}Y^*_{GG-1}(\hat{r})Y_{10}(\hat{r})Y_{GG-1}(\hat{r})\sqrt{\frac{4\pi}{3}}\\ &=-\frac{1}{2G+1},\end{aligned} \tag{D.8}$$

$$\begin{aligned}&\int d\Omega(\mathcal{Y}G-\frac{1}{2}G-1GG)^\dagger(\hat{r})\hat{r}\cdot\vec{\tau}\mathcal{Y}^{GG}_{G+\frac{1}{2}G}(\hat{r})\\ &=\int d\Omega\Big[-\sqrt{\frac{1}{2G+2}}\sqrt{\frac{2G}{2G+1}}Y^*_{G-1G-1}(\hat{r})Y_{10}(\hat{r})Y_{GG-1}(\hat{r})\sqrt{\frac{4\pi}{3}}\\ &\quad+\sqrt{\frac{2G+1}{2G+2}}\sqrt{2}Y^*_{G-1G-1}(\hat{r})Y_{1-1}(\hat{r})Y_{GG}(\hat{r})\Big]\\ &=-\frac{2\sqrt{G(G+1)}}{2G+1},\end{aligned} \tag{D.9}$$

$$\begin{aligned}\int d\Omega(\mathcal{Y}^{GG}_{G-\frac{1}{2}G})^\dagger(\hat{r})\hat{r}\cdot\vec{\tau}\mathcal{Y}^{GG}_{G+\frac{1}{2}G+1}(\hat{r}) &= \int d\Omega\Big[-\sqrt{\frac{1}{2G+1}\frac{1}{2G+3}\frac{1}{G+1}}\sqrt{\frac{4\pi}{3}}Y^*_{GG-1}Y_{10}Y_{G+1G-1}\\ &\quad+\sqrt{\frac{1}{2G+1}\frac{2G+1}{G+1}\frac{1}{2G+3}}\sqrt{\frac{4\pi}{3}}Y^*_{GG-1}Y_{1-1}Y_{G+1G}\\ &\quad-\sqrt{\frac{G}{G+1}\frac{1}{2G+3}}Y^*_{GG}Y_{10}Y_{G+1G}\\ &\quad+\sqrt{\frac{4G}{2G+3}}\sqrt{\frac{4\pi}{3}}Y^*_{GG}Y_{1-1}Y_{G+1G+1}\Big]\\ &=-\frac{2\sqrt{G(G+1)}}{2G+1},\end{aligned} \tag{D.10}$$

and

$$\begin{aligned}\int d\Omega(\mathcal{Y}^{GG}_{G+\frac{1}{2}G})^\dagger(\hat{r})\hat{r}\cdot\vec{\tau}\mathcal{Y}^{GG}_{G+\frac{1}{2}G+1}(\hat{r}) &= \int\Omega\Big[-\frac{1}{G+1}\sqrt{\frac{G}{2G+1}\frac{1}{2G+3}}Y^*_{GG-1}Y_{10}Y_{G+1G-1}\sqrt{\frac{4\pi}{3}}\\ &\quad+\frac{1}{G+1}\sqrt{\frac{G}{2G+1}\frac{2G+1}{2G+3}}Y^*_{GG-1}Y_{1-1}Y_{G+1G}\sqrt{\frac{4\pi}{3}}\\ &\quad+\frac{1}{2G+2}\sqrt{\frac{1}{2G+3}}Y^*_{GG}Y_{10}Y_{G+1G}\frac{4\pi}{3}\\ &\quad-\sqrt{\frac{1}{G+1}\frac{1}{2G+3}}Y^*_{GG}Y_{1-1}Y_{G+1G+1}\sqrt{\frac{4\pi}{3}}\\ &\quad-\frac{1}{G+1}\sqrt{\frac{2G+1}{2G+3}}Y^*_{GG}Y_{11}Y_{G+1G}\sqrt{\frac{4\pi}{3}}\\ &\quad+\frac{2G+1}{2G+2}\sqrt{\frac{1}{2G+3}}Y^*_{GG}Y_{10}Y_{G+1G}\sqrt{\frac{4\pi}{3}}\Big]\\ &=\frac{1}{2G+1}.\end{aligned} \tag{D.11}$$

$J' = G-\frac{1}{2}$		$J' = G+\frac{1}{2}$		
$L' = G-1$	$L' = G$	$L' = G$	$L' = G+1$	
0	-1	$-2\sqrt{G(G+1)}$	0	$L = G-1$ $J = G-\frac{1}{2}$
-1	0	0	$-2\sqrt{G(G+1)}$	$L = G$
$-2\sqrt{G(G+1)}$	0	0	-1	$L = G$ $J = G+\frac{1}{2}$
0	$-2\sqrt{G(G+1)}$	-1	0	$L = G+1$

Table D.1: Matrix elements of $\int d\Omega(\mathcal{Y}^{GM}_{L'J'})^\dagger(\hat{x})\hat{r}\cdot\vec{\tau}\mathcal{Y}^{GM}_{LJ}(\hat{r})$. Note there is an overall factor of $1/(2G+1)$ that needs to be multiplied.

All other matrix elements are zero because of the orthogonality of the spherical harmonic functions. The result of these calculations is given in table D.1.

D.2 Calculation of $\vec{\sigma}\cdot\hat{p}$

Next we calculate the matrix $\int d\Omega_p\big(\mathcal{Y}^{GM}_{L'J'}\big)^\dagger(\hat{p})\hat{p}\cdot\vec{\sigma}\mathcal{Y}^{GM}_{LJ}(\hat{p})$. Through a simple relabeling we can see it is equivalent to $\int d\Omega_p\mathcal{Y}^{GM}_{L'J'}(\hat{x})\hat{r}\cdot\vec{\sigma}\mathcal{Y}^{GM}_{LJ}(\hat{r})$. Naturally we now use the same identities to calculate this matrix. The elements

$$\begin{aligned}\int d\Omega_p(\mathcal{Y}^{GM}_{G-\frac{1}{2}})^\dagger(\hat{x})\hat{p}\cdot\vec{\tau}\mathcal{Y}^{GM}_{LJ}(\hat{r}) = \int d\Omega_p\sqrt{\frac{4\pi}{3}}\Big[&-\sqrt{\frac{1}{2G+1}}Y^*_{G-1G-1}Y_{10}Y_{GG-1}\\ &+2\sqrt{\frac{G}{2G+1}}Y^*_{G-1G-1}Y_{1-1}Y_{GG}\Big]\\ &=-1,\end{aligned} \tag{D.12}$$

and

$$\begin{aligned}\int d\Omega_p(\mathcal{Y}^{GG}_{G+\frac{1}{2}G})^\dagger\hat{p}\cdot\vec{\sigma}\mathcal{Y}^{GG}_{G+\frac{1}{2}G+1} = \int d\Omega_p\sqrt{\frac{4\pi}{3}}\Big[&-\frac{2}{2G+2}\sqrt{\frac{G}{2G+3}}Y^*_{GG-1}Y_{10}Y_{G+1G-1}\\ &+\frac{2}{2G+2}\sqrt{\frac{G(2G+1)}{(2G+1)(2G+3)}}Y^*_{GG-1}Y_{1-1}Y_{G+1G}\\ &+\frac{2}{2G+2}\sqrt{\frac{1}{(2G+1)(2G+3)}}Y^*_{GG}Y_{11}Y_{G+1G-1}\\ &-\frac{1}{2G+2}\sqrt{\frac{1}{2G+3}}Y^*_{GG}Y_{10}Y_{G+1G-1}\\ &-\frac{2G+1}{2G+2}\sqrt{\frac{1}{2G+3}}Y_{GG}Y_{10}Y_{G+1G}\\ &+(2G+1)\sqrt{\frac{1}{(G+1)(2G+3)}}Y_{GG}Y_{10}Y_{G+1G+1}\Big]\\ &=-1,\end{aligned} \tag{D.13}$$

and their conjugates, are the only non-zero elements of the matrix. The full matrix can then be described by table D.2.

$J'=G-\frac{1}{2}$		$J'=G+\frac{1}{2}$		
$L'=G-1$	$L'=G$	$L'=G$	$L'=G+1$	
0	-1	0	0	$L=G-1$
				$J=G-\frac{1}{2}$
-1	0	0	0	$L=G$
0	0	0	-1	$L=G$
				$J=G+\frac{1}{2}$
0	0	-1	0	$L=G+1$

Table D.2: Matrix elements of $\int d\Omega_p(\mathcal{Y}^{GM}_{L'J'})^\dagger(\hat{p})\hat{p}\cdot\vec{\sigma}\mathcal{Y}^{GM}_{LJ}(\hat{p})$.

REFERENCES

[1] I. Takyi and H. Weigel [2019]. Nucleon structure functions from the NJL-model chiral soliton, *The European Physical Journal A* **55**: 1–20.

[2] I. Takyi [2019]. *Structure functions of the nucleon in the soliton model*, PhD thesis, Stellenbosch University.

[3] J.J. Thomson [1913]. *The structure of the atom*, Academie Royale de Belgique.

[4] E. Rutherford [2012]. The scattering of α and β particles by matter and the structure of the atom, *Philosophical Magazine* **92**(4): 379–398.

[5] J. Chadwick [1932]. The existence of a neutron, *Proceedings of the Royal Society of London. Series A, Containing Papers of a Mathematical and Physical Character* **136**(830): 692–708.

[6] H. Yukawa [1935]. On the Interaction of Elementary Particles I, *Proc. Phys. Math. Soc. Jap.* **17**: 48–57.

[7] F.E. Close [1979]. *Introduction to quarks and partons*, Academic Press, Inc., New York, NY.

[8] L.H. Ryder [1996]. *Quantum field theory*, Cambridge University Press.

[9] T. Muta [2010]. *Foundation of quantum chromodynamics: an introduction to perturbative methods in gauge theories*, World Scientific, Singapore.

[10] T.P. Cheng and L.F. Li [1984]. *Gauge theory of elementary particle physics*, Clarendon press: Oxford.

[11] Tanabashi, M. et al. [2018]. Review of Particle Physics, *Phys. Rev. D* **98**(3): 030001.

[12] G. 't Hooft [1974]. A two dimensional model for mesons, *Nuclear Physics B* **75**(3): 461–470.

[13] E. Witten [1979]. Baryons in the 1/N expansion, *Nuclear Physics B* **160**(1): 57–115.

[14] B. Lampe and E. Reya [2000]. Spin physics and polarized structure functions, *Physic Reports* **332**(1–3): 1–163.

[15] Glück, M. and Reya, E. and Vogt, A. [1998]. Dynamical parton distributions revisited, *The European Physical Journal C* **5**(3): 461–470.

[16] Y. Nambu and G. Jona-Lasinio [1961]. Dynamical model of elementary particles based on an analogy with superconductivity. I, *Physical review* **122**(1): 345.

[17] S.L. Adler [1969]. Axial vector vertex in spinor electrodynamics, *Physics Review* **177**: 2426–2438.

[18] J.S. Bell and R. Jackiw [1969]. A PCAC puzzle: $\pi^0 \to \gamma\gamma$ in the σ model, *Nuovo Cim. A* **60**: 47–61.

[19] D. Ebert and H. Reinhardt [1986]. Effective chiral hadron Lagrangian with anomalies and Skyrme terms from quark flavour dynamics, *Nuclear Physics B* **271**(3-4): 188–226.

[20] R. Alkofer and H. Reinhardt and H. Weigel [1996]. Baryons as chiral solitons in the Nambu-Jona-Lasinio model, *Physics Reports* **265**(3): 139–252.

[21] C.V. Christov, A. Blotz, H.C. Kim, P. Pobylitsa, T. Watabe, T. Meissner, E. Ruiz-Arriola and K. Goeke [1996]. Baryons as non-topological chiral solitons, *Progress in Particle and Nuclear physics* **37**: 91–191.

[22] U. Vogl and W. Weise [1991]. The Nambu and Jona-Lasinio model: its implication for hadrons and nuclei, *Progress in Particle and Nuclear physics* **27**: 195–272.

[23] W. Pauli and F. Villars [1849]. On the invariant regularization in relativistic quantum theory, *Reviews of Modern Physics* **21**(3): 434–444.

[24] H. Weigel, E. Ruiz-Arriola and L. Gamberg [1999]. Hadron structure function in a chiral quark model: regularization, scaling and sum rules, *Nuclear Physics B* **560**(1): 383–427.

[25] F. Doering, C. Schueren, E.R. Arriola, T. Watabe and K. Goeke [1996]. Analytical continuation of the fermion determinant with a finite cut-off, *Nuclear Physics A* **603**(3): 415–440.

[26] K. Fujikawa and H. Suzuki [2004]. *Path Integrals and Quantum Anomalies*, Oxford University Press.

[27] C. Schuren, E. Ruiz-Arriola and K. Goeke [1992]. Explicit chiral symmetry breaking in the Nambu-Jona-Lasinio model, *Nuclear Physics A* **547**(4): 612–632.

[28] A. Dhar, R. Shankar and S.R. Wadia [1985]. Nambu-Jona-Lasinio-type effective Lagrangian: Anomalies and nonlinear Lagrangian of low-energy, large-N QCD, *Physical Review D* **31**(12): 3256.

[29] R. Alkofer and H. Reinhardt [1995]. *Chiral quark dynamics, Springer Lecture notes Physics*, Vol. 33, Springer, Berlin.

[30] F. Halzen and A.D. Martin [2008]. *Quark and Leptons: An introductory course in modern particle physics*, John Wiley and Sons, New York.

[31] H. Weigel [2008]. *Chiral Soliton Models for Baryons*, Vol. 743, Springer-Verlag, Berlin.

[32] H. Reinhardt [1989]. The chiral soliton in the proper-time regularization scheme, *Nuclear Physics A* **503**(3): 825–848.

[33] R.F. Dashen, B. Hasslacher and A. Neveu [1975]. Semiclassical bound states in an asymptotically free theory, *Physics Review D* **12**: 2443–2458.

[34] R.P. Feynman [1939]. Forces in Molecules, *Phys. Rev.* **56**: 340–343.

[35] R. Alkofer, H. Reinhardt, H. Weigel and U. Zückert [1992]. Supporting the Skyrmion from the Nambu–Jona-Lasinio model with vector and axial-vector mesons, *Physics Review Letters* **69**: 1874–1876.

[36] H. Reinhardt and R. Wünsch [1989]. Topological solitons of the Nambu-Jona-Lasinio model, *Physics Letters B* **230**(1): 93–98.

[37] Th. Meissner and F. Grümmer and K. Goeke [1989]. Solitons in the Nambu-Jona-Lasinio model, *Physics Letters B* **227**(3): 296–300.

[38] R. Alkofer [1990]. The soliton of the Nambu-Jona-Lasinio model, *Physics Letters B* **236**(3): 310–314.

[39] P. Ring and P. Schuck [2004]. *The nuclear many-body problem*, Springer-Verlag, Berlin.

[40] G. Holzwarth and B. Schwesinger [1986]. Baryons in the Skyrme model, *Reports on Progress in Physics* **49**(8): 825.

[41] T. Frederico and G.A. Miller [1994]. Deep-inelastic structure function of the pion in the null-plane phenomenology, *Physics Review D* **50**: 210–216.

[42] F. Gross [2008]. *Relativistic quantum mechanics and field theory*, John Wiley & Sons.

[43] M.E. Peskin and D.V. Schroeder [1995]. *Introduction to QFT*, Persues Books, Cambridge, Massachusetts.

[44] M. Wakamatsu and T. Kubota [1998]. Chiral symmetry and the nucleon structure functions, *Physics Review D* **57**: 5755–5766.

[45] R.L. Jaffe [1975]. Deep-inelastic structure functions in an approximation to the bag theory, *Phys. Rev. D* **11**: 1953–1968.

[46] H. Weigel, L. Gamberg and H. Reinhardt [1996]. Unpolarised structure functions in the Nambu-Jona-Lasinio chiral soliton model, *Modern Physics Letters A* **11**(38): 3021–3034.

[47] H. Weigel, L. Gamberg and H. Reinhardt [1997]. Nucleon structure functions from a chiral soliton, *Physics Letters B* **399**(3): 287–296.

[48] D.I. Diakonov, V.Y. Petrov, P.V. Pobylitsa, M.V. Polyakov and C. Weiss [1997]. Unpolarized and polarized quark distributions in the large-N_c limit, *Phys. Rev. D* **56**: 4069–4083.

[49] Jaffe, RL [1981]. Operators in a translation invariant two-dimensional bag model, *Annals of Physics* **132**(1): 32–52.

[50] Gamberg, L and Reinhardt, H and Weigel, H [1998]. Nucleon structure functions from a chiral soliton in the infinite momentum frame, *International Journal of Modern Physics A* **13**(32): 5519–5534.

[51] I. Takyi [20-3-2023]. private communication.

[52] Press, William H and Teukolsky, Saul A and Vetterling, William T and Flannery, Brian P [1997]. *Numerical recipes in Fortran 77 and Fortran 90: Source code for recipes and example programs*, Cambridge University Press, Cambridge.

[53] Ito, Hiroaki and Kitazawa, Masakiyo [2023]. Gravitational form factors of a kink in 1 + 1 dimensional ϕ^4 model, *JHEP* **08**: 033.

[54] Varshalovich, D and Moskalev, A and Khersonski, V [1988]. *Quantum Theory of Angular Momentum World Scientific Publishing*, Singapore.